ARCHIVES OF ACOUSTICS
12, 2, 75–87 (1987)

IN SEARCH FOR THE CRITERIA OF ABSOLUTE PITCH

ANDRZEJ RAKOWSKI, MARIETTA MORAWSKA-BÜNGELER

Department of Music Acoustics, Academy of Music in Warsaw
(ul. Okólnik 2, 00-368 Warszawa)

A series of experiments has been performed in order to find specific features of pitch memory in persons possessing the so-called absolute pitch.

Sixty one music students were given a test of passive absolute pitch (pitch-naming test); then a part of this group was subjected to another test in order to determine their ability to produce required musical pitch without being given any reference tone (active absolute pitch). A criterion for absolute pitch was proposed on the basis of the evaluation of the precision of tuning a pure-tone generator to the required musical pitch. Finally, two musicians, one of them possessing absolute-pitch, were given a task of tuning a pure-tone generator to the pitch of a standard after various delay times. The results were presented in the form of pitch-forgetting curves.

1. Introduction

Absolute pitch is the ability, possessed by some people, to recognize exactly or reproduce musical pitch without reference tones. The ability to recognize musical pitch of tones is called passive absolute pitch, while the ability to imagine and then reproduce a given pitch is called active absolute pitch. People without absolute pitch usually can recognize and reproduce the pitch of definite musical tone only when they are presented with another tone and know its name. In such a case the so-called relative pitch is employed, i.e., the knowledge of the learned and permanently memorized musical intervals. Absolute pitch is only possessed by a small part of the human population, probably about one to several percent. It is positively related to other music talents, though not necessarily a condition for their occurence. Hitherto, absolute pitch has been the subject of many investigations. Results of some of these works have been recently discussed by WARD and BURNS [1].

It is accepted by most authors that absolute pitch is an inborn talent and that people with this talent differ greatly from people without absolute pitch in the domain of pitch recognition. However, many musicians who initially did not distinguish absolute pitch of tones developed this ability to a certain extent through

practice and utilization of additional evaluation criteria. Such additional criteria usually consist of remembering one musical pitch and having it as a standard reference point in evaluating pitch of other tones. In some people the phenomenon of absolute pitch is limited to recognizing the pitch of tones of one familiar instrument, or it consists of remembering a specific colour of a given musical key.

The present experiments were designed to investigate in detail some of the unknown properties of absolute pitch, compare the features of auditory memory in people with absolute and relative pitch, and try to determine criteria for both types of audition.

2. Investigations of passive absolute pitch

Sixty one listeners, who were students at the Academy of Music in Warsaw, participated in the experiment. Every student had completed at least a two-year course in ear training at secondary music school and currently attended courses on this subject at the Academy. Students listened to tests recorded on tape and reproduced from a loudspeaker at a comfortable listening level of approximately 75 dB *SPL*. Listeners were divided into 6 groups, each consisting of about ten persons.

The listeners' task was to recognize the names and tone registers (octaves) of 24 or 23 notes of the musical scale presented in random order. Each tone was presented only once in a test; it lasted for two seconds and was separated from the next tone by a two-second time interval. Identification of tones and octaves was performed by subjects to make the process of answering as quick and simple as possible. The answer was given by marking out one of twelve names of tones (chromatic tones were marked twofold, e. g. *G♯/A♭*) and additionally, by marking out one of eight octaves on a draft piano keyboard (see Fig. 1).

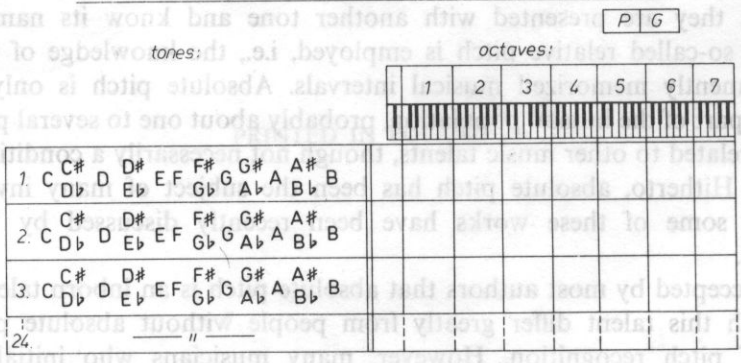

Fig. 1. Part of the answer sheet in a pitch-naming test

There were two versions of the test: first, with the application of piano tones recorded on tape (*P*), second, with the application of pure tones from a generator (*G*). Tones with the lowest frequency were not presented in the generator test due to technical difficulties. Instead other tones from the low register were presented, and the number of tones was decreased to 23; there were 24 tones in the piano test. The piano test was conducted first, and the generator test followed after a few days.

Figure 2 shows the distribution of all errors made by the listeners during the first presentation of both tests. Both non-octave (false tone name) and octave (falsely determined octave) mistakes were included. Also a lack of an answer was considered as an error.

The results in Fig. 2 show that fewer mistakes were made in the piano test than in the generator test. Most probably this was caused by better familiarity of the

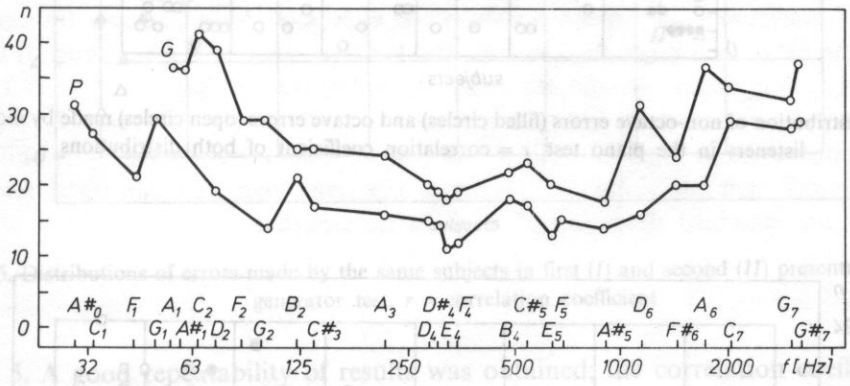

Fig. 2. Distribution of errors made by 61 listeners when 24 piano tones (*P*) and 23 pure tones from a generator (*G*) were presented for the first time

listeners with the timbre of piano tones than with the timbre of pure tones from the generator. It can also be noted that sounds from the middle tone register were recognized better than those from extreme registers.

Figure 3 presents the distribution of errors made by individual listeners during the first presentation of the piano test. This distribution, arranged according to the increasing number of non-octave errors, is shown as filled circles. The corresponding octave errors are presented as open circles. In groups of listeners, who had made equal numbers of non-octave errors, sequential arrangements of listeners (affecting their octave-error distributions) were randomized. The correlation coefficient, calculated for so-arranged distributions of non-octave and octave errors in the whole group of 61 listeners, equalled -0.45.

The tests were repeated with a part of the previous group of listeners two weeks after the first presentation; 31 listeners participated in the repeated piano test and 30 listeners in the generator test. The distributions of errors made by the listeners in the first and second presentations of the piano and generator tests are shown in Figs. 4

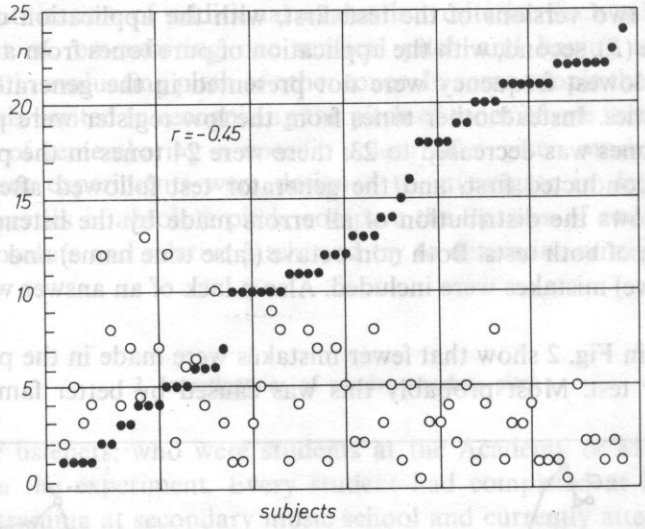

Fig. 3. Distribution of non-octave errors (filled circles) and octave errors (open circles) made by individual listeners in the piano test. r = correlation coefficient of both distributions

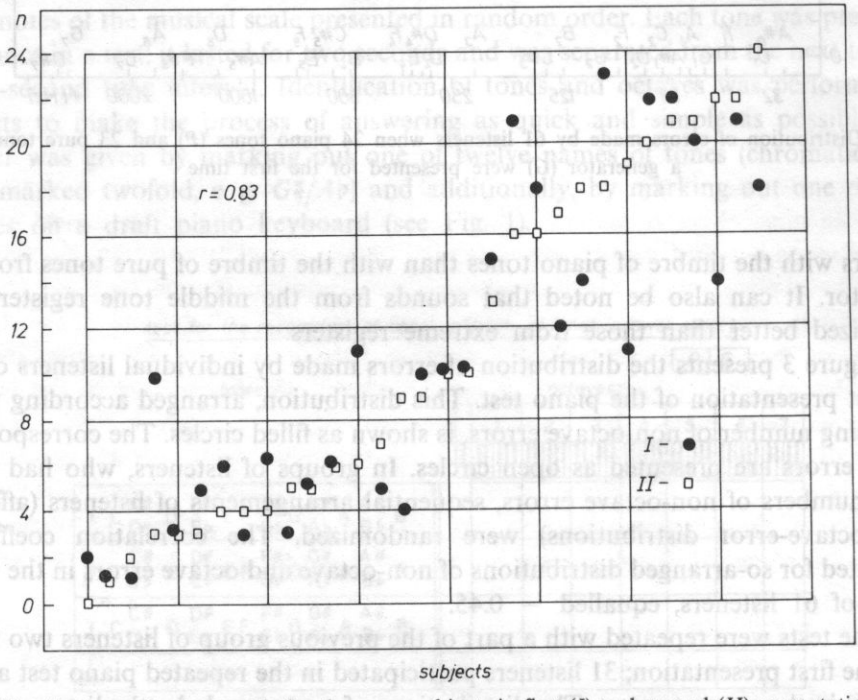

Fig. 4. Distributions of errors made by the same subjects in first (I) and second (II) presentation of the piano test. r = correlation coefficient

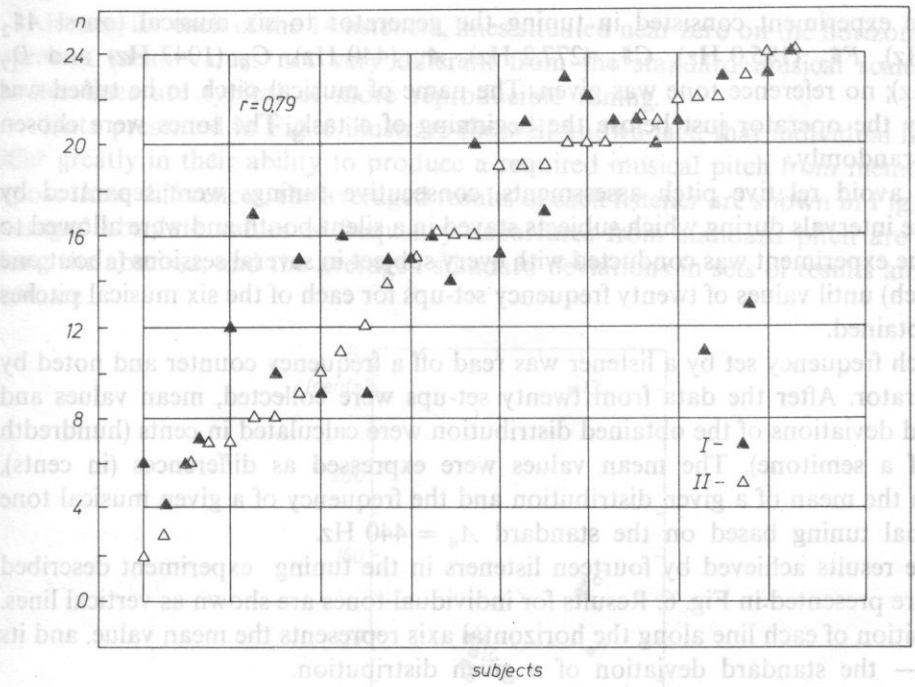

Fig. 5. Distributions of errors made by the same subjects in first (*I*) and second (*II*) presentation of the generator test. r = correlation coefficient

and 5. A good repeatability of results was obtained; the correlation coefficients of distributions were +0.83 and +0.79 for piano and generator tests, respectively.

3. Investigations of active absolute pitch

Fourteen subjects, members of a group which participated in the tests of passive absolute pitch, took part in the next experiment concerning active absolute pitch. Some subjects were selected because they achieved best results in the first test of piano tones recognition, while the others were picked randomly.

Each of the 14 subjects was given a task of tuning a sine-tone generator to a series of musical pitches. Experiments were carried out in individual sessions, in an acoustically isolated booth with the use of high quality binaural earphones at a loundness level of 40 phons. Subjects tuned the tone generator starting alternately from the upper or lower position outside the audible range. Tuning was done with one knob. The scale of the generator was covered, and all other visual or mechanical criteria were also eliminated, so listeners could only employ their auditory memory in tuning the required pitch.

The experiment consisted in tuning the generator to six musical tones: $A\sharp_2$ (116.5 Hz), $F\sharp_3$ (185.0 Hz), $C\sharp_4$ (277.2 Hz), A_4 (440 Hz), C_6 (1047 Hz) and D_7 (2349 Hz); no reference tone was given. The name of musical pitch to be tuned was given by the operator just before the beginning of a task. The tones were chosen pseudo-randomly.

To avoid relative pitch assessments, consecutive tunings were separated by 4-minute intervals during which subjects stayed in a silent booth and were allowed to read. The experiment was conducted with every subject in several sessions (about one hour each) until values of twenty frequency set-ups for each of the six musical pitches were obtained.

Each frequency set by a listener was read off a frequency counter and noted by the operator. After the data from twenty set-ups were collected, mean values and standard deviations of the obtained distribution were calculated in cents (hundredth parts of a semitone). The mean values were expressed as differences (in cents), between the mean of a given distribution and the frequency of a given musical tone in normal tuning based on the standard $A_4 = 440$ Hz.

The results achieved by fourteen listeners in the tuning experiment described above are presented in Fig. 6. Results for individual tones are shown as vertical lines. The position of each line along the horizontal axis represents the mean value, and its length – the standard deviation of a given distribution.

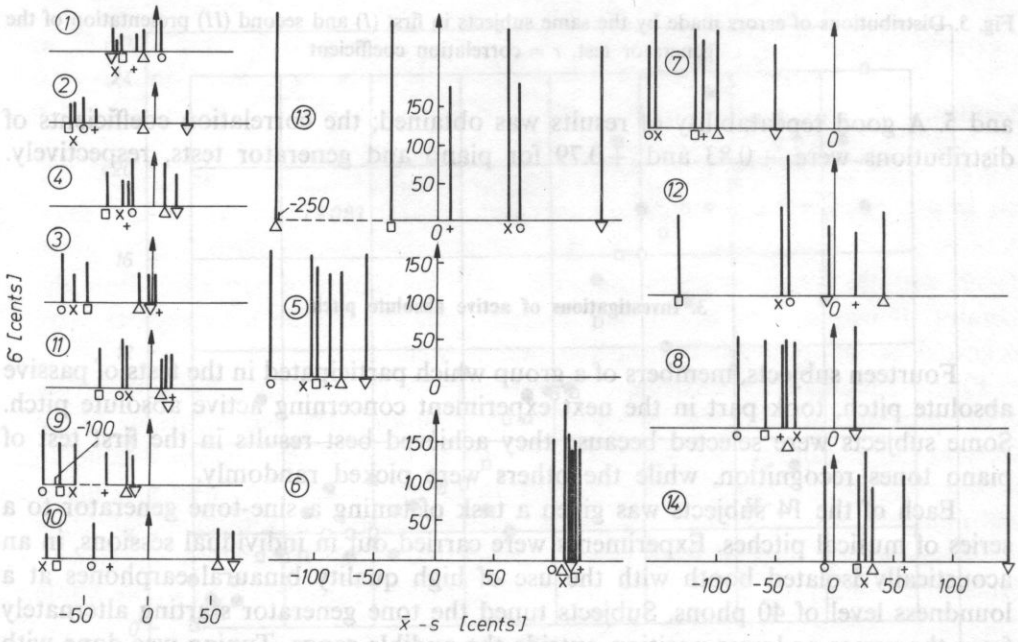

Fig. 6. Results of fourteen subjects in tuning six tone frequencies to the required musical pitch. Departures of average values of twenty tunings from standard frequencies S ($A\sharp_2$ – ○, $F\sharp_3$ – ×, $C\sharp_4$ – □, A_4 – +, C_6 – △, D_7 – ▽) are shown on the horizontal axis. Values of standard deviations of individual distributions are shown along the vertical axis

Hence, for each of the 14 listeners, lines situated near zero on the horizontal axis represent mean values not very different from the standard musical scale, while shorter lines are typical of more reproducible tuning.

Data presented in Fig. 6 illustrate the well-known fact, that individual listeners differ greatly in their ability to produce a required musical pitch from memory. To expose these differences, the averaged results of each listener are shown in Fig. 7. The averaged absolute values of frequency departures from standard pitch are shown along the abscissa, and the averaged standard deviations in sets of results along the ordinate.

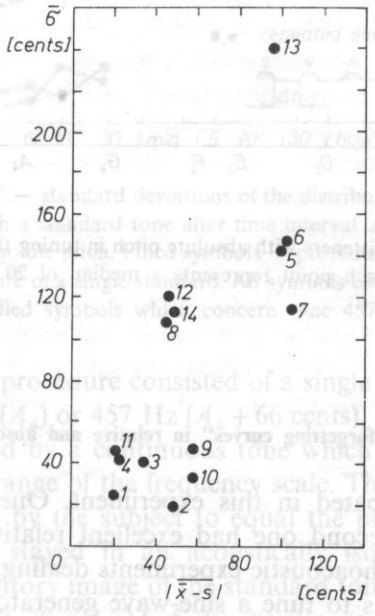

Fig. 7. Averaged values of standard deviations σ and averaged values of constant errors $(\bar{x}-s)$ obtained in free tuning of six music tones by fourteen listeners

The next experiment was carried out with the participation of three new subjects, who were students, possessing a very good absolute pitch, according to the opinion of their teachers. Subjects were told to tune a sine-wave generator to 13 musical notes from C_4 to C_5. The experiment was conducted under conditons similar to those in the previous one. Tunings were performed in a pseudo-random order with 5-minute time intervals in between, in order to eliminate the influence of short-term memory and relative pitch. About 13 frequency set-ups, corresponding to 13 chromatic tones, were obtained during a one-hour session. Twenty sessions were conducted with each subject within approximately one month; the medians of the distributions are shown in Fig. 8. It appears that all three listeners tended to raise the frequency of lower tones and reduce the frequency of higher tones in relation to standard tuning.

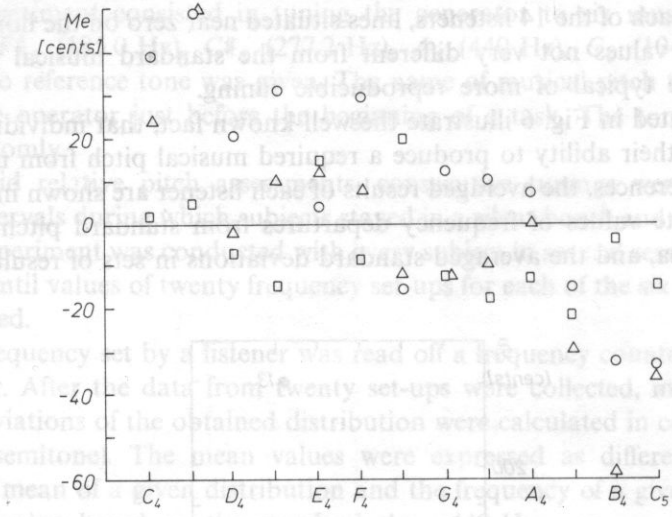

Fig. 8. Results achieved by three listeners with absolute pitch in tuning thirteen tones of the musical scale from C_4 to C_5. Each point represents a median of 20 frequency set-ups

4. "Pitch forgetting curves" in relative and absolute pitch

Two subjects participated in this experiment. One of them had very good absolute pitch, and the second one had excellent relative pitch. Both had considerable experience in psychoacoustic experiments dealing with pitch discrimination.

The subjects' task was to tune a sine-wave generator to match the pitch of a standard tone at various time intervals between the standard and variable tones. Time intervals between these tones varied from one second to 30 minutes. (In addition, data for a 24-hour time interval were obtained using a procedure which will be described later). Listeners performed 20 tunings for each value of the time interval. Two procedures were applied: one in the range of short time intervals only (procedure of a repeated standard), and a second one in both short and long time interval ranges (procedure of a single standard).

In the procedure of a repeated standard, 3-second pulses of the standard and variable tones were presented interchangeably, separated by time interval a Δt. The variable tone (subject to tuning) was additionally signalled by a light. The tones were presented binaurally through headphones at a loudness level of 40 phons while the subject was seated in a sound-isolated booth. The presentation of stimuli was continuous until the subject announced that tuning was completed. Twenty frequency set-ups were taken at each of the 4 values of Δt (1, 5, 10 and 25 s), and standard deviations calculated. The results are presented in Fig. 9.

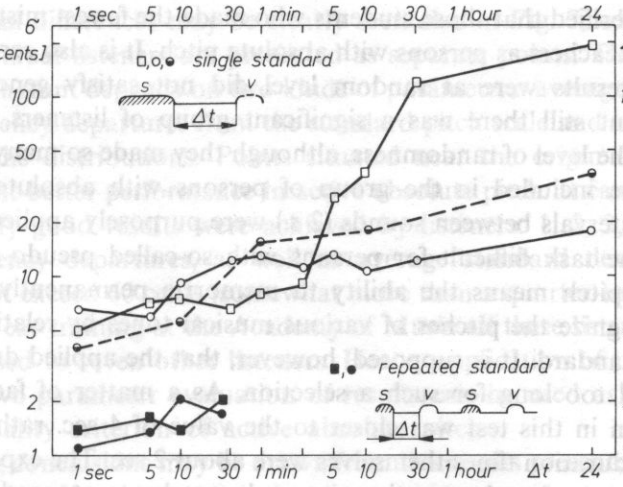

Fig. 9. "Pitch forgetting curves" – standard deviations of the distributions of frequency set-ups of tuning a pure tone to equal pitch with a standard tone after time interval Δt. Squares – subject with relative pitch; circles – subject with absolute pitch. Filled symbols – procedure of a repeated standard; open and half–filled symbols – procedure of a single standard. All symbols concern tuning of a tone 440 Hz (A_4), exluding half-filled symbols which concern tone 457 Hz (A_4+66 cents)

The single standard procedure consisted of a single presentation of a 10-second standard tone of 440 Hz (A_4) or 457 Hz (A_4+66 cents). After a time interval Δt, this presentation was followed by a continuous tone which appeared alternatively in a very high or a very low range of the frequency scale. This second stimulus (variable tone) had to be adjusted by the subject to equal the pitch of the previously-heard standard tone. Subjects stayed in an acoustically isolated booth and were encouraged to keep the auditory image of the standard tone in mind during the silence time intervals Δt. (1, 5, 10, 30 s, 1, 2.5, 5, 10, 30 min; each value applied at separate session or group of sessions). They were visually informed about the time remaining until the appearance of the variable tone, which was also signalled by light 3 seconds ahead. In the case of 24-hour time intervals, this procedure was not used, and the results were obtained just after the arrival of the listener at the laboratory, knowing that he had participated in the experiments with the same standard on the day before. Although the time of tuning was not limited, it generally did not exceed 3 seconds. By shortening the tuning process, subjects tried to minimize the interfering effect of a variable tone on the memorized pitch of a standard.

5. Discussion and conclusions

As can be seen in Figures 3–5, the experiment on pitch identification (pitch-naming test) did not give results sufficient for establishing a criterion for absolute pitch. The distribution of errors made by the subjects in the tests was rather continuous.

However, it was verified that those students who made the fewest mistakes would be qualified by their teachers as persons with absolute pitch. It is also certain that those listeners, whose results were at random level did not satisfy general criteria of absolute pitch. But still there was a significant group of listeners, whose results greatly exceeded the level of randomness, although they made so many mistakes that they could not be included in the group of persons with absolute pitch.

Short time intervals between sounds (2 s.) were purposely applied in the test in order to make the task difficult for persons with so-called pseudo-absolute pitch. Pseudo-absolute pitch means the ability to memorize permanently one standard pitch and to recognize the pitches of various musical tones by relative judgements refering to that standard. It is supposed, however, that the applied duration of time intervals was still too long for such a selection. As a matter of fact the time for making a decision in this test was closer to the value of 4 sec. rather than 2 sec., because the tone duration times themselves were about 2 sec. The experiment should be repeated in future for shorter time intervals or shorter tone durations.

Although the experiment on pitch identification did not enable the identification of all possessors of absolute pitch, it led to another very important observation. It can be seen in Fig. 3 that persons who made a small number of non-octave mistakes, had rather poor results in distinguishing octaves. The correlation between octave and non-octave errors was negative ($r = -0.45$). This result strongly supports the theory of a two-dimensional character of musical pitch sensations (REVESZ [2]; BACHEM [3]). These two dimensions of pitch are: pitch quality ("chroma") and pitch register (octave). The following hypotheses can be made to explain the negative correlation between distributions of non-octave and octave errors:

1. The recognition of the "musical name" of a tone (i.e. chroma) as a pitch category is done nearly independently of the recognition of its pitch register (octave).

2. Listeners with the ability of chroma recognition (those, who have "absolute pitch") usually do not exibit any specific ability of octave recognition better than that exibited by listeners with relative pitch.

3. The fact that listeners who made fewer non-octave mistakes had worse results than other listeners in tests of octave recognition was explained in the following way: Listeners who were sure of their abilities in pitch naming (recognition of pitch names) and who justly considered this part of the test as fundamental, devoted more attention to it, as well as a greater part of the limited answering time. Recognition of the octave was considered by them as secondary, and they spent less time on this task. Listeners, who knew from practice that recognition of chroma is for them practically impossible, acted appositely. They spent most of the time on the task which they justly considered as solvable, i.e. on recognition of the octave. This way they had a lower percent of octave errors.

Experiments on pitch tuning were supplementary to identification experiments and led to establishing criteria of active absolute pitch. It can be concluded from Fig. 6 that individual listeners differed greatly in the precision of tuning individual

tones. Individual differences may be clearly seen also in Fig. 7, where the averaged results of individual listeners are presented as separate points. The arrangement of points in the diagram depends on two kinds of parameters: averaged absolute values of tuning frequency departures from the standard pitch scale and averaged standard deviations of the distributions. Points situated near the origin of the coordinate system represent better performance in active absolute pitch. It can be seen in Fig. 7 that particularly good results were achieved by listeners: 1, 2, 3, 4, 9, 10 and 11. Average frequency departures, as well as average standard deviations for these listeners did not exceed 60 cents (somewhat more than a quarter-tone). According to the teachers of ear training at the Academy of Music all these listeners had absolute pitch, as opposed to seven other listeners. Hence, application of the active method (tuning) and two-parameter evaluation of results can be used as a foundation for operational quality criterion of active absolute pitch.

Interesting conclusions may be drawn from the results presented in Fig. 8. In the process of tuning thirteen chromatic tones within an octave, a distinct effect appeared as raising low tones and lowering high tones. The explanation of this may be following. Due to prolonged operation within a limited memory standard range (one octave) an effect of partial assimilation of the standards occured in the subjects. This resulted in deviations of these standards in the direction of the centre of gravity of the whole set. Such effects have been observed by psychologists with respect to various sensations. Harris (1948) described them with respect to short-term pitch memory and introduced the term "effective standard". They may also be explained in terms of the adaptation level theory (Helson [5]). Results presented in Fig. 8 reveal this phenomenon in the domain of absolute pitch.

The experiment which led to the construction of "pitch forgetting curves" enabled a more detailed observation of the mechanism of short – and long – term memory in subjects with relative and absolute pitch (Fig. 9). First of all, a very high precision of tuning was observed in both listeners when the repeated standard was applied. The values of standard deviation at $\Delta t = 1$ sec can be interpreted as frequency discrimination thresholds measured with the method of adjustments. The standard deviations increase when the interval between stimuli is increased to 25 sec, but still they remain within a range of 2 cents (1/50 of a semitone). This experiment reveals a surprising accuracy of the short-term pitch memory in experienced musical subjects. It is also worth mentioning that although only one subject possessed absolute pitch, both of them achieved similar results. This is in agreement with previously obtained results (Rakowski and Hirsch [6]) showing that absolute pitch does not interfere with short-term auditory memory.

While comparing the repeated and single standard precedures, one can see that the results obtained with the latter one are much less precise (i.e., standard deviations are larger). This is due both to the disturbing effect of the variable tone in the initial phase of tuning and to the lack of the possibility of repeated comparisons when the method of single standard is applied. With this procedure, the results obtained from

both listeners differ significantly at most of the time intervals applied. At shorter time intervals, the results of the absolute-pitch listener appear to be somewhat worse than those of his relative-pitch colleague; however, at Δt longer than 5 minutes they are definitely better. This fact can be explained in the following way: The listener with absolute pitch from the very first presentation of a standard knows that he is dealing with the musical tone A_4. He can tune this tone easily using the internal pitch standard stored in his long-term auditory memory. Such a tuning strategy is somewhat less accurate than the application of short-term memory, but it is less tiring and does not require such great concentration. Hence, it may be assumed that our absolute-pitch subject changed his strategy at time intervals of about 10 sec, and for longer time delays used his long-term pitch memory. In such a case his tuning operations were practically independent of the time delays applied, and his results were more or less constant.

The situation was different in the case of a listener not possessing absolute pitch. He did not have any internal pitch standards at his disposal, therefore he tried to prolong the contact with the external standard by straining his short-term memory. The short-term memory for pitch is very accurate; therefore up to a 3-min delay he achieved even better results than the absolute-pitch subject. But at a time interval of several minutes the short-term memory trace of the non-absolute pitch listener was rapidly decaying and the accuracy of his tuning became worse.

The results achieved by the subject with absolute pitch appeared to be somewhat less accurrate, when the standard frequency was changed from 440 Hz (A_4) to 457 Hz ($A_4 + 66$ cents). This leads to an important conclusion: Absolute pitch is not equivalent with readiness for retentive remembering of a new pitch standard. The process of remembering such a pitch, differing from twelve pitch standards stored in the long-term memory, is carried out by comparing it with these standards and appropriate verbalization. For example the subject states: "This tone is somewhat lower than $A\sharp$". Consequently, the reproduction process of that pitch is more complex; it consists of two phases: 1) recalling the nearest standard; and 2) producing the estimated microinterval in relation to it. Hence, a greater variance results.

It may be concluded, that the "pitch forgetting curves" presented in Fig. 9 are a good illustration of memory processes characteristic of absolute and relative pitch.

References

[1] W. D. WARD, E. M. BURNS, *Absolute pitch.* In: D. Deutsch, ed., The Psychology of Music, Academic Press, London–New York (1982).

[2] G. RÉVÉSZ, *Zur Grundlagen der Tonpsychologie*, Veit, Leipzig, 1913.

[3] A. BACHEM, *Various types of absolute pitch*, J. Acoust. Soc. Am., **9**, 146–158 (1937).

[4] J. D. HARRIS, *Discrimination of pitch-suggestions towards method and procedure*, Am. J. Psychol., **61**, 309–322 (1948).

[5] H. HELSON, *Adaptation level theory*. In: S. Koch, (ed.), Psychology: A Study of Science, McGraw Hill, New York–Toronto–London (1959).

[6] A. RAKOWSKI, I. J. HIRSH, *Post-stimulatory pitch shifts for pure tones*, J. Acoust. Soc. Am., **68**, 467–474 (1980).

Received on May 15, 1986; revised version on September 22, 1986.

ARCHIVES OF ACOUSTICS
12, 2, 89–111 (1987)

SPECTRAL ANALYSIS OF VIBRATIONS IN CONTROL INVESTIGATIONS OF VIBROACOUSTIC HEADS KGS-320

TADEUSZ ZAKRZEWSKI

Mechanization Center of the Mining Industry KOMAG
(44-100 Gliwice, ul. Pszczyńska 37, Poland)

Diagnostic investigations were performed in order to evaluate the usability of the spectral analysis of vibrations in the process of control diagnostics of vibroacoustic arm heads of combined cutter loaders *KGS* 320. Tests were carried out at the acceptance inspection stand during idle running of the head with the consideration of both directions of rotation of the output shaft.

Frequency components corresponding to rotational speeds of some kinematic elements of the system under investigation were isolated on the basis of the spectral analysis of vibrations. A comparison of discrete amplitudes obtained from vibration spectra, allowed to evaluate the range of variability of vibration levels in determined frequency bands, as well as to isolate some kinematic pairs, which are characterised by the maximal vibration intensity. It was found that the rotation direction of the output shaft influences values of amplitudes of some vibration parameters in frequency bands, which contain characteristic frequencies of some elements of the system.

1. Introduction

The question of providing a longlasting reliability of technical objects produced by many branches of industry is one of the important problems of production enterprises. Progress in the domain of construction and technology of production and control of operation processes of determinate machine elements has led to the formation of many various, frequently complex, technical objects. The practical usability of such objects is determined by the type and occurance frequency of failures, and by the repair time. Therefore, in order to improve the quality of technical objects, their dynamic properties have to be investigated during control diagnostics. The physics of processes leading to failures constitute the basis of a scientifically-founded choice of the most effective construction and technologic method, which would increase or the life of basic machine elements [10]. In view of rapid development of technology and high requirements for machinery, concerning their reliability, production precision, life, etc. technical diagnostics should enable to

determine the condition of a machine on the basis of its certain parameters, without disassembly or interruption of the technologic cycle. Hence, indirect methods, in which the condition evaluation is performed on the basis of investigations of processes accompanying machine functioning, have to be applied [4]. Such methods are utilized in vibroacoustic diagnostics which infer about the dynamic state of an object from investigations of the vibroacoustic process generated in various points of the body of an investigated object [12, 5]. Vibroacoustic phenomena correspond to most significant physical processes, which take place in the machine and which determine correctness of functioning, such as for example: strain, stress, cooperation of elements etc. Various estimators of a deterministic character, which describe these phenomena, and the dynamic state of dynamic pairs of the machine can be determined by averaging the process in the domain of time, frequency or amplitude.

Performed vibroacoustic investigations were aimed at the relative evaluation of the dynamic state of arm heads in mining combined cutter loaders. The evaluation was carried out on the basis of results of a vibration spectral analysis, which included $n = 10$ heads during idle running with the consideration of both rotation directions of the getter.

2. Applied measuring system

The choice of the research method, which would enable useful signal separation from disturbing signals, is the main problem of vibroacoustic diagnostics. At present, three fundamental separation methods are applied [8]. They concern the domains of: space, time and frequency. The method of signal separation in the domain of time is based on time gating (sampling) of signals with respect to the dynamics of the material system and on obtaining information contained in time intervals of the gate opening. The frequency signal separation method consists in the transformation of the time function into the domain of frequency and then in the analysis of this function in adequate diagnostic bands. The choice of an analysis method depends on the type of machine under investigation and is based on an assumption that the useful signal can be found in certain frequency ranges, while outside these ranges disturbing signals or signals carrying little information, prevail.

At present, the spectral analysis method is measuring method most frequently applied in machine diagnostics [14, 16]. Due to the randomness of vibroacoustic processes related to machine work, the diagnosis of the state of an object is based on signal estimators achieved through analogue or digital signal processing. Analogue signal processing finds wide application in practice, especially when the dynamic state of a machine can be determined from the measurement and analysis of only few estimators of the vibroacoustic signal [15].

Digital processing allows quicker and more complex investigation and analysis of a signal, according to a previously programmed algorithm of digital processing. It

should find wider application in vibroacoustic diagnostics of machines in the nearest future.

In order to estimate the dynamic state of arm heads two series of measurements were carried out, and rms and peak values of vibration parameters were recorded respectively for the right and left rotation of the output shaft. Including the assumption that the dynamic state of heads is conditioned by the so-called vibration rate and that the frequency of the primary motion of main drive elements is low (below 50 Hz), it can be approximately accepted that this rate should be:

1) proportional to the displacement amplitude of vibrations, conditioned by the play misalignment of drive shafts,

2) proportional to the velocity amplitude of vibrations, caused by incorrect mating of toothed wheels,

3) proportional to the acceleration amplitude of vibrations, due to manipulative and assembly errors of rolling bearings.

Vibration parameters were measured with a piezoelectric sensor and then the voltage from the transducer was recorded on magnetic tape. The block diagram of the system for direct registration of vibration parameters is presented in Fig. 1. The registered signal was filtered in order to reduce the influence of disturbances with high and very low frequencies. The block diagram of the laboratory system for amplitude – frequency analysis is shown in Fig. 2. Rms and peak values of measured parameters were read off directly from the vibrometer during investigations.

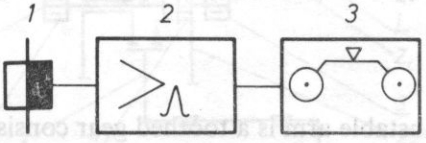

Fig. 1. Block diagram of the system for measurements of vibration parameters: 1) *ACC/U* transducer type 4370, 2) vibrometer type 2511, 3) magnetic recorder "Tandberg" type 115D

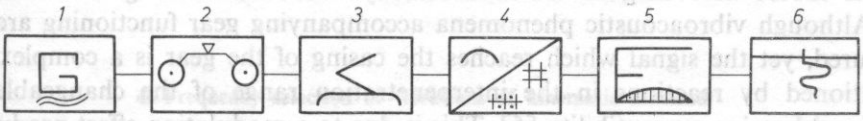

Fig. 2. Block diagram of the system for frequency analysis of vibration parameters: 1) beat frequency generator type 1022 (path calibration), 2) magnetic recorder "Tandberg" type 115*D*, 3) voltage amplifier type 2606, 4) digital recorder type 7502, 5) third-octave analyser type 2113 or heterodyne analyser type 2010, 6) level recorder type 2305

3. Localization of measuring points

The localization of measuring points on the body of a head is a very important problem in vibroacoustic measurements. As the greatest surpluses of dynamic forces in machines with rotational elements are transfered by bearings and transmissions of

kinematic elements, thus measuring points were located in the direct nearness of bearings of main drive units of the head, such as idle wheels, main shafts, layshafts, planetary gear. Tab. 1 presents the distribution diagram of measuring points adjoining mentioned kinematic elements of the system. In principle, such measurements should be done in three perpendicular directions, but in our case (head with mainly rotational elements) measurements were limited to the radial and axial direction, what is absolutely sufficient [3].

Table 1. List of revolutions frequencies and mesh frequencies of specified toothed wheels

Measurement point number	Gear wheel	Bearing	Measurement directions
1	Z3	5	radial
2	Z1	–	radial
3	Z2	4; 3	radial
4	Z4	6	radial
5	Z4	6	axial
6	Z5	7	radial
7	Z4; Z5	7	axial
8	Z10; Z11	13	axial
9	Z8	11	radial
10	Z9; Z10; Z11	10	radial
11	Z7	9	axial
12	–	14; 15	radial

A head with an adjustable arm is a toothed gear consisting of several cylindrical gears and a planetery gear, which drives directly the output shaft of the mining organ, as the last transmission. The mining organ is supplied with power from an electric motor according to the kinematic system shown in Fig. 3.

Although vibroacoustic phenomena accompanying gear functioning are easily measured, yet the signal which reaches the casing of the gear is a complex signal conditioned by reactions in the interpenetration range of the changeable (with rotations) bearing susceptibility [5]. This is due to a modulation effect produced by the series connection of dynamic reactions in the range of interpenetration of dynamic reactions of ball bearings. Furthermore, the casing of the gear has a very complex resonance structure and thus various filtration effects will occur in various signal reception points on the casing and a modified signal corresponding to gear functioning will be obtained.

The evaluation of the technologic state of a gear and its elements with the vibroacoustic method is difficult, because of complicated paths of reactions from the range of interpenetration to individual vibration reception points on the casing of the gear.

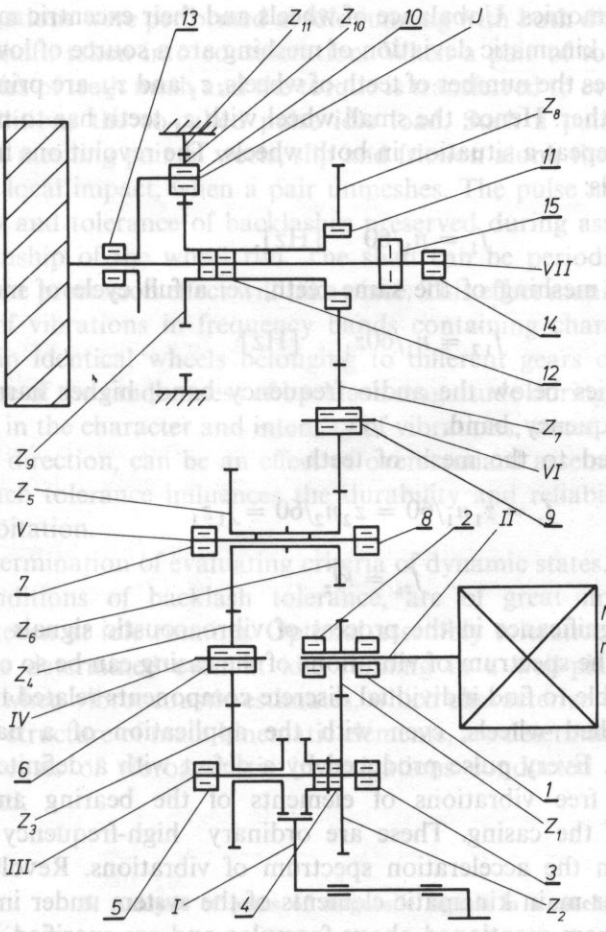

Fig. 3. Kinematic diagram of a head with a specification of shafts (I–VII), toothed wheels ($Z_1 - Z_{11}$) and bearings (1–15)

4. Frequency selection of vibrations of kinematic elements

Toothed gears, ball or barrel bearings are fundamental elements of most machines. In order to compare adequate components of the spectrum of vibrations, frequencies of forced vibrations of definite kinematic elements of the head, such as main shafts, layshafts and toothed wheels, have to be determined.

Every element of a toothed gear is an elastic body and can be excited to vibrate and generates a signal, which has a spectrum of a rather wide frequency range. The level of vibrations is especially high in certain frequency bands of the spectrum, especially for frequencies which are an integral multiple of the excitation frequency [11]. This means that the highest power in toothed wheels is emitted at mesh

frequencies and its harmonics. Unbalance of wheels and their excentric mounting on the shaft as well as the kinematic deviation of meshing are a source of low frequency vibrations. In most cases the number of teeth of wheels, z_1 and z_2, are prime numbers with respect to each other. Hence, the small wheel with z_1 teeth has to make z_2 full rotations in order to repeat a situation in both wheels. The revolutions frequency of the small wheel equals:

$$f_1 = n_1/60 \quad [\text{Hz}]. \tag{1}$$

The frequency of meshing of the same teeth, i.e. a full cycle of mesh, equals

$$f_{12} = n_1/60z_1 \quad [\text{Hz}] \tag{2}$$

and most frequently lies below the audio frequency band; higher harmonics can overlap the audio frequency band.

Frequencies related to the mesh of teeth

$$f_z = z_1 n_1/60 = z_2 n_2/60 = f_1 z_1 \tag{3}$$

and their harmonics

$$f_{zk} = kf_z \tag{3a}$$

are of fundamental significance in the process of vibroacoustic signals generation.

Due to bearings, the spectrum of vibrations of the casing can be so complicated that it may be impossible to find individual discrete components related to rotations and meshing of toothed wheels, even with the application of a narrow-band spectrum analyser [2]. Every pulse produced by a defect with a definite excitation frequency will cause free vibrations of elements of the bearing and then of neighbouring parts of the casing. These are ordinary high-frequency vibrations observed sometimes in the acceleration spectrum of vibrations. Revolutions and meshing frequencies for main kinematic elements of the system under investigation have been calculated from mentioned above formulae and are specified in Table 2.

Table 2. Measuring points assigned to specified kinematic elements

Rotation frequency $[s^{-1}]$ [Hz]	Meshing frequency $[s^{-1}]$ [Hz]
$f_{II} = 24.3$	$F_{Z1} = 464.1$
$f_{III} = 9.06$	$F_{Z2} = 464.1$
$f_{IV} = 6.5$	$F_{Z2'} = 309.4$
$f_V = 4.64$	$F_{Z3} = 182$
$f_{VI} = 2.82$	$F_{Z4} = 182$
$f_{VII} = 0.64$	$F_{Z5} = 182$
	$F_{Z6} = 78.9$
	$F_{Z7} = 78.9$
	$F_{Z8} = 78.9$
	$F_{Z9} = 62.1$
	$F_{Z10} = 30.9$

Investigations were performed at idle running with both directions of rotation of the output shaft, taken into consideration. When a pair of toothed wheels rotates, following pairs of teeth mesh and the torque is transferred to every pair of teeth. This process conditions the so-called pulse idle load. Such a pulse consists of a local collision of a meshing pair of weels, slip and friction along the side contact parts of teeth, and a local impact, when a pair unmeshes. The pulse magnitude depends on the accuracy and tolerance of backlashes preserved during assembly, as well as on the workmanship of the wheel rim. The shaft can be periodically forces by these factors and the precession effect will take place. This effect manifests in the amplitude magnitude of vibrations in frequency bands containing characteristic frequencies. Backlashes in identical wheels belonging to different gears of the same type will differ, because of the randomness of backlash magnitude during assembly. Significant divergencies in the character and intensity of vibrations, stated also after a change of the rotation direction, can be an effect of overstandard assembly tolerance of head elements. Such tolerance influences the durability and reliability of such a system during exploitation.

The determination of evaluating criteria of dynamic states, which correspond to optimal conditions of backlash tolerance, are of great importance in control diagnostics, even at idle running. Optimal assembly tolerance, of some elements at least, can be determined even at idle running in a well-planned and performed experiment, when vibroacoustic estimates, which characterize definite parameters of the dynamic structure of main kinematic elements, are determined. This will facilitate and reduce costs of vibroacoustic investigations conducted presently at variable dynamic load.

5. Analysis of paths of diagnostic signals in a machine

A signal undergoes distorsions and disturbances due to other sources of vibrations on its path from the source to the transducer, in the dynamic system of a machine. The received signal often is a superposition of all generated signals, because of complex paths and size of signals which reach the receiving point on the machine body. It depends on the transmittance structure of the system under investigation. Therefore, the separation of characteristic frequencies in the spectrum of vibrations is a very complex problem. In order to present the complexity of this problem the influence of transmittance on power spectral density functions are analysed in a simple line system during the change of the rotation direction of the output shaft.

Many papers on machine diagnostics neglect a very important problem of the path of a signal $x(t)$ from the source of vibrations to the point of signal reception by a transducer mounted most frequently on the machine body. Instead of the real signal $x(t)$ we obtain signal $y(t)$ on the machine body. If we assume a line dynamic system (shown in Fig. 4), then the relationship between the power spectral density function of input $x(t)$ and output $y(t)$ signals is as follows

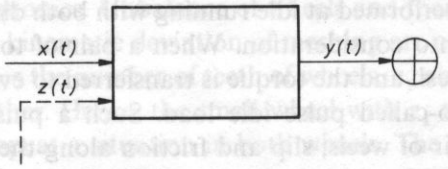

Fig. 4. Simplified diagram of a single input line system

$$G_y(f) = |H(f)|^2 G_x(f), \tag{4}$$

where: $G_x(f)$, $G_y(f)$ – one-sided power spectral density functions of signals $x(t)$ and $y(t)$, $H(f)$ – transmittance of the system, corresponding to the amplitude-phase characteristic of the path of the signal.

Having the power spectral density $G_x(f)$ of the input signal and the gain coefficient $H(f)$ of the system, we can determine the power spectral density $G_y(f)$ of the output signal.

Let us consider now a superposition of n line systems (Fig. 5) with constant parameters, with q strictly determined output signals $x_i(t)$, $i = 1, 2, 3, \ldots, q$, measu-

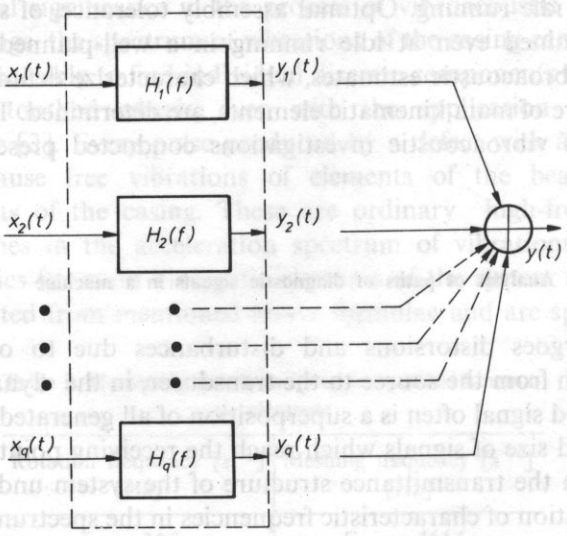

Fig. 5. Diagram of a multi input line system

red at the output through the global output signal $y(t)$. This signal will be a sum of n components of output signals

$$y(t) = \sum_{i=1} y_i(t). \tag{5}$$

Several typical transformations based on the Fourier transform lead to the following form of the expression for the power spectral density of the output signal:

$$G_y(f) = \sum_{i=1}^{q} \sum_{j=1}^{q} H_i^*(f) H_j(f) G_{ij}(f), \tag{6}$$

where: $G_{ij}(f)$ – mutual power spectral density of signals $x_i(t)$ and $x_j(t)$, $H^*(f)$ – complex function conjugated with function $H(f)$.

For uncorrelated processes we have:

$$G_y(f) = \sum_{i=1}^{q} |H_i(f)|^2 G_i(f). \tag{6a}$$

A change of the rotation direction of the output shaft should not lead to transmittance changes of the system. Hence, we can accept that the transmittance of point n on the head casing is constant for a right (P) and left (L) rotation

$$\{|H_i(f)|2\}_n^{P,L} = \text{const}. \tag{7}$$

In such a case power spectral densities of signals registered in a given point can be expressed as

$$G_y^P(f) = \sum_{i=1}^{q} |H_i(f)|^2 G_i^P(f), \qquad G_y^L(f) = \sum_{i=1}^{q} |H_i(f)|^2 G_i^L(f). \tag{8}$$

This means that the power spectral density in a given measuring point will not have the error of transmittance estimation when the direction of rotation is changed. Differences in the power spectral density structure occuring in various points after a change of the rotation direction should be conditioned mainly by the assymetry of precession, which takes place in motion dynamics of definite kinematic pairs.

6. Results and discussion

Such fundamental parameters of vibration as displacement, velocity and acceleration, have been measured and analysed. Their comparison in certain frequency intervals has lead to a classification of heads under investigation with respect to intensity of emitted vibration signals. The spectral analysis of vibration parameters, presented in the form of amplitude-frequency characteristics, enabled us to determine dominating frequencies and to assign them adequate revolutions frequencies of certain kinematic elements of the investigated system.

6.1. Line spectrum of vibrations displacement

A narrow-band analysis in the frequency range 0–50 Hz has been performed at both rotation directions of the output shaft, in order to determine amplitude-frequency distribution of vibrations displacement in individual measuring points on heads under investigation. Displacement spectra of vibrations for right rotations,

recorded in point $n = 7$ of casings of heads numbered $N = 27$ and $N = 28$, respectively, are shown in Fig. 6. These heads have significantly diversified displacement amplitudes in certain frequency bands, especially in the sub-audio range. Rms values of amplitudes were determined from obtained spectrograms of displacement of vibrations. Considerations were limited to a frequency range 0–30 Hz due to a lack of sufficient amplitude resolution for frequencies exceeding 30 Hz. Figs. 7 and 8 present graphically the displacement spectra of

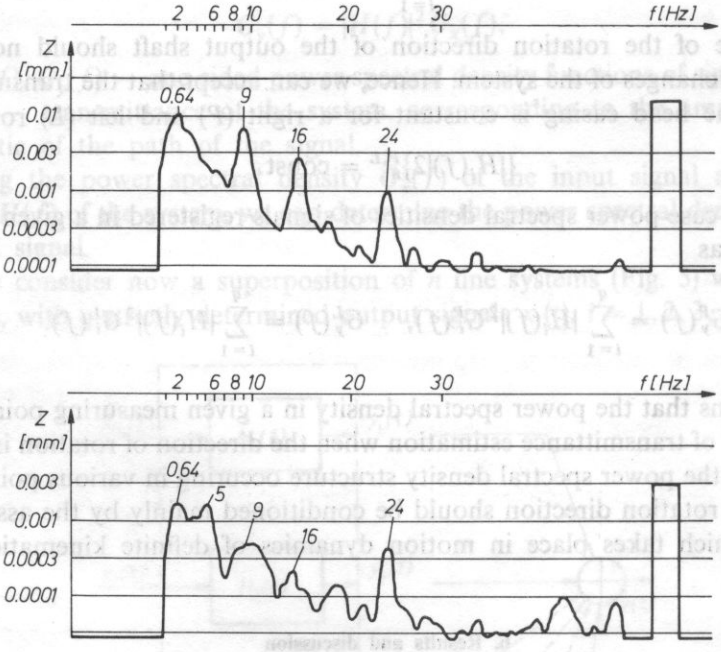

Fig. 6. Line spectra of vibrations displacement: a) Head no 27, point 7, right rotation of the output shaft, b) Head no 28, point 7, right rotation of the output shaft

vibrations for heads $N = 27$, 28, determined respectively for points $n = 2$ and $n = 12$, for a right (P) and left (L) rotation of the system. A considerable amplitude-frequency variability has been observed in registered spectra of displacements in most measuring points of the casing. It results from the spectral analysis, presented in the form of a frequency distribution of amplitudes for all measuring points, that displacement amplitude maxima of vibrations occur mainly in bands with mid-band frequencies: $f = 1$, 2, 4, 6, 9, 16 and 25 Hz.

A comparison of calculated characteristic frequencies corresponding to rotational speeds of shafts and certain toothed wheels (Table 1), with the graphic frequency distribution of displacement of vibrations proves that frequencies dominating in the frequency spectrum determine bands which contain calculated characteristic frequencies. Global changes of displacement of vibrations averaged with respect to all

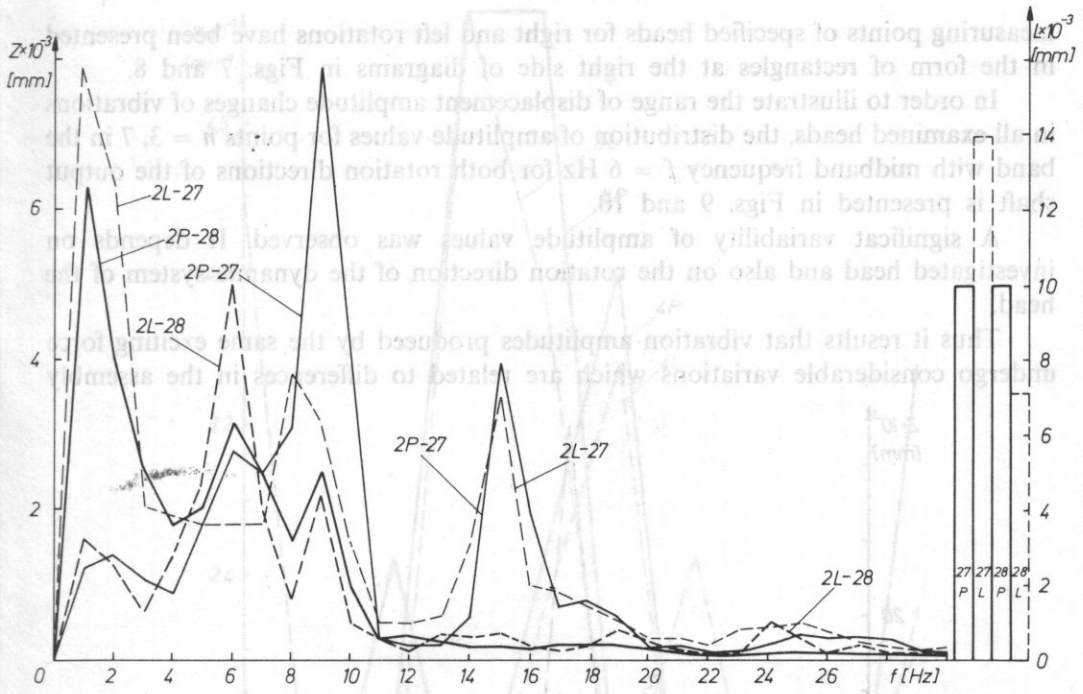

Fig. 7. Frequency analysis of vibration displacement for heads $N = 27$ and 28 in measuring point 2; ——— — right rotation; — — — — left rotation

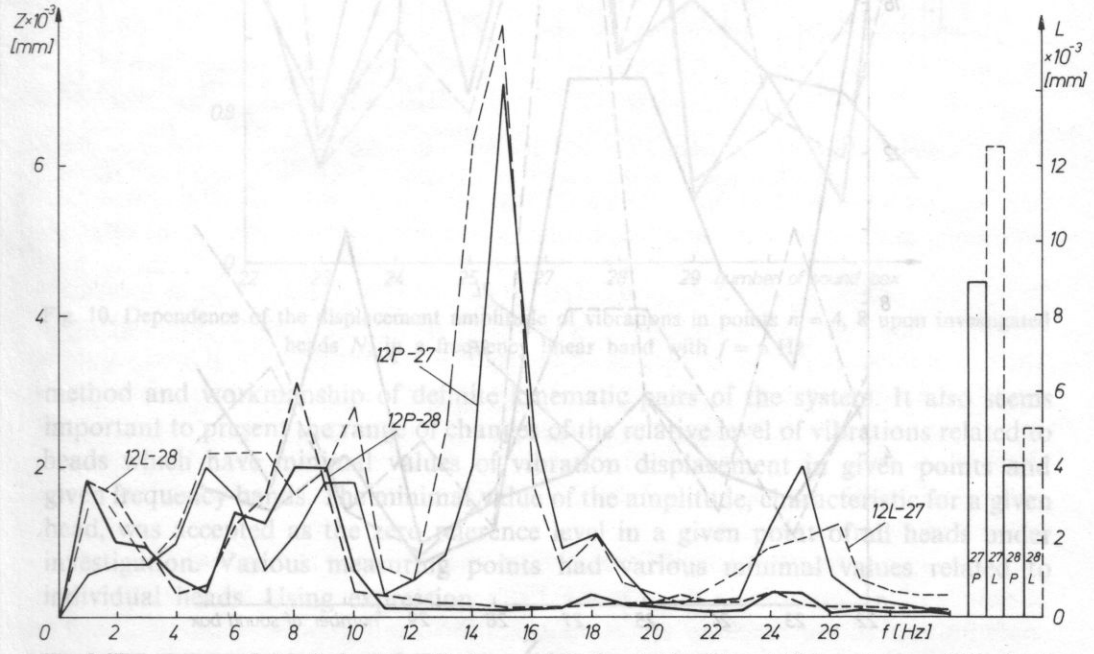

Fig. 8. Frequency analysis of vibrations displacement for heads $N = 27$ and 28 in point $n = 12$ for both directions of rotation (P — right rotations, L — left rotations)

measuring points of specified heads for right and left rotations have been presented in the form of rectangles at the right side of diagrams in Figs. 7 and 8.

In order to illustrate the range of displacement amplitude changes of vibrations in all examined heads, the distribution of amplitude values for points $n = 3, 7$ in the band with midband frequency $f = 6$ Hz for both rotation directions of the output shaft is presented in Figs. 9 and 10.

A significat variability of amplitude values was observed. It depends on investigated head and also on the rotation direction of the dynamic system of the head.

Thus it results that vibration amplitudes produced by the same exciting force undergo considerable variations which are related to differences in the assembly

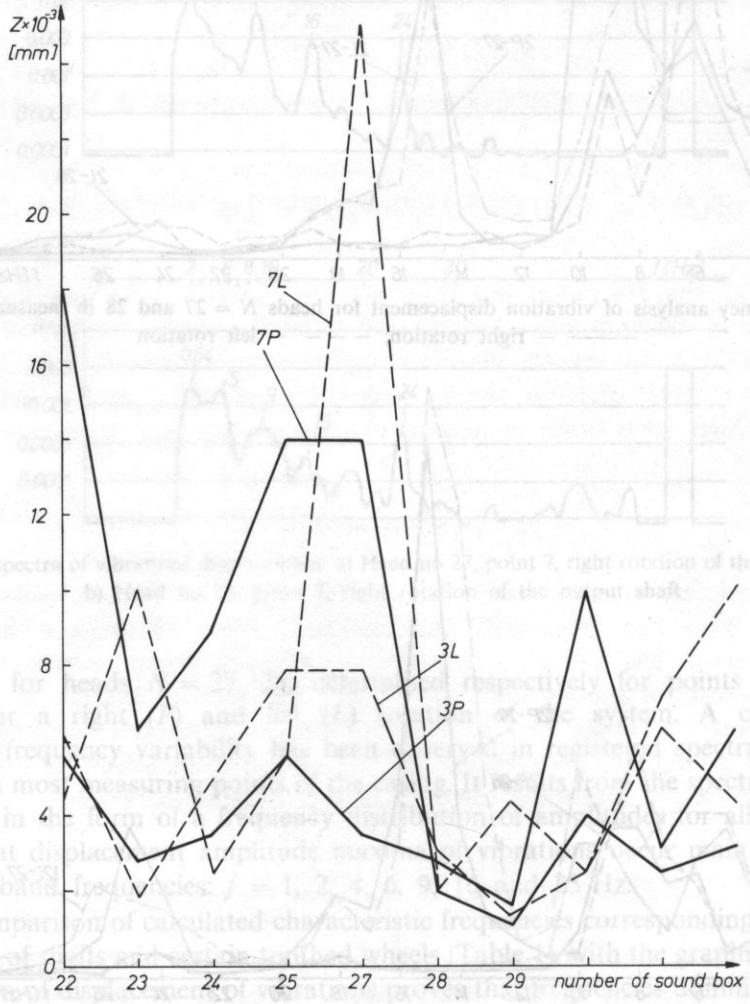

Fig. 9. Dependence of the displacement amplitude of vibrations in points $n = 3, 7$ upon investigated heads N, in a frequency linear band with $f = 2$ Hz

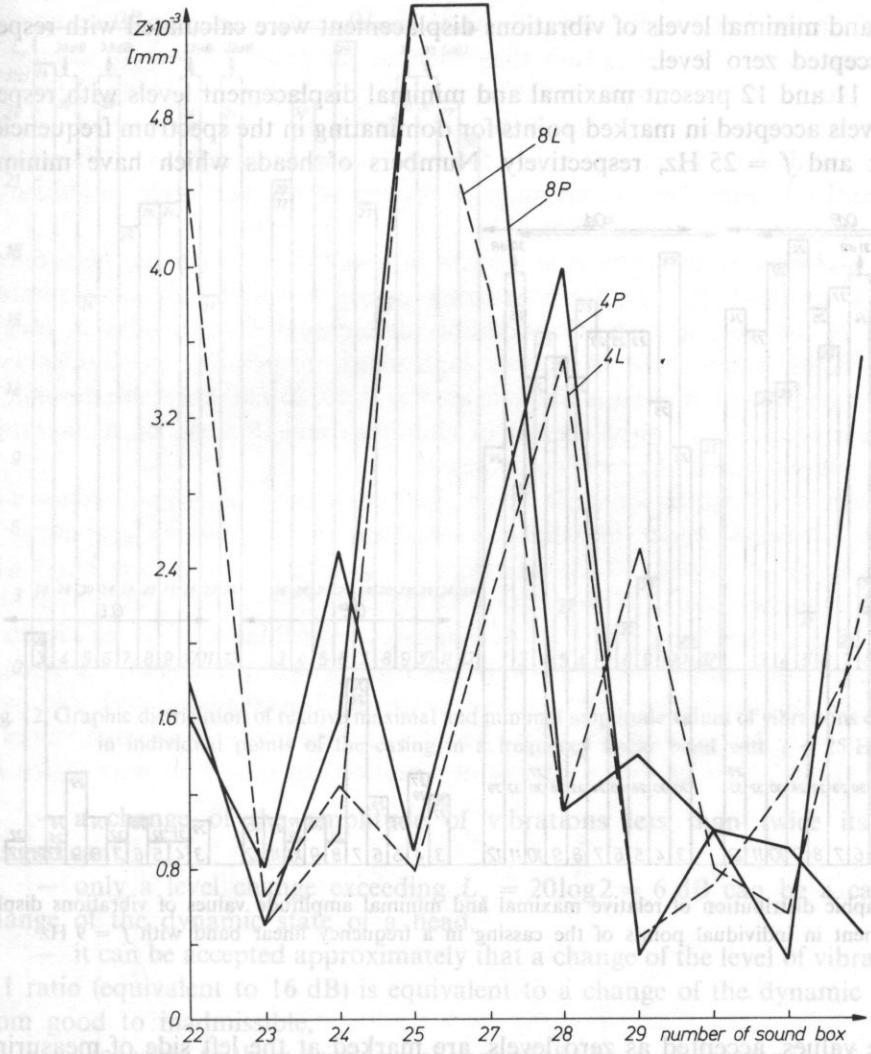

Fig. 10. Dependence of the displacement amplitude of vibrations in points $n = 4$, 8 upon investigated heads N, in a frequency linear band with $f = 6$ Hz

method and workmanship of definite kinematic pairs of the system. It also seems important to present the range of changes of the relative level of vibrations related to heads which have minimal values of vibration displacement in given points and given frequency bands. The minimal value of the amplitude, characteristic for a given head, was accepted as the zero reference level in a given point of all heads under investigation. Various measuring points had various minimal values related to individual heads. Using expression

$$L_z = 20\log\frac{Z_{sk(\max)}}{Z_{sk(\min)}} \quad [\text{dB}],$$

maximal and minimal levels of vibrations displacement were calculated with respect to the accepted zero level.

Figs. 11 and 12 present maximal and minimal displacement levels with respect to zero levels accepted in marked points for dominating in the spectrum frequencies: $f = 9$ Hz and $f = 25$ Hz, respectively. Numbers of heads which have minimal

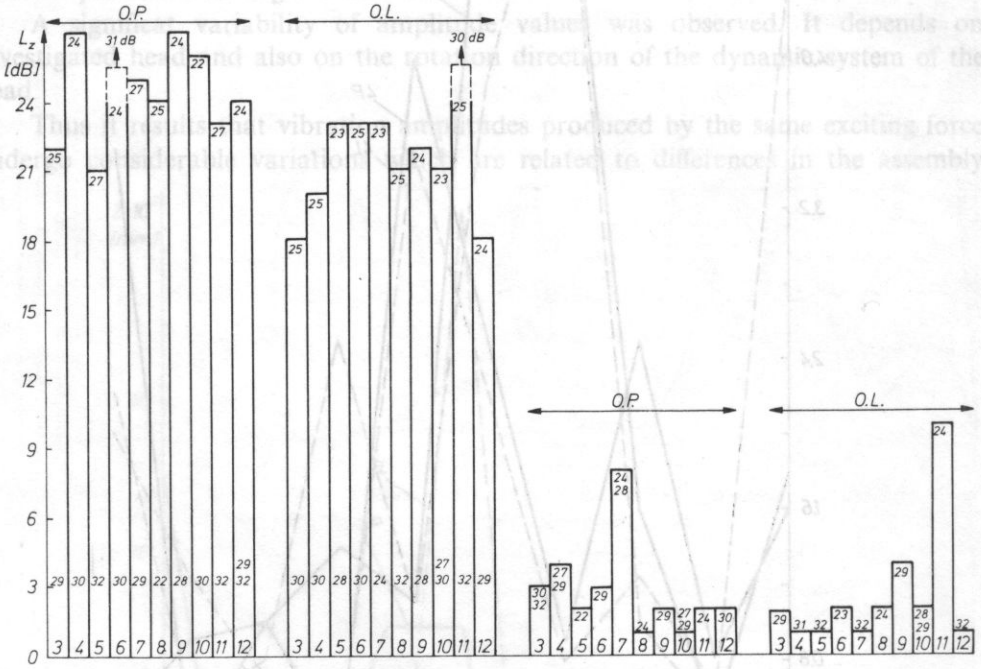

Fig. 11. Graphic distribution of relative maximal and minimal amplitude values of vibrations displacement in individual points of the cassing in a frequency linear band with $f = 9$ Hz

amplitude values, accepted as zero levels, are marked at the left side of measuring points. While heads with maximal displacement levels of vibrations are marked at the top of these diagrams. Diagrams on the right side express minimal level values of specified heads (numbers in the top part) with respect to the same reference levels as in the previous case. It is worth mentioning that level changes range from 0 to 33 dB. This is an effect of a great diversification of dynamic processes taking place in individual heads. Also a change of the direction of rotation significantly influences generated dynamic processes.

A very important conclusion results from criteria stated in standard *ISO* 3945 – a change of the level of vibrations in a 6:1 ratio is always a cause for a change of the classification of the machine vibration condition from good to inadmissible. The following classification of the dynamic state can be accepted on the basis of this standard:

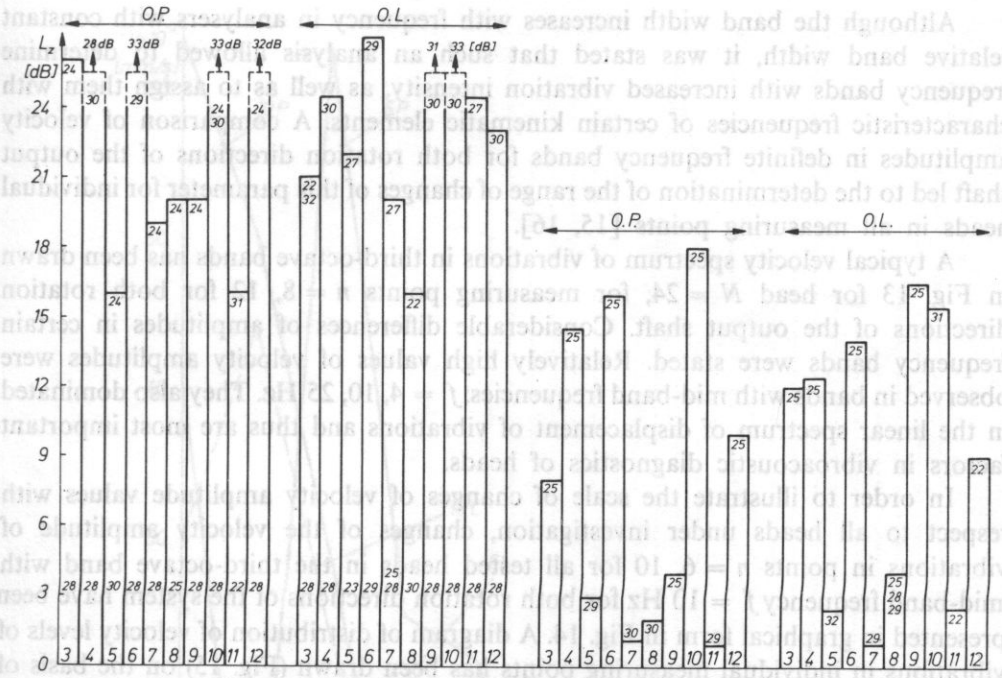

Fig. 12. Graphic districution of relative maximal and minimal amplitude values of vibrations displacement in individual points of the casing in a frequency linear band with $f = 25$ Hz

– a change of the amplitude of vibrations less than twice its value is insignificant,

– only a level change exceeding $L_x = 20\log 2 = 6$ dB can be a cause for a change of the dynamic state of a head,

– it can be accepted approximately that a change of the level of vibrations in a 6:1 ratio (equivalent to 16 dB) is equivalent to a change of the dynamic condition from good to inadmissible,

– according to these criteria a change of the level of vibrations which exceeds 16 dB should be equivalent to a transition to a supralimiting state, in which the head is unfit for exploitation.

If the presented above classification is taken into account, heads in the supralimiting state can be separated on the basis of diagrams of distributions of limiting levels of vibrations.

6.2. Third-octave spectrum of velocity of vibrations

On the basis of a third-octave spectrum analysis of the vibration velocity in a frequency range 1–200 Hz and in measuring points of the same heads, frequency bands with maximal velocity amplitude values of vibrations were determined.

Although the band width increases with frequency in analysers with constant relative band width, it was stated that such an analysis allowed to determine frequency bands with increased vibration intensity, as well as to assign them with characteristic frequencies of certain kinematic elements. A comparison of velocity amplitudes in definite frequency bands for both rotation directions of the output shaft led to the determination of the range of changes of this parameter for individual heads in all measuring points [15, 16].

A typical velocity spectrum of vibrations in third-octave bands has been drawn in Fig. 13 for head $N = 24$, for measuring points $n = 8$, 12 for both rotation directions of the output shaft. Considerable differences of amplitudes in certain frequency bands were stated. Relatively high values of velocity amplitudes were observed in bands with mid-band frequencies: $f = 4$, 10, 25 Hz. They also dominated in the linear spectrum of displacement of vibrations and thus are most important factors in vibroacoustic diagnostics of heads.

In order to illustrate the scale of changes of velocity amplitude values with respect to all heads under investigation, changes of the velocity amplitude of vibrations in points $n = 6$, 10 for all tested heads in the third-octave band with mid-band frequency $f = 10$ Hz for both rotation directions of the system have been presented in graphical form in Fig. 14. A diagram of distribution of velocity levels of vibrations in individual measuring points has been drawn (Fig. 15) on the basis of results of the amplitude-frequency analysis in the third-octave band with mid-band frequency $f = 16$ Hz in order to isolate heads with maximal and minimal values of levels. Maximal values of velocity levels of vibrations in this band were stated for

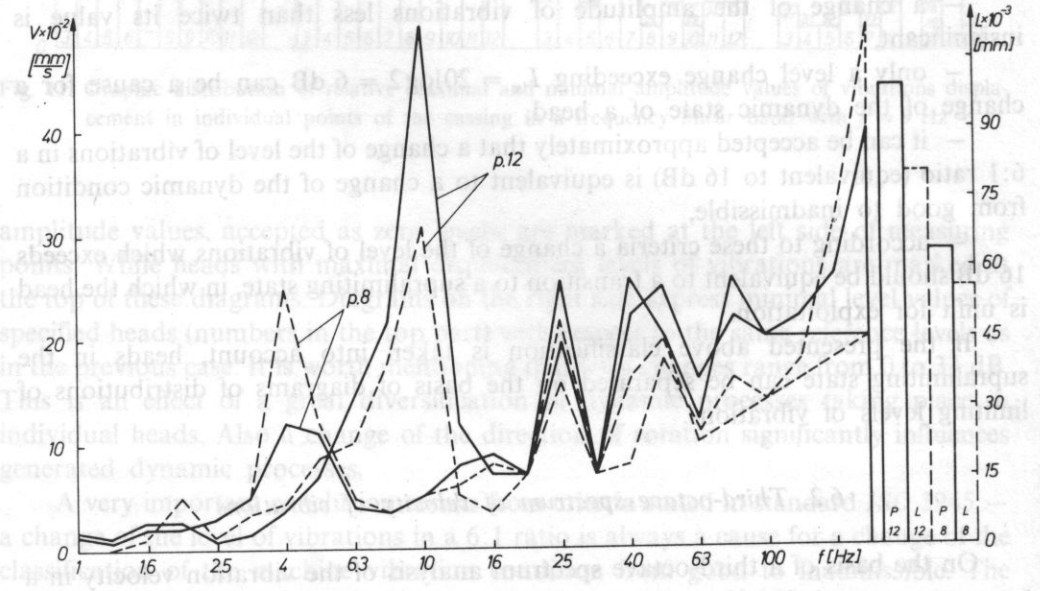

Fig. 13. Frequency analysis of velocity of vibrations in third-octave bands for head $N = 24$ in points $n = 8$, 12; ——— — right rotations, — — — — left rotations

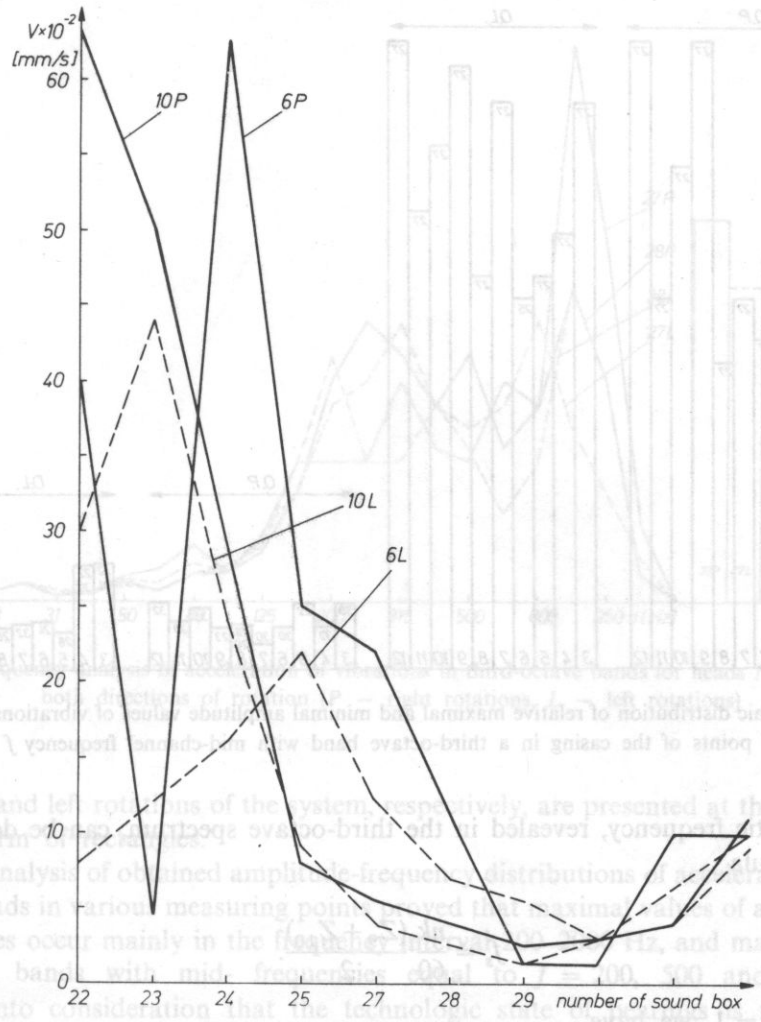

Fig. 14. Dependence of the velocity amplitude of vibrations in points $n = 6, 10$ upon investigated heads N in a third-octave band with mid-channel frequency $f = 10$ Hz

head $N = 27$ in nearly all measuring points for right and left rotations of the system. Hence, this frequency band dominates for this head. Highest values of the maximal velocity level for this band occured in points $n = 9, 12$, situated radially with respect to the main shaft of the planetary gear. Mid-band frequency $f = 16$ Hz, which dominates in the third-octave spectrum, corresponds to the characteristic frequency dependent on the superposition of vibrations generated by a series connection of a system consisting of a toothed planet wheel $Z_{10} = 19$, $m = 10$ and a toothed sleeve $Z_9 = 29$, $m = 10$ (Table 1). Taking mentioned above data into consideration, the

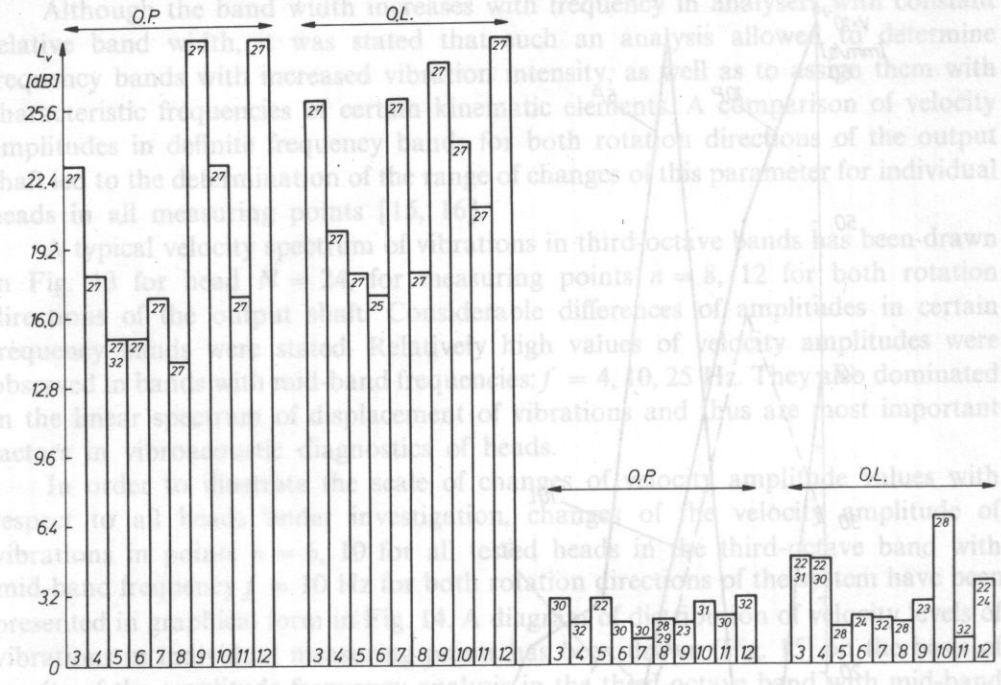

Fig. 15. Graphic distribution of relative maximal and minimal amplitude values of vibrations velocity in individual points of the casing in a third-octave band with mid-channel frequency $f = 16$ Hz

characteristic frequency, revealed in the third-octave spectrum, can be determined from formula

$$f_s = \frac{nk}{60} \cdot \frac{(Z_9 + Z_{10})}{2}.$$

For $k = 1$, we have

$$f_s = 16 \text{ Hz}.$$

This characteristic frequency was also found in the line displacement spectrum of vibrations (Fig. 7) in points $n = 9$, 12 of some of the investigated heads.

6.3. *Third-octave spectrum of acceleration of vibrations*

Also a spectral analysis of vibrations acceleration in third-octave bands was performed in frequency range 20–2000 Hz for all measuring points on bodies of investigated heads. A typical spectrum is shown in Fig. 16. It is a spectrum registered in measuring point $n = 12$ for heads $N = 27$, 28 in bands with marked mid-band frequencies. Rms acceleration values averaged with respect to all measuring points

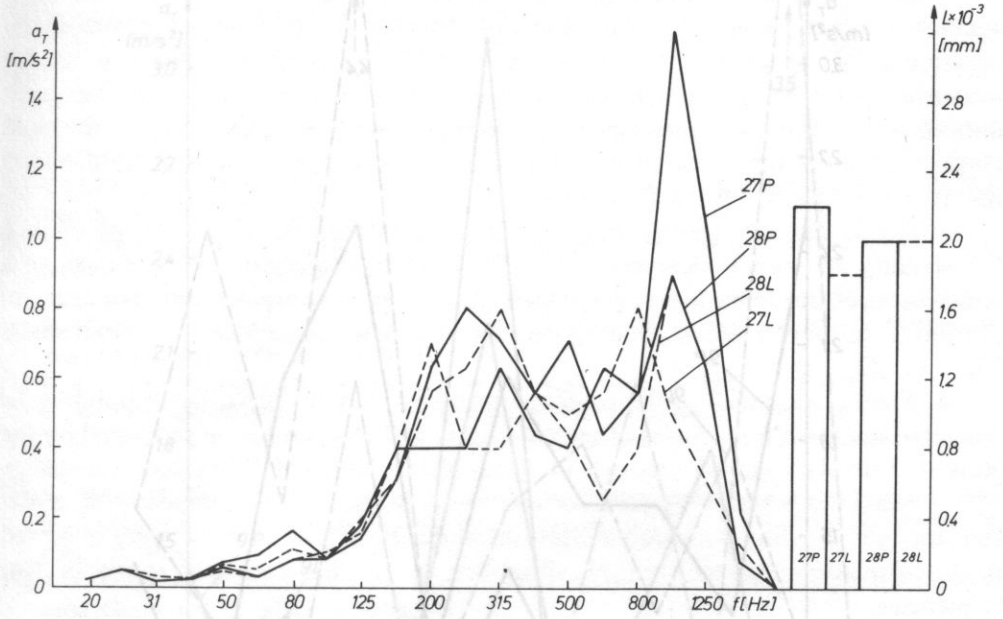

Fig. 16. Frequency analysis of acceleration of vibrations in third-octave bands for heads $N = 27, 28$ for both directions of rotation (P – right rotations, L – left rotations)

for right and left rotations of the system, respectively, are presented at the right side in the form of rectangles.

An analysis of obtained amplitude-frequency distributions of acceleration for all tested heads in various measuring points proved that maximal values of acceleration amplitudes occur mainly in the frequency interval 200–2000 Hz, and main maxima occur in bands with mid- frequencies equal to $f = 200$, 500 and 1000 Hz. Taking into consideration that the technologic state of bearings is represented relatively best by acceleration [2], it can be accepted that these maxima can reflected principally by peripheral wavines or bearing cage backlash and run-out, which occur in some rolling bearings. It results from calculations of characteristic frequencies of vibrations related to mentioned above defects, that acceleration spectra of vibrations in bands with specified above midband frequencies contain the following characteristic frequencies: $f_w = 194$ Hz (bearing 4), $f_w = 173$ Hz (bearing 1) and $f_w = 501$ Hz (bearing 2) (Fig. 3). Various values of acceleration amplitudes of vibrations in these frequency bands can reflect the dynamic state of specified bearings.

Figs. 17 and 18 present changes of acceleration amplitudes of vibrations in points $n = 9$, 10 of investigated heads in bands with mid- frequencies equal to $f = 800$ Hz and 1000 Hz. In these bands these amplitudes dominate in mentioned measuring points. Various values of acceleration amplitudes, which occur here, depend mainly on the investigated head (its dynamic state) and also on the rotation

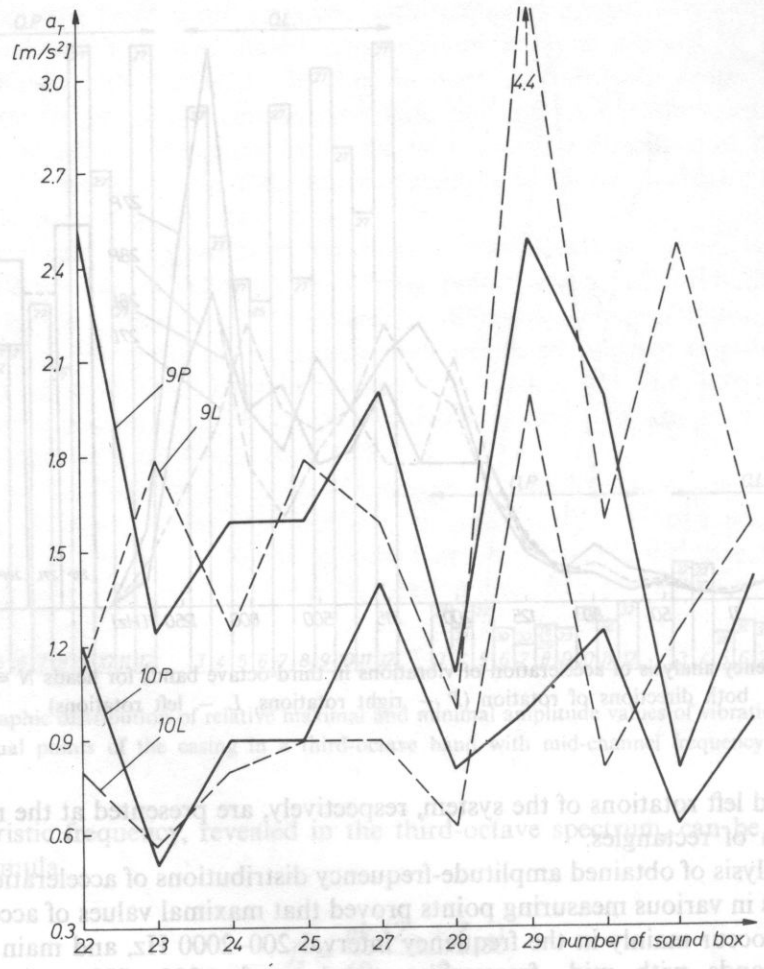

Fig. 17. Dependence of the acceleration amplitude of vibrations in points $n = 9$, 10 upon investigated heads N in a third-octave band with mid- frequency $f = 800$ Hz

direction of the output shaft. It is impossible to evaluate the importance of accelerations of dominating frequencies revealed in the third-octave spectrum at this stage of research. However, they may be of great importance in the process of vibraacoustic diagnostics.

7. Conclusions

Results of the amplitude-frequency analysis have indicated that the structure of vibrations received in individual points on the body of investigated heads is distinctly diversified. Frequency intervals with characteristic frequencies of certain kinematic

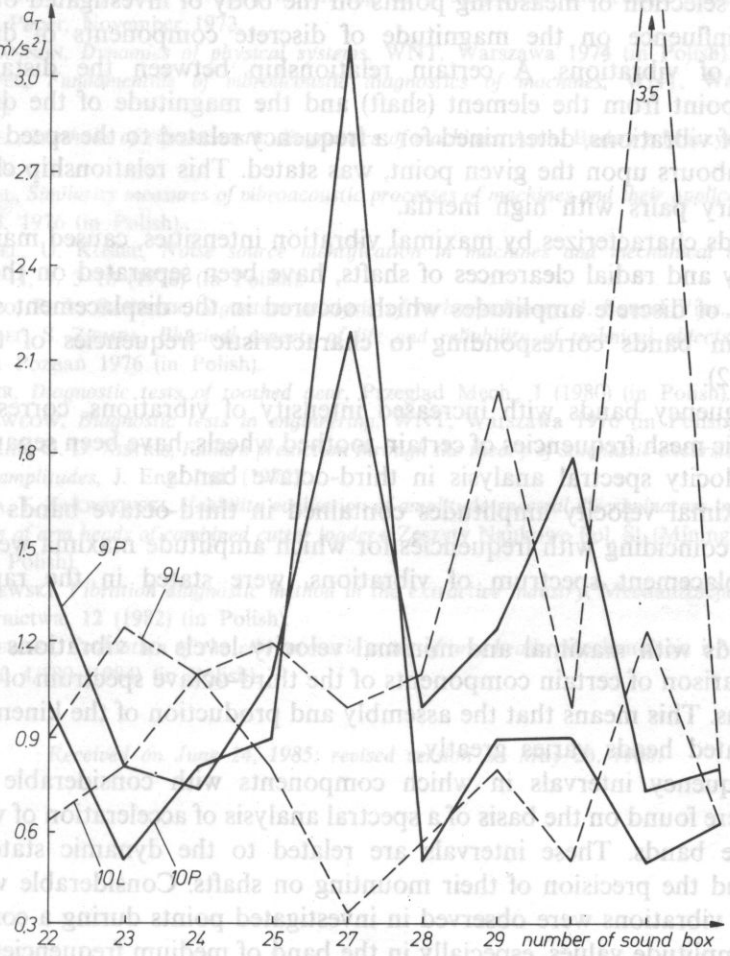

Fig. 18. Dependence of the acceleration amplitude of vibrations in points $n = 9$, 10 upon investigated heads N in a third-octave band with mid-channel frequency $f = 1$ kHz

elements of the system have been determined on their basis. A comparison of amplitudes in adequate frequency bands led to the determination of the range of maximal variations of measured parameters. A significant influence of the rotation direction on the structure of generated vibroacoustic signals was indicated. An analysis of measurement results has led to the following conclusions:

1. A spectral analysis of vibration displacements has disclosed discrete components related to revolutions frequencies of all main shafts and layshafts (Table 2), which testifies to their good frequency correlation. Considerable relative displacement amplitude level changes of vibrations, which were determined for revealed discrete components in definite points on the body of investigated heads, are due to unbalance or backlash in adequate rotary pairs or lack of their coaxiality.

2. The selection of measuring points on the body of investigated objects has a significant influence on the magnitude of discrete components of displacement amplitudes of vibrations. A certain relationship between the distance of the measuring point from the element (shaft) and the magnitude of the displacement amplitude of vibrations, determined for a frequency related to the speed of the shaft which neighbours upon the given point, was stated. This relationship characterizes mainly rotary pairs with high inertia.

3. Heads characterizes by maximal vibration intensities, caused mainly by lack of coaxiality and radial clearences of shafts, have been separated on the basis of a comparison of discrete amplitudes which occured in the displacement spectrum of vibrations in bands corresponding to characteristic frequencies of these shafts (Figs. 11, 12).

4. Frequency bands with increased intensity of vibrations, corresponding to characteristic mesh frequencies of certain toothed wheels, have been separated on the basis of velocity spectral analysis in third-octave bands.

5. Maximal velocity amplitudes contained in third-octave bands with center frequencies coinciding with frequencies for which amplitude maxima were observed in the displacement spectrum of vibrations, were stated in the range of low frequencies.

6. Heads with maximal and minimal velocity levels of vibrations were found from comparison of certain components of the third-octave spectrum of the velocity of vibrations. This means that the assembly and production of the kinematic system of investigated heads varies greatly.

7. Frequency intervals in which components with considerable amplitudes occured, were found on the basis of a spectral analysis of acceleration of vibrations in third-octave bands. These intervals are related to the dynamic state of rolling bearings and the precision of their mounting on shafts. Considerable variations of the level of vibrations were observed in investigated points during a comparison of maximal amplitude values, especially in the band of medium frequencies. This gives evidence of dynamic cooperation non-homogeneities of definite elements of tested heads.

8. The rotation direction of the output shaft influences significantly the value of discrete components in described spectra of vibrations. It is not unlikely that differences of values of definite spectral estimates, conditioned by the rotation direction of the output shaft, can carry important information about the assembly correctness and cooperation of certain elements of the system.

If detailed classification criteria would be worked out on the basis of many investigated objects of the same type, then the described method could become one of more effective quality inspection methods of produced heads.

References

[1] J. S. BENDAT, A. G. PIERSOL, *Methods of analysis and measurement of random signals*, PWN, Warszawa 1976 (in Polish).

[2] M. P. BLAKE, W. S. MITCHELL, *Vibration and acoustic measurement handbook*, New York–Washington, Spartan Books 1972.

[3] Ch. R. BOWES, *Shipboard vibration monitoring as a diagnostic maintenance tool*, ENDEVCO Technical Paper, November 1973.
[4] R. H. CANNON, *Dynamics of physical systems*, WNT, Warszawa 1974 (in Polish).
[5] Cz. CEMPEL, *Fundamentals of vibroacoustic diagnostics of machines*, WNT, Warszawa 1982 (in Polish).
[6] Cz. CEMPEL, *Methods of vibroacoustic diagnostics of machines*, Arch. Budowy Maszyn, **2**, 391 1978 (in Polish).
[7] Cz. CEMPEL, *Similarity measures of vibroacoustic processes of machines and their application*, IMTPP Report 23, 1976 (in Polish).
[8] Cz. CEMPEL, U. KOSIEL, *Noise source identification in machines and mechanical devices*, Arch. Akustyki, **11**, 1, 3–18 (1976) (in Polish).
[9] V. DONATO, R. L. BANISTER, *Signature analysis of turbomachinery*, J. Sound Vibr., **9** (1971).
[10] Z. HANDZEL, S. ZIEMBA, *Physical aspects of life and reliability of technical objects*, IPPT-PAN, Warszawa–Poznań 1976 (in Polish).
[11] L. MÜLLER, *Diagnostic tests of toothed gear*, Przegląd Mech., **1** (1980) (in Polish).
[12] B. W. PAWŁOW, *Diagnostic tests in engineering*, WNT, Warszawa 1976 (in Polish).
[13] T. S. SANKAR, G. D. XISTRIS, *Failure prediction through the theory of stochastic excursions of extreme vibration amplitudes*, J. Eng. Ind. (1972).
[14] W. SIKORA, T. ZAKRZEWSKI, *Usability evaluation of amplitude-spectral discriminators in vibroacoustic diagnostics of arm heads of combined cutter loaders*, Zeszyty Naukowe Pol. Śl. (Mining), **137**, 99–139 (1985) (in Polish).
[15] T. ZAKRZEWSKI, *Vibration diagnostic method in the extractive industry*, Mechanizacja i Automatyzacja Górnictwa, **12** (1982) (in Polish).
[16] T. ZAKRZEWSKI, *Evaluation of the vibroacoustic state of arm heads*, Mechanizacja i Automatyzacja Górnictwa, 4/180 (1984) (in Polish).

Received on June 24, 1985; revised version on May 26, 1986.

ARCHIVES OF ACOUSTICS
12, 2, 113–128 (1987)

THE REFLECTION OF A GAUSSIAN PULSE OF A PLANE ULTRASONIC WAVE FROM RIGID AND ELASTIC SPHERES IN WATER

LESZEK FILIPCZYŃSKI, TAMARA KUJAWSKA

Department of Ultrasonics, IFTR, Polish Academy of Sciences
(00-049 Warszawa, ul. Świętokrzyska 21)

The authors have determined shapes and amplitudes of Gaussian pulses with limit frequencies equal to 2, 3, 10 and 20 kHz, which were reflected backwards from rigid and steel spheres with a 0.5 m radius, immersed in water. For this purpose spectral analysis, transmittance theorem and inverse Fourier transform were used. Reflected pulses exhibited two maxima corresponding to a specular reflection from the face surface of the sphere and to a creeping travelling wave around the sphere. These maxima were masked by many resonances inside of the elastic sphere. The masking effect decreases with the decrease of the limit frequency of the Gaussian pulse incident upon the sphere. In such a case the shape of the reflected pulse tends to a time derivative of the incident pulse. The peak to peak pressure of the reflected pulse remains unchanged in the range of limit frequencies under investigation. The measurement of the time interval between the first and second maximum of the reflected pulse makes it possible to determine the radius of the elastic sphere, if the limit frequency is sufficiently low.

Notation

A_m – auxiliary function
a – sphere radius
B_m – auxiliary function
c – wave velocity in water
c' – velocity of creeping wave
c_1 – velocity of longitudinal wave in the sphere
c_2 – velocity of transverse wave in the sphere
c_m – expansion coefficient
D_m – auxiliary function
E_m – auxiliary function
F_m – auxiliary function
f_g – limit frequency
f_∞ – shape function of the sphere
$h^{(2)} = j_m - jn_m$ – spherical Hankel function of the second type
$h_m^{(2)'}$ – derivation of function $h_m^{(2)}$ with respect to the argument
$j = \sqrt{-1}$

j_m – spherical Bessel function
j'_m – derivative of function j_m with respect to the argument
G_i – spectrum of the incident wave pulse
$k = \omega/c$ – wave number
m – natural number
n_m – spherical Neumann function
n'_m – derivative of function n_m with respect to the argument
P_m – Legendre polynomial
p_i – acoustic pressure of the incident wave
p_0 – acoustic pressure amplitude of the incident wave
p_s – acoustic pressure of scattered wave
q – constant
r – radial coordinate
s – constant
t – time
$x = \omega a/c$
$x_1 = \omega a/c_1$
$x_2 = \omega a/c_2$
β – constant
η_m – auxiliary quantity
θ – azimuth
$\lambda_g = c/f_g$ – limit wave length
ξ – auxiliary variable
ϱ – water density
ϱ_s – density of the sphere
τ – normalized time
ω – angular frequency
ω_g – limit angular frequency

1. Introduction

The reflection of ultrasonic waves from spherical objects immersed in water is of fundamental significance to many problems of ultrasound technology, such as hydroacoustic surveying. This problem has been undertaken in many papers. The first one to solve this problem theoretically for elastic spheres and a continuous wave was FARAN [4]. Later, other authors have pointed out a small mistake in FARAN'S very complex formulae [3, 12, 16]. Experimental research in the domain of the reflection effect, performed with the application of aluminium and brass spheres immersed in water in the range of $ka = 4.1 \div 57$, has confirmed the theory [8].

This paper deals with the effect of backward reflection of a Gaussian pulse of an ultrasonic wave incident upon rigid and elastic spheres immersed in water. It was accepted that a plane wave pulse, which is a time function near to a Dirac pulse, assumes a shape close to a Gauss pulse, due to imperfect generation and propagation conditions in water. Such a pulse incident upon a fixed sphere, is reflected from it and returns in the direction from which it was emited.

This paper is aimed at the determination of the shape and amplitude of the reflected pulse. It also tries to answer the question: Can any information concerning

the reflecting sphere be obtained on this basis? HASEGAWA'S formulae [9, 10, 11] describing the reflection of a continuous plane wave from an elastic sphere, with the correction made by ANSON and others [1], have been applied in this paper.

The procedure introduced by RUDGERS [18] and HICKLING [12] will be applied in order to analyse the reflection of pulses.

2. Gaussian pulse of an ultrasonic wave

A system of polar coordinates is being accepted (Fig. 1A). Considering axial symmetry we have two coordinates: r and θ. A Gaussian pulse of a plane wave moving along the z-axis ($z = r\cos\theta$) is the following time function (at a fixed value of z)

$$p_i = p_0 \exp(-\beta^2 t^2). \tag{1}$$

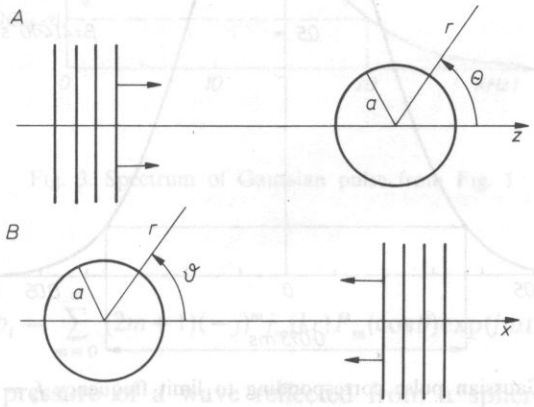

Fig. 1. A – Applied coordinate system – a plane progressive wave is incident upon sphere with radius a along the z-axis. This system was applied by authors of papers [4, 5, 11, 18]. B – Coordinate system applied by RSHEVKIN ([17], p. 258)

Assuming $p_0 = 1$ and applying a Fourier transform [13], we achieve the pulse spectrum in the following form

$$G_i(\omega) = \int_{-\infty}^{+\infty} p_i(t)\exp(-j\omega t)dt = \frac{\sqrt{\pi}}{\beta}\exp(-\omega^2/4\beta^2), \tag{2}$$

where the identity [6]

$$\int_{-\infty}^{+\infty} \exp(-u^2 s^2 \pm qs)ds = \frac{\sqrt{\pi}}{u}\exp(q^2/4u^2) \quad \text{for } u > 0, \tag{3}$$

was applied.

If we define the limit frequency f_g (as well as the limit angular frequency ω_g), as a frequency at which the spectrum amplitude is equal to 1/10 of the maximum value, then we have

$$\beta = \pi f_g / \sqrt{|\ln 0.1|} = 2.07 f_g = 0.329 \omega_g. \tag{4}$$

The shape of the Gaussian pulse which corresponds to the limit frequency $f_g = 20$ kHz is presented in Fig. 2, while its spectrum is shown in Fig. 3.

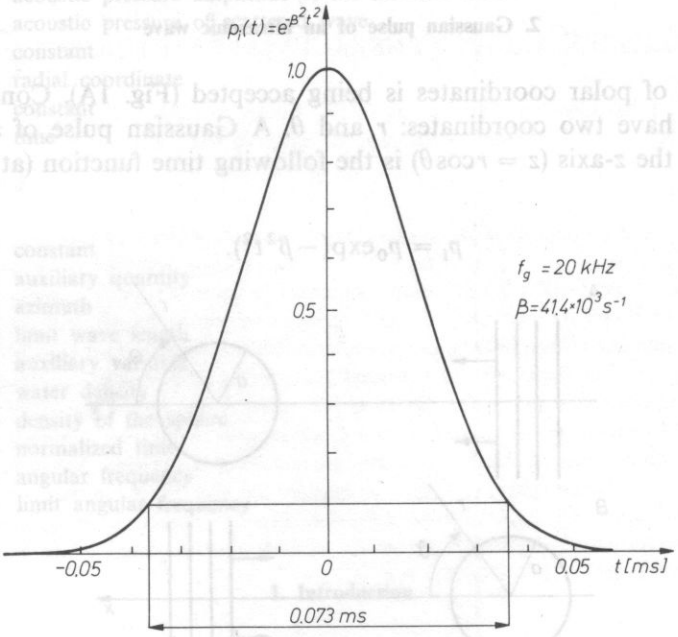

Fig. 2. Gaussian pulse corresponding to limit frequency $f_g = 20$ kHz

In further analysis we will introduce a dimensionless quantity $ka = \omega a/c$ in place of the angular frequency ω. Hence, we achieve the following expression, if we include factor a/c in the exponent in expression (2) and also include (4)

$$G_i(ka) = \frac{\sqrt{\pi}}{0.329\,\omega_g} \exp\left[-(ka)^2 / 0.433 \left(\frac{\omega_g a}{c} \right)^2 \right]. \tag{5}$$

3. Reflection of a continuous wave and a Gaussian pulse from rigid spheres

First of all we will determine the value of a continuous wave reflected from a rigid sphere. The acoustic pressure of a harmonic plane wave propagating in the direction $z = r\cos\theta$ (Fig. 1) has the following form [11, 9, 10]

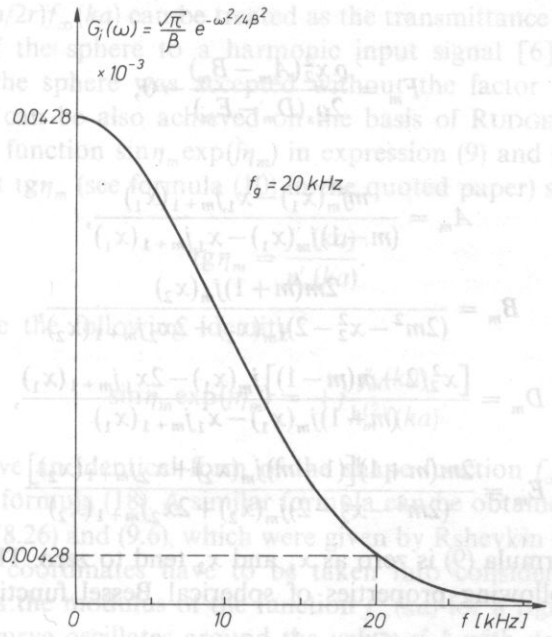

Fig. 3. Spectrum of Gaussian pulse from Fig. 1

$$p_i = \sum_{m=0}^{\infty} (2m+1)(-j)^m j_m(kr) P_m(\cos\theta)\exp(j\omega t) \tag{6}$$

while the acoustic pressure of a wave reflected from a sphere is expressed as

$$p_s = \sum_{m=0}^{\infty} (2m+1)(-j)^m c_m h_m^{(2)}(kr) P_m(\cos\theta)\exp(j\omega t). \tag{7}$$

Coefficient c_m is determined from boundary conditions on the surface of the sphere. In the case of an elastic sphere this coefficient is a function of: velocity of a longitudinal and transverse waves in the sphere, sphere density, wave velocity in the fluid surrounding the sphere, fluid density, frequency and radius of the sphere. This relationship becomes simpler in the case of a rigid sphere, because the velocity of longitudinal and transverse waves tends to infinity. Hence,

$$(c_1 \to \infty,\ c_2 \to \infty) \Rightarrow x_1 \to 0 \quad \text{and} \quad x_2 \to 0, \tag{7a, b}$$

and HASEGAWA'S formulae [8, 11, 1] for an elastic sphere can be simplified to the form for a rigid sphere, because then

$$c_m = \left[x j_m(x) - F_m j_m(x)\right] / \left[F_m h_m^{(2)}(x) - x h_m^{(2)\prime}(x)\right] \to -j_m'(x)/h_m^{(2)\prime}(x) \tag{8}$$

as

$$F_m = \frac{\varrho x_2^2 (A_m - B_m)}{2\varrho_s (D_m - E_m)} \to 0, \tag{9}$$

where

$$A_m = \frac{m j_m(x_1) - x_1 j_{m+1}(x_1)}{(m-1) j_m(x_1) - x_1 j_{m+1}(x_1)}, \tag{10}$$

$$B_m = \frac{2m(m+1) j_m(x_2)}{(2m^2 - x_2^2 - 2) j_m(x_2) + 2x_2 j_{m+1}(x_2)}, \tag{11}$$

$$D_m = \frac{[x_2^2/2 - m(m-1)] j_m(x_1) - 2x_1 j_{m+1}(x_1)}{(m-1) j_m(x_1) - x_1 j_{m+1}(x_1)}, \tag{12}$$

$$E_m = \frac{2m(m+1)[(1-m) j_m(x_2) + x_2 j_{m+1}(x_2)]}{(2m^2 - x_2^2 - 2) j_m(x_2) + 2x_2 j_{m+1}(x_2)}. \tag{13}$$

The limit of formula (9) is zero as x_1 and x_2 tend to zero. This could be shown by applying the following properties of spherical Bessel functions [15]

$$\frac{j_{m+1}(\xi)}{j_m(\xi)} \to \frac{\xi}{2m+3} \quad \text{for } \xi \to 0 \tag{14}$$

and the de l'Hospitals principle twice with respect to (9). Approximating the Hankel function by an asymptotic expression ([17], p. 211) for a distance much greater than the radius of the sphere, $r \gg a$

$$h_m^2(kr) = \frac{1}{kr} \exp\left[-j\left(kr - \frac{m+1}{2}\pi\right)\right] \tag{15}$$

including identity

$$(-j)^m \exp[j(m+1)\pi/2] = +j, \tag{16}$$

and assuming backward reflection ($\theta = 180°$)

$$P_m(\cos\theta) = (-1)^m \tag{17}$$

we achieve from formulae (7) and (8) the final form of the formula for the acoustic pressure of a continuous wave reflected from a rigid sphere [5]

$$p_s = \frac{a}{2r}\left[\frac{-2}{ka} \sum_{m=0}^{\infty} j(2m+1)(-1)^m \frac{j_m'(ka)}{h_m^{(2)'}(ka)}\right] \exp[-j(kr - \omega t)]$$

$$= \frac{a}{2r} f_\infty(ka) \exp[-j(kr - \omega t)]. \tag{18}$$

The expression in first square brackets in formula (18) is called the shape function of the backward reflection from a sphere in the far field. It is denoted by

$f_\infty(ka)$. Function $(a/2r)f_\infty(ka)$ can be treated as the transmittance of the sphere which is the response of the sphere to a harmonic input signal [6]. In paper [6] the transmittance of the sphere was accepted without the factor $a/2r$.

Formula (18) can be also achieved on the basis of RUDGERS paper [18]. The author introduced function $\sin\eta_m \exp(j\eta_m)$ in expression (9) and (11) in his paper. It can be proved that $\operatorname{tg}\eta_m$ (see formula (10) in the quoted paper) satisfies relationship

$$\operatorname{tg}\eta_m = \frac{j'_m(ka)}{n'_m(ka)}. \tag{19}$$

Then we have the following identity

$$\sin\eta_m \exp(j\eta_m) = +j\frac{j'_m(ka)}{h_m^{(2)\prime}(ka)}. \tag{20}$$

Hence, we have an identical form of the shape function $f_\infty(ka)$ as in the first square brackets in formula (18). A similar formula can be obtained also on the basis of formulae (8.24), (8.26) and (9.6), which were given by Rshevkin [17]. In such a case differently defined coordinates have to be taken into consideration (Fig. 1B).

Fig. 4 presents the modulus of the function $f_\infty(ka)$ for a rigid sphere (curve R). For $ka > 10$ this curve oscillates around the value of 1 with decaying oscillations.

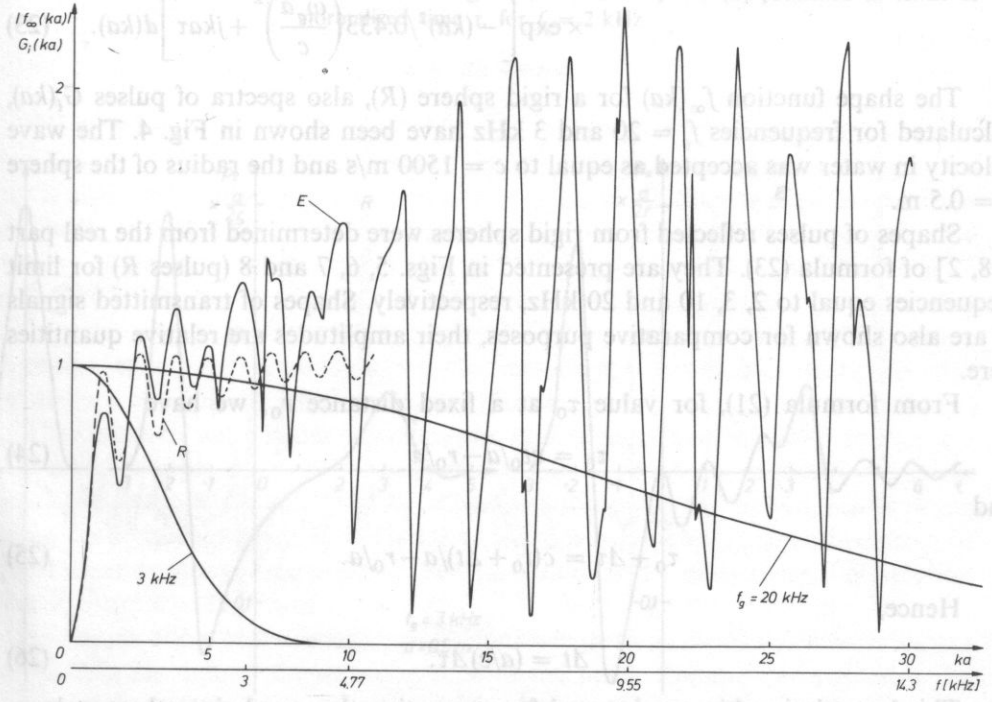

Fig. 4. Shape function $f_\infty(ka)$ for a rigid (R) and steel (E) sphere, and spectra of a Gaussian pulse with limit frequency $f_g = 20$ kHz and 3 kHz (related to the maximal value). Sphere radius $a = 0.5$ m

When the wave incident upon the sphere has the shape of a pulse, then two variables, r and t, are substituted by one dimensionless variable in the following form [18]

$$\tau = (ct - r)/a. \tag{21}$$

This procedure is justifiable, because the same shape of a pulse is obtained at a fixed time t when its shape is observed in terms of distance r, or on the contrary at a fixed distance r when its shape is observed in time t.

The pulse of a reflected wave will be presented in the domain of time normalized by expression (21) with the application of the linear theory of networks [14]. To this end an inverse Fourier transform was determined from the product of the transmittance of the sphere, $a/2rf_\infty(ka)$, and pulse spectrum $G_i(ka)$. Including formulae (18) and (5) we have

$$p_s(\tau) = \frac{1}{2\pi}\int_{-\infty}^{+\infty} \frac{a}{2r} f_\infty(ka) G_i(ka) \exp(jka\tau) d(ka) \tag{22}$$

or in full notation

$$p_s(\tau) = \frac{a}{4\pi r}\int_{-\infty}^{+\infty} \left[\frac{-2}{ka}\sum_{m=0}^{\infty} j(2m+1)(-1)^m \frac{j'_m(ka)}{h_m^{(2)\nu}(ka)}\right] \frac{\sqrt{\pi}}{0.329\omega_g} \times$$

$$\times \exp\left[-(ka)^2/0.433\left(\frac{\omega_g a}{c}\right)^2 + jka\tau\right] d(ka). \tag{23}$$

The shape function $f_\infty(ka)$ for a rigid sphere (R), also spectra of pulses $G_i(ka)$, calculated for frequencies $f_g = 20$ and 3 kHz have been shown in Fig. 4. The wave velocity in water was accepted as equal to $c = 1500$ m/s and the radius of the sphere $a = 0.5$ m.

Shapes of pulses reflected from rigid spheres were determined from the real part [18, 2] of formula (23). They are presented in Figs. 5, 6, 7 and 8 (pulses R) for limit frequencies equal to 2, 3, 10 and 20 kHz, respectively. Shapes of transmitted signals T are also shown for comparative purposes, their amplitudes are relative quantities here.

From formula (21), for value τ_0 at a fixed distance r_0, we have

$$\tau_0 = ct_0/a - r_0/a \tag{24}$$

and

$$\tau_0 + \Delta\tau = c(t_0 + \Delta t)/a - r_0/a. \tag{25}$$

Hence,

$$\Delta t = (a/c)\Delta\tau. \tag{26}$$

This last relationship can be used for converting the τ-scale into the t-scale – different for every radius a of the sphere.

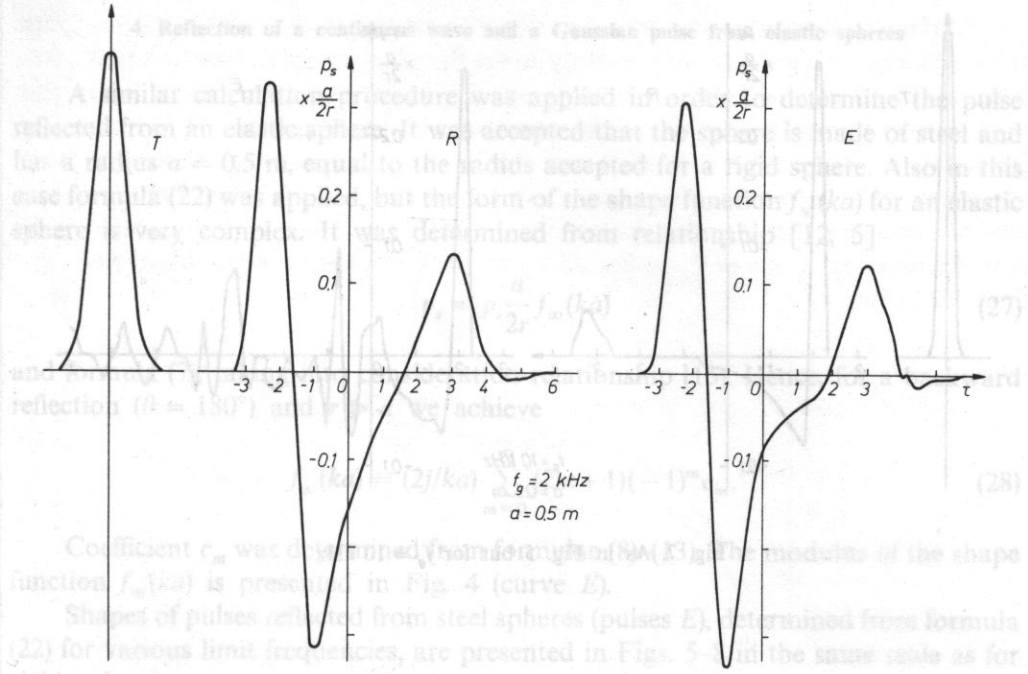

Fig. 5. Transmitted pulse (T), reflected from a rigid (R) and steel sphere (E) presented in terms of normalized time τ, for $f_g = 2$ kHz

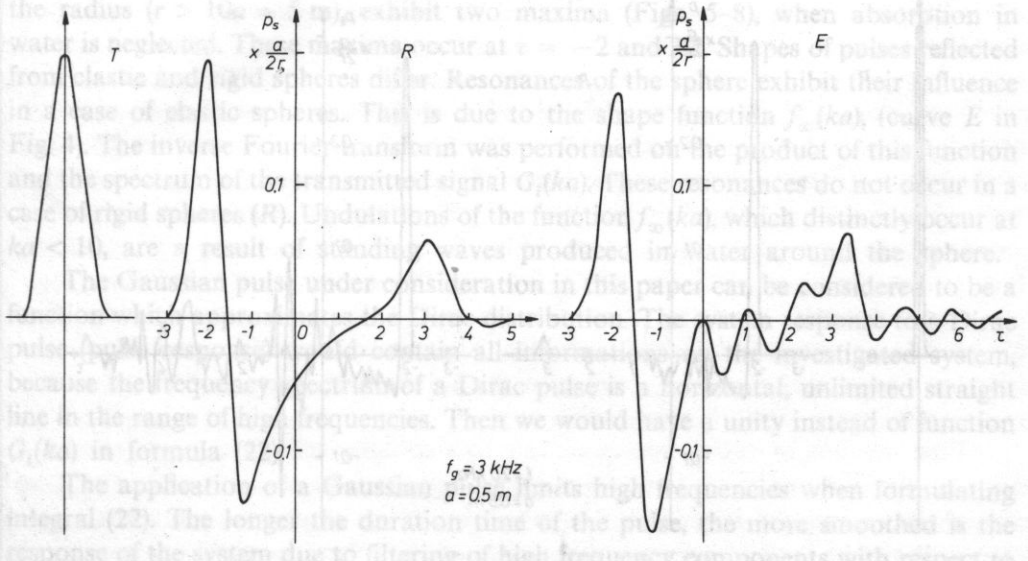

Fig. 6. As in Fig. 5 but for $f_g = 3$ kHz

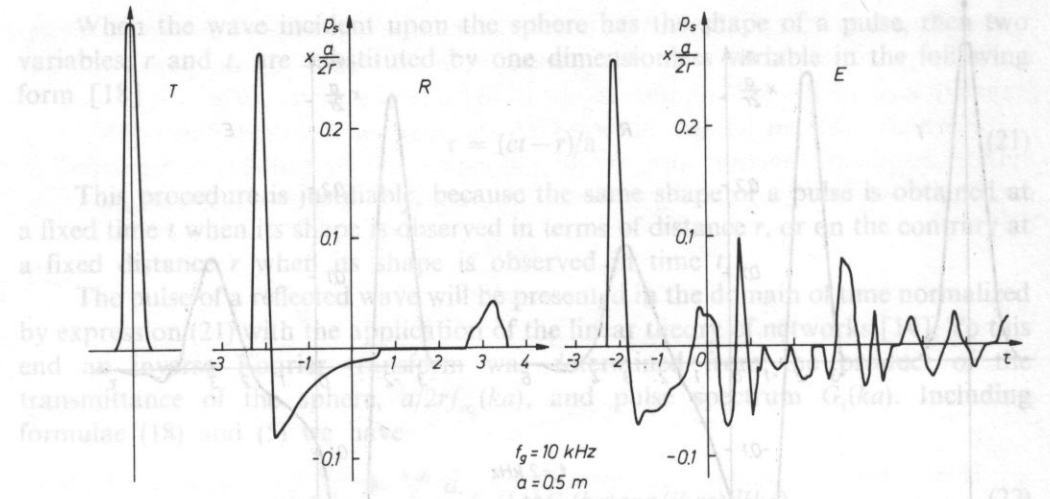

Fig. 7. As in Fig. 5 but for $f_g = 10$ kHz

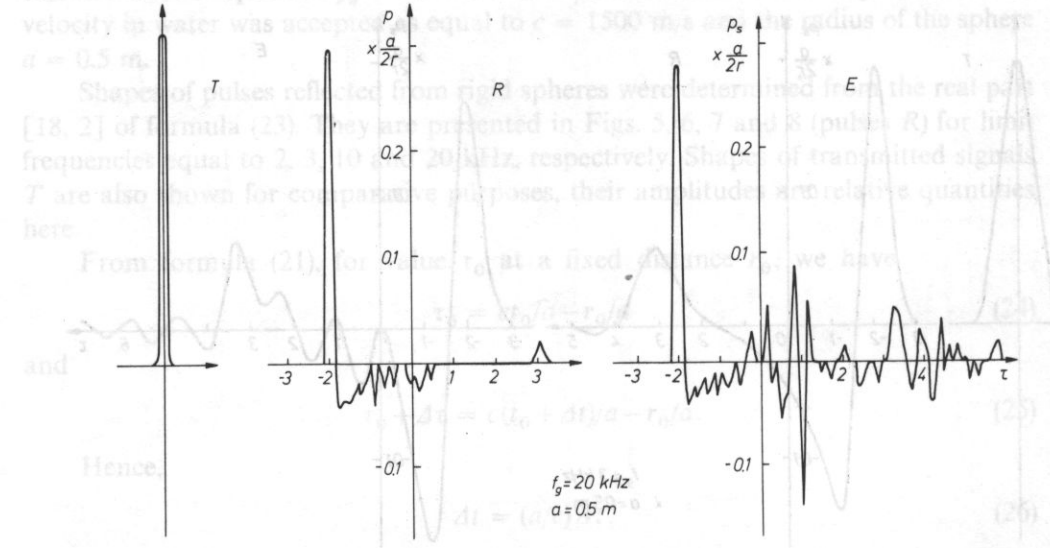

Fig. 8. As in Fig. 5 but for $f_g = 20$ kHz

4. Reflection of a continuous wave and a Gaussian pulse from elastic spheres

A similar calculation procedure was applied in order to determine the pulse reflected from an elastic sphere. It was accepted that the sphere is made of steel and has a radius $a = 0.5$ m, equal to the radius accepted for a rigid sphere. Also in this case formula (22) was applied, but the form of the shape function $f_\infty(ka)$ for an elastic sphere is very complex. It was determined from relationship [12, 5]

$$p_s = p_i \frac{a}{2r} f_\infty(ka) \tag{27}$$

and formula (7), taking into consideration relationship (15). Hence, for a backward reflection ($\theta = 180°$) and $r \gg a$ we achieve

$$f_\infty(ka) = (2j/ka) \sum_{m=0}^{\infty} (2m+1)(-1)^m c_m. \tag{28}$$

Coefficient c_m was determined from formulae (8)–(13). The modulus of the shape function $f_\infty(ka)$ is presented in Fig. 4 (curve E).

Shapes of pulses reflected from steel spheres (pulses E), determined from formula (22) for various limit frequencies, are presented in Figs. 5–8 in the same scale as for rigid spheres.

5. Results and discussion

Pulses reflected backwards from rigid spheres at a great distance with respect to the radius ($r > 10a = 5$ m), exhibit two maxima (Figs. 5–8), when absorption in water is neglected. These maxima occur at $\tau = -2$ and 3.2. Shapes of pulses reflected from elastic and rigid spheres differ. Resonances of the sphere exhibit their influence in a case of elastic spheres. This is due to the shape function $f_\infty(ka)$, (curve E in Fig. 4). The inverse Fourier transform was performed on the product of this function and the spectrum of the transmitted signal $G_i(ka)$. These resonances do not occur in a case of rigid spheres (R). Undulations of the function $f_\infty(ka)$, which distinctly occur at $ka < 10$, are a result of standing waves produced in water around the sphere.

The Gaussian pulse under consideration in this paper can be considered to be a function which approximates the Dirac distribution. The system response to a Dirac pulse (pulse response) would contain all informations on the investigated system, because the frequency spectrum of a Dirac pulse is a horizontal, unlimited straight line in the range of high frequencies. Then we would have a unity instead of function $G_i(ka)$ in formula (22).

The application of a Gaussian pulse limits high frequencies when formulating integral (22). The longer the duration time of the pulse, the more smoothed is the response of the system due to filtering of high frequency components with respect to the transmittance function of the sphere.

Maximal amplitudes of reflected pulses with respect to the limit frequency f_g are shown in Fig. 9. They are only slightly lower for steel spheres than for rigid ones. This is due to great differences between specific acoustic impedances of water and steel, so only a small part of the energy penetrates into steel spheres, while it does not penetrate into rigid spheres at all. These amplitudes decrease rapidly when the limit frequency f_g is decreased. However, if we take into consideration the overshoot, which is observed directly after the first maximum (for $-2 < \tau < 0$), then we observe that the maximal value of the reflected signal peak to peak is independent from the limit frequency.

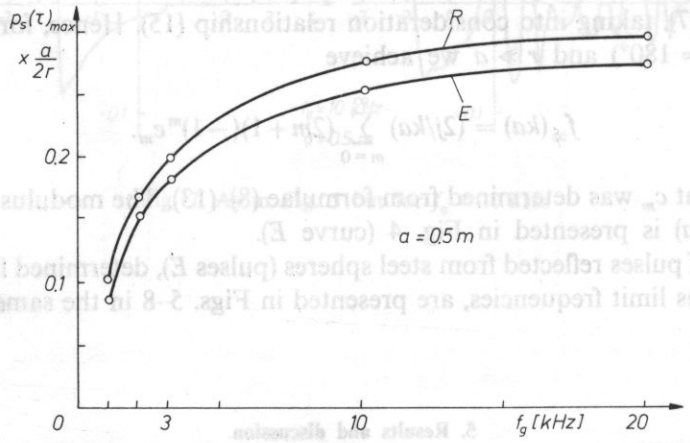

Fig. 9. Maximal amplitudes (positive) of a pulse reflected from rigid (R) and elastic (E) spheres in terms of limit frequency f_g (at $\tau = -2$)

Figs. 10 and 11 present transmitted pulses and first maxima of received pulses placed over them for $f_g = 20$ and 3 kHz. In the second case it is visible that the shape of the reflected pulse approaches the shape of the time derivative of the transmitted pulse. This can be explained by the shape of the transmittance curve $(a/2rf_\infty(ka)$ for small values of ka (at $a/2r = \text{const}$) (Fig. 4) similarly as for a differentiating four-terminal network RC, for which it would be a straight inclined line.

The differentiation of the reflected pulse can be also explained by the fact that for $ka < 1$ components of the waves incident upon the sphere with higher frequencies (shorter wave lengths) are reflected from the sphere with greater amplitudes than components with lower frequencies.

First maxima of pulses, corresponding to a specular reflection, occur always at $\tau = -2$, because the initial time $t = 0$ was accepted in the moment when the wave propagating along the z-axis (Fig. 1A) would reach the origin of coordinates, $r = 0$. Hence, the wave is incident upon the surface of the sphere in point $r = -a$ in the time $t = -a/c$. Substituting these in formula (21) we achieve $\tau = -2$.

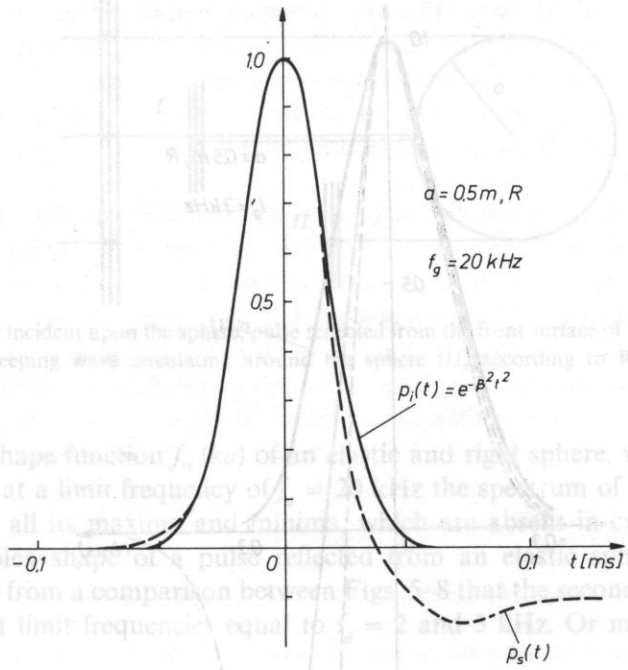

Fig. 10. Shape of transmitted pulse p_i with the first maximum of the pulse p_s reflected from a rigid sphere drawn over it, for f_g = 20 kHz

The second maximum of a reflected pulse was observed in all cases at $\tau = 3.2$. Its value is much lower than that of the first maximum. Because this effect also occurs with rigid spheres, it must be related to phenomena occuring outside the sphere. Such an effect had been observed by RUDGERS [18] in his theoretical paper. He related it to a creeping wave, which propagates around the sphere with a velocity only slightly lower than that in water. The path of a creeping wave, according to this author, is shown in Fig. 12. The first maximum is produced by a direct reflection of a pulse from the front surface of the sphere; the second one occurs much later, when the wave has propagated around the sphere. The difference of propagation time was equal to $\Delta\tau = 5.2$ in all cases. This corresponds to velocity

$$c' = \pi a/(\Delta\tau a/c - 2a/c) = 0.98c, \tag{29}$$

where the numerator denotes the path around the hemisphere travelled by the pulse of a creeping wave, and the denominator denotes the time of this process, calculated from relationship (26).

The idea of a wave travelling around the sphere seems justfiable by the fact that the curve $f_\infty(ka)$ exhibits an oscillatory behaviour for a rigid sphere. For, this testifies to the existence of waves around the sphere, which cause inteferences in the steady state (see curve R in Fig. 4).

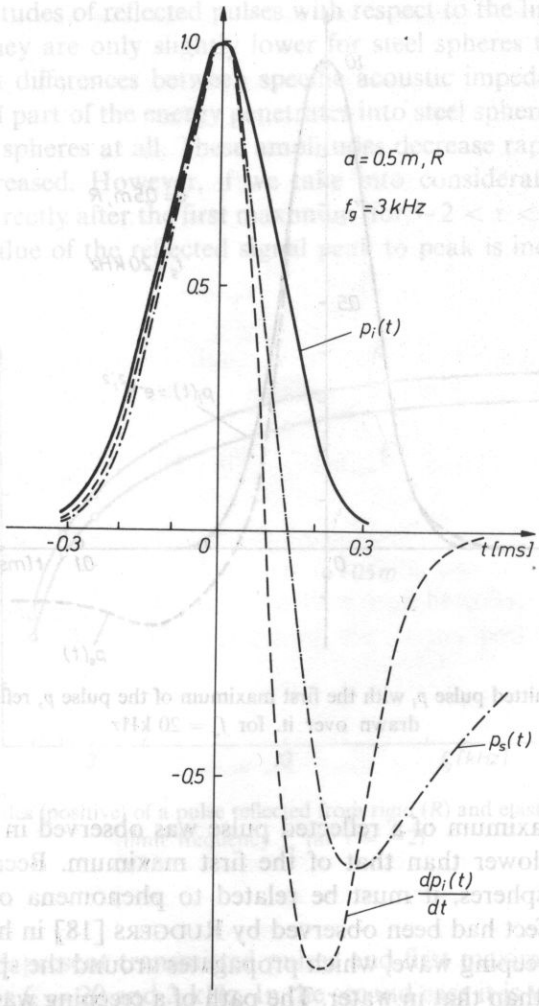

Fig. 11. Shape of transmitted pulse p_i with the derivative dp_i/dt and first maximum of the pulse p_s reflected from a rigid sphere drawn over it, for f_g = 3 kHz; in order to compare more easily these functions, they have been shifted in time and their maximal positive values have been equalized

Therefore, it is possible to determine the unknown radius of the sphere on the basis of the time interval $\Delta t_{\mathrm{I-II}}$ measurement, from formula

$$a = c' \Delta t_{\mathrm{I-II}} (\pi + 2c'/c)^{-1} \approx c \Delta t_{\mathrm{I-II}} (\pi + 2)^{-1}. \tag{30}$$

However, it may be difficult to determine the second maximum for a case of real (elastic) spheres. It can be seen from comparison between Figs. 5–8 that the shape of a pulse reflected from an elastic sphere becomes similar to a pulse reflected from a rigid sphere at lower limit frequencies. This effect can be explained on the basis of Fig. 4. The spectrum of a Gaussian pulse at a limit frequency of 3 kHz includes such

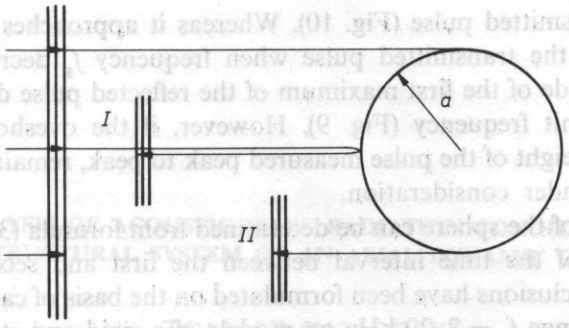

Fig. 12. Pulse (T) incident upon the sphere, pulse reflected from the front surface of the sphere (I) and pulse of a creeping wave circulating around the sphere (II) according to RUDGERS [18]

parts of the shape function $f_\infty(ka)$ of an elastic and rigid sphere, which have similar shape. While at a limit frequency of $f_g = 20$ kHz the spectrum of this pulse includes curve E with all its maxima and minima, which are absent in curve R. Hence, we have a complex shape of a pulse reflected from an elastic sphere (Fig. 8E).

It results from a comparison between Figs. 5–8 that the second maximum can be determined at limit frequencies equal to $f_g = 2$ and 3 kHz. Or more general in the case when

$$\lambda_g/a = 1\text{–}1.5. \tag{31}$$

Besides a creeping wave which circulates the sphere once, also cases of repeated circulation can take place, but amplitudes of these waves are two orders of magnitude smaller [18]. Therefore, they can be neglected.

6. Conclusions

a) A Gaussian pulse of a plane ultrasonic wave incident upon a sphere produces a reflected pulse, which exhibits two maxima for a rigid sphere model. The first maximum is formed due to a direct specular reflection of a wave from the front surface of a sphere (at $\tau = -2$, see curves R in Figs. 5–8), while the second one (at $\tau = 3.2$) is formed due to a creeping wave which circulates the sphere.

b) The second maximum in the case of an elastic sphere (steel) is masked by many maxima and minima, produced by internal resonances of the sphere (see curve E in Figs. 5–8).

c) The second maximum can be determined when relationship (31) is satisfied. The masking effect decays then.

d) The lower the limit frequency f_g the higher the value of the second maximum, equally for a rigid and elastic sphere. The second maximum becomes more easily detectable then.

e) At a limit frequency of $f_g = 20$ kHz, the shape of the first maximum is very

much like the transmitted pulse (Fig. 10). Whereas it approaches the shape of the time derivative of the transmitted pulse when frequency f_g decreases (Fig. 11).

f) The amplitude of the first maximum of the reflected pulse decreases with the decrease of the limit frequency (Fig. 9). However, if the oveshoot is taken into account, then the height of the pulse measured peak to peak, remains constant in the frequency range under consideration.

g) The radius of the sphere can be determined from formula (30) on the basis of the measurement of the time interval between the first and second maximum.

The above conclusions have been formulated on the basis of calculations carried out in frequency range $f_g = 2$–20 kHz on models of a rigid and steel sphere with a radius of $a = 0.5$ m. It was found that at low frequencies the incident Gaussian pulse does not "see" the interior of the sphere – is unresponsible to its internal structure. While at the same time the magnitude of the echo is independent from frequency, because of the overshoot in the reflected pulse.

References

[1] I. ANSON, R. CHIVERS, H. STOCKDALE, *The calculation of Y_p for suspended sphere radiometer targets*, Acustica, **48**, 304 (1981).

[2] D. CHAMPENEY, *Fourier transforms and their physical applications*, Academic Press, London, 14, 1973.

[3] L. DRAGONETTE, M. VOGT, L. FLAX, W. NEUBAUER, *Acoustic reflection from elastic spheres II. Transient analysis*, J. Acoust. Soc. Am., **23**, 4, 405–418 (1974).

[4] J. FARAN, *Sound scattering by solid cylinders and spheres*, J. Acoust. Soc. Am., **23**, 4, 405–418 (1951).

[5] L. FILIPCZYŃSKI, *Detectability of calsifications in breast tissues by the ultrasonic echo method*, Archives of Acoustics, **8**, 3, 209 (1983).

[6] C. GAZANHES, J. SESSAREGO, J. HERAULT, J. LEANDRE, *Fonctions de transfert et reponses impulsionnelles de shperes rigides et elastiques*, Acoustica, **52**, 5, 267 (1983).

[7] I. GRADSHTEIN, I. RISHIK, *Tablicy integralow, sum, rjadow i proizwedenii*, Nauka, Moskwa, 321, 1971.

[8] L. HAMPTON, C. MCKINEY, *Experimental study of the scattering of acoustic energy from solid metal spheres in water*, J. Acoust. Soc. Am., **33**, 5, 664–673 (1961).

[9] T. HASEGAWA, *Comparison of two solutions for acoustic pressure on a sphere*, J. Acoust. Soc. Am., **61**, 6, 1445–1448 (1971).

[10] T. HASEGAWA, Y. WATANABE, *Acoustic radiation pressure on an absorbing sphere*, J. Acoust. Soc. Am., **63**, 6, 1733–1737 (1978).

[11] T. HASEGAWA, K. YOSIOKA, *Acoustic radiation force on a solid elastic sphere*, J. Acoust. Soc. Am., **46**, 5 P2, 1139–1143 (1969).

[12] R. HICKLING, *Analysis of echoes from a solid elastic sphere in water*, J. Acoust. Soc. Am., **39** (1966).

[13] P. HWEI HSU, *Fourier analysis, Simon and Schuster*, New York, 74, 1970.

[14] Z. KLONOWICZ, Z. ZURZYCKI, *Theory of networks*, t. I, PWN, Warszawa 1983 (in Polish).

[15] P. MORSE, K. INGARD, *Theoretical acoustics*, McGraw-Hill, New York, 338, 1968.

[16] W. NEUBAUER, M. VOGT, L. DRAGONETTE, *Acoustic reflection from elastic spheres*, I. Steady-state signals, J. Acoust. Soc. Am., **55**, 1123–1129 (1974).

[17] C. RSHEVKIN, *Kurs lekcij po teorii zwuka*, Izd. Moskovskovo Universiteta, Moskwa 1960.

[18] A. RUDGERS, *Acoustical pulses scattered by a rigid sphere in a fluid*, J. Acoust. Soc. Am., **45**, 4, 900–910 (1969).

Received on June 12, 1986; revised version on January 15, 1987.

ARCHIVES OF ACOUSTICS
12, 2, 129–147 (1987)

AN ANALYSIS OF ACOUSTIC WAVE RADIATION CONDITIONS WITHIN THE STRUCTURAL SYSTEM OF AN AXIAL DYNAMIC GENERATOR

TOMASZ ZAMORSKI

Department of Acoustics Institute of Physics, Higher Pedagogic School in Rzeszów
(35-310 Rzeszów, ul. Rejtana 16a)

This paper analysis radiation conditions of an acoustic wave in an axial generator with outlets of the stator entering a common horn with a ring-shaped cross section. Acoustic properties of the generator horn, including the wave reflected from the outlet, were considered. The influence of the impedance misfit in the outlets of stater openings-horn inlet system, on the acoustic power emission was estimated. A theoretical and experimental analysis was performed in order to determine the influence of a finite horn length on the power emission and generator efficiency.

1. Introduction

Acoustic axial dynamic generators belong to a group of flow generators which convert energy of compressed air into acoustic energy. The vertical section in Fig. 1

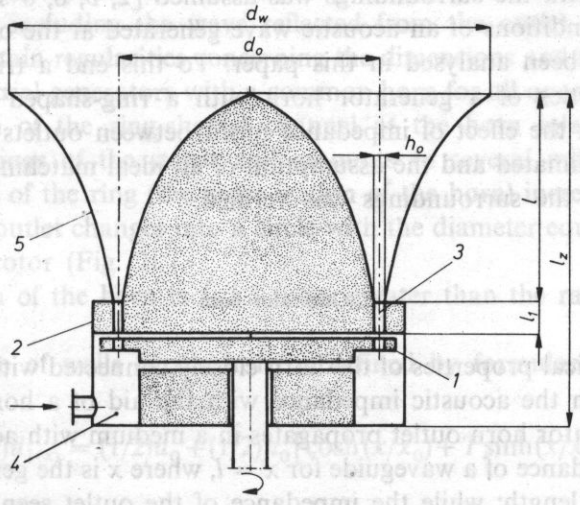

Fig. 1. Axial section of an axial dynamic generator

shown main elements of the structural system of an axial dynamic generator. An air flux which escapes the pressure chamber (4) through channels (3) in the plate of the stator (2) is periodically cut-off by a rotating rotor (1) with openings spaced in a regular manner on its perimeter. Thus, a sound wave is generated at the outlet of the stator channel and radiated outside through the horn (5).

In first constructions of generators [2] the stator was equipped with few holes only. Every one of them had a separate acoustic horn. Such a structure is still applied in audio frequency, high power generators [11]. Trials of constructing generators of high frequency waves have led to structural changes in the stator-horn system, such as increasing the number of openings (from tens to several hundred) with small diameter (several milimeters), spaced regularly on the perimeter of the rotor and stator. All openings are opened into a common horn with a ring-shaped cross section, because building seperate horns for every channel of the stator was impossible for technological reasons. Such a structural model of an axial generator is most frequently applied at present [5, 7–10].

Presented above trials of obtaining high acoustic frequencies generally were not accompanied by an analysis of radiation conditions of generated waves, although they were subjected to significant changes. Introduced structural modification causes an impedance misfit between outlets of the stator and inlet of the horn, thus inevitable losses of radiated acoustic power. This problem has not hitherto attracted attention of scientists, mainly because the theory of acoustic horns with ring-shaped cross sections has not been sufficiently developed. Calculations of generators with a common horn for all openings of the stator are at present limited to approximations which accept that the impedance of the generator horn outlet with a ring-shaped section is expressed by an identical formula as for a horn with an identical wall profile, but with a circular section [8, 9]. Furthermore, an ideal acoustic matching of the horn outlet with the surroundings was assumed [2, 5, 6, 8–10, 12–15, 18, 19].

Radiation conditions of an acoustic wave generated at the outlet of the stator channel (3) have been analysed in this paper. To this end a trial of determining acoustical properties of a generator horn with a ring-shaped section has been undertaken. Then the effect of impedance misfit between outlets of the stator and horn inlet was estimated and the assumption of an ideal matching of the generator horn outlet with the surroundings was verified.

2. Generator horn

Certain physical properties of the horn closely connected with its geometry are required to match the acoustic impedance with the aid of a horn. A wave which reaches the generator horn outlet propagates in a medium with acoustic impedance equal to the impedance of a waveguide for $x = l$, where x is the generator axis of the horn and l is its length; while the impedance of the outlet seen from the outside depends on the shape of the outlet, as well as on the shape of the isophase surface

and length of the wave leaving the horn. If real parts of both impedances are equal and their imaginary parts are equal to zero, then a wave which reaches the horn outlet will be radiated into the surrounding medium without obstacles and the generator will radiate outside maximum of the acoustic energy. The equality of real parts of the impedance prevents a reflection of the wave from the outlet, while the absence of their imaginary parts means that a phase shift between the pressure and vibration velocity of particles of the medium does not occur. Such a specific case of ideal impedance matching at the outlet is called a "horn with infinite length" [16], because only in a hypothetical, infinite horn a wave propagating towards the outlet is not accompanied by a reflected wave. In such a case the total acoustic power is released on the real part of the outlet impedance. This impedance can be considered focused. An analysis of impedance frequency characteristics of the outlet as well as of an arbitrary horn at the outlet proves that a given horn approaches the ideal of an infinite waveguide when the wavelength decreases with respect to the dimensions of the outlet. Then real parts of both impedances approach the acoustic self-resistance of the medium and imaginary parts approach zero.

Mentioned above arguments concern a plane wave. The enlargement of transverse dimensions of the horn with respect to the wavelength could lead to amplified transverse vibrations of the medium in the horn. It would have an adverse influence on power radiation, because it causes reflections of the wave from walls of the horn and accumulation of a part of the energy inside the waveguide. Therefore, the diameter of the horn outlet can not be arbitrarily increased, even when the construction demands concerning generator dimensions and weight are neglected.

In practice we have to choose from opposed postulated when determining the dimension of a horn and then the impedance matching at the outlet can greatly differ from the ideal of an infinite waveguide.

Therefore, in this paper we will calculate the generator horn as a "horn with finite length", i.e. including the wave reflected from the outlet.

There are certain regularities concerning the dimensions and shape of a horn in constructions of axial generators with a common horn for all openings of the stator:

– the width of the ring-shaped channel at the horn inlet is equal to the diameter of openings of the stator and amounts to several milimeters,

– the width of the ring (the cross-section of the horn) increases from inlet to outlet and at the outlet changes into a circle with the diameter equal to the doubled diameter of the rotor (Fig. 2),

– the length of the horn is 1–1.5 times greater than the radius of the outlet opening,

– the profile of walls of the horn is defined by formulae [17]

$$(1/2)d_{1(x)} = (1/2)d_0 + (1/2)h_0[\cosh(x/x_0) + T\sinh(x/x_0)], \tag{1}$$

$$(1/2)d_{2(x)} = (1/2)d_0 - (1/2)h_0[\cosh(x/x_0) + T\sinh(x/x_0)], \tag{2}$$

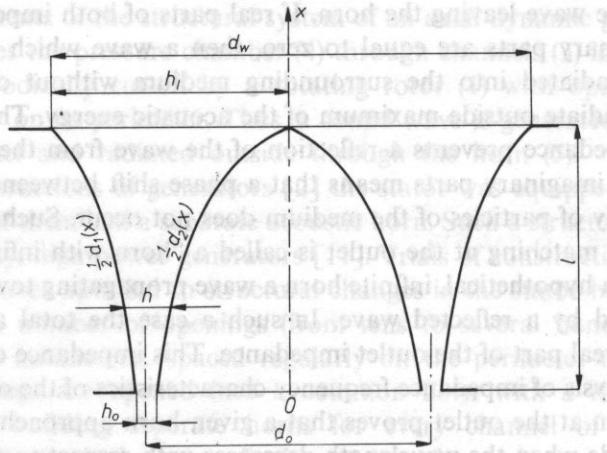

Fig. 2. Axial section of the horn of an axial generator

where x_0 is a constant determining the rate of flare. In practice parameter T most frequently equals one or zero, what corresponds to an exponential or catenoidal profile of walls, respectively. Hence, we will limit further consideratons to the case of $T \in [0, 1]$.

It results from formulae (1) and (2) that the crosssectional area S of the generator horn has the following form

$$S = S_0(\cosh\alpha + T\sinh\alpha), \tag{3}$$

where $\alpha = x/x_0$, $S_0 = \pi d_0 h_0$ is the area of the inlet. On the basis of [16] and [17] it can be stated that the equation of wave propagation in a horn (3) has the following form

$$d^2F/d\alpha^2 + [\mu^2 - V_{(\alpha)}]F = 0, \tag{4}$$

where F is the so-called wave function, μ is the dimensionless frequency and function $V_{(\alpha)}$, which characterizes the geometry of the horn, is expressed by

$$V_{(\alpha)} = 1/2 - (1/4)\mathrm{tgh}^2(\alpha + \Omega), \tag{5}$$

where Ω is an abbreviated notation of

$$\Omega = \mathrm{arctgh}\, T. \tag{6}$$

It should be noted that equation (4) describes the propagation of a plane harmonic wave, which propagates in the generator horn without energy loss [16]. This equation can be solved in an approximate manner for values $T \in [0, 1)$, while for $T = 1$ we achieve a linear differential equation with constant coefficients and with an accurate solution in the finite form [3].

Let us consider closer the case of $T = 1$. From (6) and (5) it results that wave equation (4) will accept the following form

$$d^2F/d\alpha^2 + K^2F = 0 \tag{7}$$

where K is independent of position and is expressed by formula

$$K^2 = \mu^2 - 1/4. \tag{8}$$

The solution of equation (7) has the following form [16]

$$F = Ae^{\pm iK\alpha}, \tag{9}$$

where A is independent of position. It results from (8) and (9) that the frequency which delimits periodic solutions from aperiodic ones, and is frequently called the cut-off frequency of a horn, is equal to

$$\mu_{gr} = 1/2. \tag{10}$$

From the theory of acoustical horns [16] we know that for a case of K independent of position, the admittance* of a horn with finite length is expressed by formula

$$\beta = \frac{K}{\mu}\operatorname{ctgh}\left\{\pi\left[\varepsilon - i\left(\delta - \frac{K\alpha}{\pi}\right)\right]\right\} + \frac{i}{2\mu}\frac{dS}{Sd\alpha}. \tag{11}$$

The real and imaginary part of the expression under the hyperbolic cotangent characterize the amplitude decrease and phase shift of the wave reflected from the horn outlet, respectively. Within the framework of mathematic formalizm accepted in the theory of horns [16], quantity $2\pi\varepsilon$ is equal to the amplitude ratio of the reflected and incident wave, and expression $2\pi(\delta - K\alpha/\pi)$ characterizes the phase shift between the wave progressing towards the outlet and the reflected wave.

Including (3), (8), (11) in the case of the horn $T = 1$ under consideration, $\mu > \mu_{gr}$, we achieve the following formula for admittance

$$\beta = \sqrt{1 - \frac{1}{4\mu^2}}\operatorname{ctgh}\left\{\pi\left[\varepsilon - i\left(\delta - \frac{\sqrt{\mu^2 - \frac{1}{4}}}{\pi}\alpha\right)\right]\right\} + \frac{i}{2\mu}. \tag{12}$$

Quantities ε and δ can be derived from the boundary condition

$$\beta_l = \beta_w, \tag{13}$$

where β_l is the elementary relative admittance of the horn outlet, while β_w is the elementary relative admittance of the outlet opening of the horn seen from the outside. β_l is obtained by substituting $\alpha = \alpha_l$ in (12), where α_l is the dimensionless abscissa of the horn outlet. β_w can be achieved by rearranging the well-known

* At this stage of considerations we will use the notion of admittance in place of impedance in order to simplify used formulae.

Rayleigh formula for elementary acoustic relative impedance of a circular piston in an infinite baffle. Thus, introducing abbreviated notations, condition (13) has the following form

$$\operatorname{ctgh}[\pi(\varepsilon - i\sigma_l)] = Q + iW, \tag{14}$$

where

$$\sigma_l = \delta - \frac{\sqrt{\mu^2 - \frac{1}{4}}}{\pi}\alpha_l, \tag{15}$$

$$Q = \left(1 - \frac{1}{4\mu^2}\right)^{-1/2} \frac{w^2 - 2wI_{1(w)}}{[w - 2I_{1(w)}]^2 + 4[S_{1(w)}]^2}, \tag{16}$$

$$W = \left(1 - \frac{1}{4\mu}\right)^{-1/2} \frac{2wS_{1(w)}}{[w - 2I_{1(w)}]^2 + 4[S_{1(w)}]^2} - \frac{1}{2\sqrt{\mu^2 - \frac{1}{4}}} \tag{17}$$

$I_{1(w)}$ and $S_{1(w)}$ denote Bessel and Struve functions of the first order, while

$$w = kd_w \tag{18}$$

where k is a wave number and d_w is the diameter of the horn outlet.

Rather arduous rearrangements allow us to determine ε and σ_l from (14):

$$2\pi\varepsilon = \operatorname{arctgh}[2Q/(1 + Q^2 + W^2)] \tag{19}$$

$$2\pi\sigma_l = \operatorname{arctgh}[2W/(Q^2 + W^2 - 1)]. \tag{20}$$

Then, having σ_l we can determine δ from (15)

$$\delta = \sigma_l + \frac{\sqrt{\mu^2 - \frac{1}{4}}}{\pi}\alpha_l. \tag{21}$$

When we include (21) in the imaginary part of the expression under the hyperbolic cotangent in formula (12), we reach a conclusion that the phase shift between the wave reflected from the horn outlet and the incident wave, is a linear function in terms of position on the horn axis:

$$\sigma_{(\alpha)} = \sigma_l + \frac{\sqrt{\mu^2 - \frac{1}{4}}}{\pi}(\alpha_l - \alpha). \tag{22}$$

Whereas, quantity ε, which characterizes the amplitude ratio of the reflected and incident wave, is constant (formula (19)) and depends solely on the impedance at the horn outlet.

At present we will consider cases of $\mu = \mu_{gr}$ and $\mu < \mu_{gr}$. Two methods can be applied to the limiting case, $\mu = \mu_{gr}$ (i.e. $K = 0$). The first one consists in a rather complicated rearrangement of formula (12) with repeated application of the de l'Hospital principle; while the second one is based on the solution of the wave equation. In the case of $K = 0$ this solution has the following form:

$$d^2F/d\alpha^2 = 0, \tag{23}$$

Both methods lead to the same final result

$$\beta = i[1-2/(C+\alpha)], \tag{24}$$

where C is expressed by

$$C = 2\left\{\frac{i[w^2-2wI_{1(w)}]-2wS_{1(w)}}{[w-2I_{1(w)}]^2+4[S_{1(w)}]^2}+1\right\}^{-1}-\alpha_l. \tag{25}$$

In the case of $\mu < \mu_{gr}$, in formula (12) we accept

$$K = -i\sqrt{\frac{1}{4}-\mu^2} \tag{26}$$

and reach

$$\beta = \frac{-i\sqrt{\frac{1}{4}-\mu^2}}{\mu}\operatorname{ctgh}\left\{\pi\left[\left(\varepsilon+\frac{\sqrt{\frac{1}{4}-\mu^2}}{\pi}\alpha\right)-i\delta\right]\right\}+\frac{i}{2\mu}. \tag{27}$$

Introducing $\alpha = 0$ in formulae (12), (22), (24) and (27) we achieve the admittance and thus – the impedance of the horn inlet. This is the most useful quantity in the analysis of wave radiation conditions in the structural system of a generator.

To conclude our considerations of the case of $T = 1$ we will present a numerical example and calculate the elementary relative impedance of the horn outlet in terms of frequency on the basis of formulae (12), (24) and (27). The following dimensions of the horn were accepted for calculations:

- width of the horn channel at the inlet $h_0 = 1.5 \cdot 10^{-3}$ m,
- inside diameter of the ring-shaped horn channel $d_0 = 10^{-1}$ m,
- diameter of the horn outlet $d_w = 2 \cdot 10^{-1}$ m,
- horn length $l = 15 \cdot 10^{-2}$ m.

These dimensions are typical for designs of axial flow generators.

Diagrams in Figs. 3 and 4 illustrate calculation results. Oscillations caused by the reflection of the wave from the horn outlet can be seen in frequency characteristics of real and imaginary parts of the inlet impedance. In the range of low frequencies oscillations of the inlet impedance are considerable and can influence the acoustic power emission and efficiency of the generator.

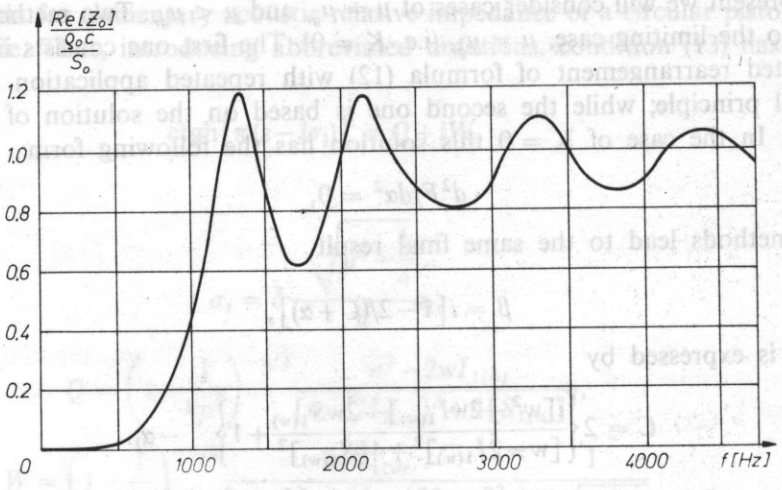

Fig. 3. Inlet acoustic resistance of the generator horn with an exponential profile

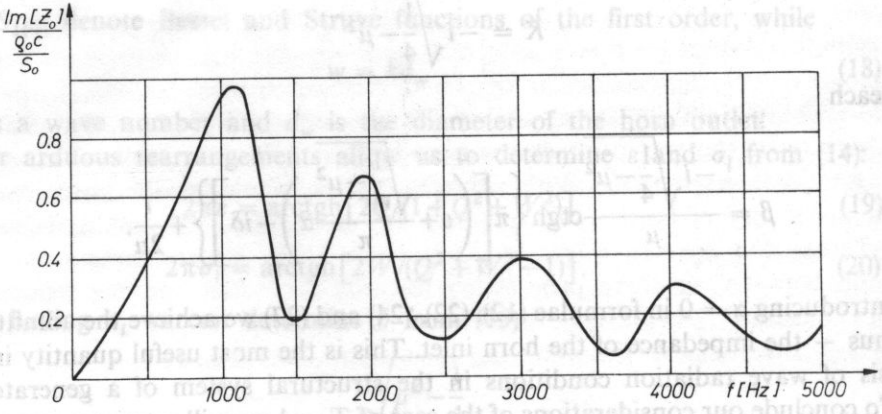

Fig. 4. Inlet acoustic reactance of the generator horn with an exponential profile

Now we will consider the case of $T \in [0, 1)$. It results from (4) that the frequency delimiting periodic ($\mu^2 \geqslant V_{(\alpha)}$) and aperiodic ($\mu^2 < V_{(\alpha)}$) solutions is equal to

$$\mu_{gr} = = \sqrt{1/2 - (1/4)\mathrm{tgh}^2(\alpha + \Omega)}. \tag{28}$$

We can see from formula (28) that the cut-off frequency is a function of the position on the axis of the horn, when values from interval $[\mu_{gr1}, \mu_{gr2}]$ are accepted. While,

$$\mu_{gr_1} = \sqrt{1/2 - (1/4)\mathrm{tgh}^2(\alpha_l + \Omega)}, \tag{29}$$

$$\mu_{gr_2} = \sqrt{1/2 - (1/4)\mathrm{tgh}^2\,\Omega}. \tag{30}$$

This is the so-called broadening of the cut-off frequency of a horn and it has been described in [17]. An approximate method of solving the wave equation of a horn, which was given in [18] will be applied in order to calculate the admittance. This method consists in the approximation of function $V_{(\alpha)}$ by a broken line. Horn $T \in [0, 1)$ is considered to be a polyadic horn and every unit corresponds to one segment of the broken line. A rearrangement of formulae given in [18] results in an expression for the elementary relative impedance of the n-unit of the horn

$$\beta_n = \frac{-i}{\mu}\left\{\frac{\sqrt{C_n(\alpha+b_n)}[I_{-\frac{2}{3}}(\frac{2}{3}\xi^{3/2}) - D_n I_{\frac{2}{3}}(\frac{2}{3}\xi^{3/2})]}{I_{\frac{1}{3}}(\frac{2}{3}\xi^{3/2}) + D_n I_{-\frac{1}{3}}(\frac{2}{3}\xi^{3/2})} - \frac{1}{2}\operatorname{tgh}(\alpha+\Omega)\right\}, \tag{31}$$

where C_n – slope of the n-segment of the broken line, $b_n = (\mu^2 - V_{(\alpha n-1)})/C_n$, $V_{(\alpha n-1)}$ denotes the value of function $V_{(\alpha)}$ at the inlet of the n-unit of the horn, D_n – constant derived by equating the outlet admittance of the n-unit and the inlet admittance of the $(n+1)$-unit of the horn.

Quantity ξ, which is found in the argument of the Bessel function in formula (31), is expressed by the following expression

$$\xi = C_n^{1/3}(\alpha + b_n). \tag{32}$$

Formula (31) is valid for $\xi > 0$. Rearranging general relationships given in [18] we reach an expression for the admittance of horns under consideration for a case of $\xi = 0$ and $\xi < 0$:

for $\xi = 0$

$$\beta_n = \frac{-i}{\mu}\left[\frac{(3C_n)^{1/3}\Gamma(\frac{2}{3})}{D_n\Gamma(\frac{1}{3})} - \frac{1}{2}\operatorname{tgh}(\alpha+\Omega)\right], \tag{33}$$

where Γ is the Euler function:

and for $\xi < 0$

$$\beta_n = \frac{-i}{\mu}\left\{\frac{-i\sqrt{C_n|\alpha+b_n|}[I_{-\frac{2}{3}}(-i\frac{2}{3}|\xi|^{3/2}) - D_n I_{\frac{2}{3}}(-i\frac{2}{3}|\xi|^{3/2})]}{I_{\frac{1}{3}}(-i\frac{2}{3}|\xi|^{3/2}) + D_n I_{-\frac{1}{3}}(-i\frac{2}{3}|\xi|^{3/2})} - \frac{1}{2}\operatorname{tgh}(\alpha+\Omega)\right\}. \tag{34}$$

The admittance of the horn inlet should be calculated in several stages, beginning from the outlet and ending at the inlet. First of all, the inlet admittance of the end unit has to be found by accepting it as equal to the outlet load of the preceeding unit, then the inlet admittance of this unit has to be found, etc. In numerical calculations based on formulae (31)–(34) a catenoidal horn ($T = 0$), with dimensions identical to those of the exponential horn analysed before, was considered. As in case of $T = 1$ it was accepted that the horn $T = 0$ is loaded at the outlet with the impedance of a circular piston with the diameter equal to the diameter of the horn outlet, which vibrates in an infinite baffle. Calculation results are illustrated in Figs. 5 and 6. Diagrams of real and imaginary parts of the elementary relative impedance of the horn outlet in terms of frequency exhibit

oscillations due to the reflection of a wave from the outlet. A comparison between Figs. 5, 6 and Figs. 3, 4 shows that a change of the horn profile from exponential to catenoidal at constant dimensions of its inlet, outlet and length, leads to significant quantitative changes in frequency characteristics of impedance. In particular the average level of the real part of the relative impedance becomes higher with a simultaneous increase of the first maximum with respect to the other ones. On the other hand resonant and antiresonant frequencies of the horn undergo only slight changes.

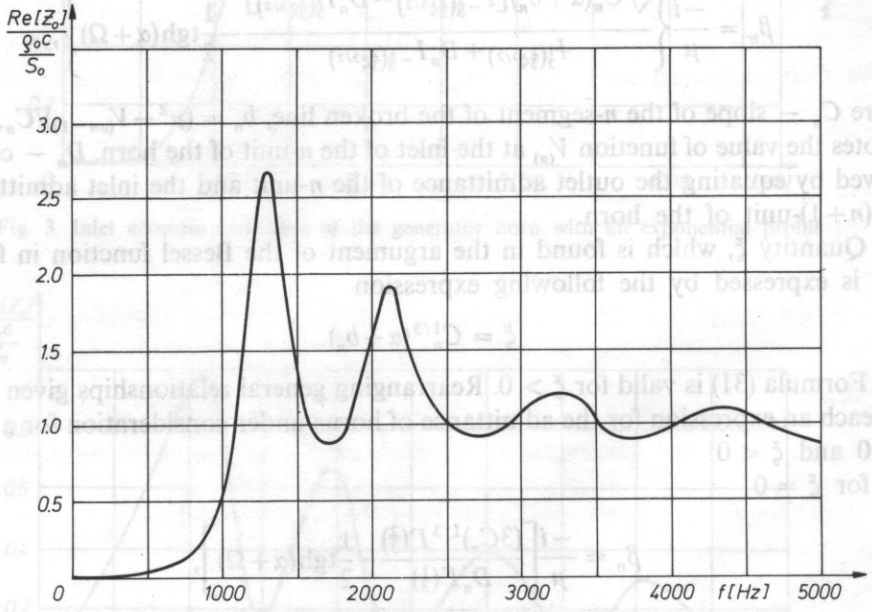

Fig. 5. Inlet acoustic resistance of the generator horn with an catenoidal profile

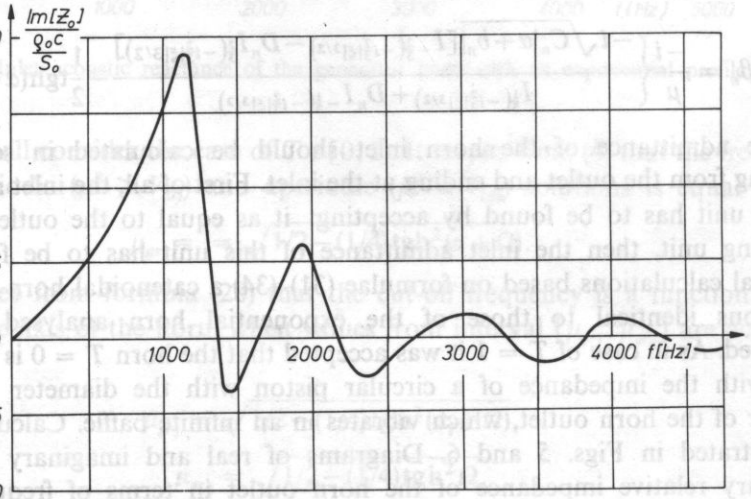

Fig. 6. Inlet acoustic reactance of the generator horn with an catenoidal profile

3. Horn with a stator

The acoustic wave is produced in an axial generator at the inlet of the stator channel. The condition of its radiation to the surroundings depends not only on the horn, but also on other elements of the generator structure (see Fig. 1). In order to analyse this problem in detail we will make use of the generalized theoretical model of an axial dynamic generator [9]. Model [9] accepts that the pressure chamber and the stator channel with the horn are acoustic four-terminal networks in a series connection and the acoustic impedance of the inlet opening of the stator channel is a sum of:

– the input impedance of the pressure chamber Z_1, which loades the inlet of this channel,

– the input impedance of the stator channel Z_2, which can be called the input impedance of the stator-horn system.

It was proved in [9] that Z_1, excluding frequencies close to resonant and antiresonant frequencies of the pressure chamber, can be neglected in calculations of typical axial generators. In such a situation the input impedance of the stator channel with the horn Z_2 is decisive for acoustic power radiation of the generator. The stator channel can be considered to be a cylindrical pipe loaded at the outlet by the impedance of the horn inlet. Hence, the conditions of acoustic power radiation by the generator should improve when the length of these channels is decreased and when their number is increased. In theory best radiation conditions can occur when all openings of the stator join together into a ring-shaped inlet opening of the horn. This corresponds to a situation in which the input impedance of the stator-horn system changes into the impedance of the horn inlet. Therefore, in order to estimate the influence of the stator (as a separate element in the acoustic system of the generator) on the conditions of acoustic power emission, the frequency characteristic of the input impedance of the stator channel together with the horn should be compared with an analogic characteristic of the inlet of the horn itself. In particular frequency characteristics of real parts of both impedances should be compared, because the real part of the relative impedance of the horn inlet, or another matching system, is known in acoustic literature [16] as the so-called coefficient of transmission and characterizes acoustic power transmission.

Let us assume that a plane wave propagates in the stator channel. Then the acoustic impedance of the inlet of the stator channel and horn can be expressed as

$$Z_2 = \frac{\dfrac{\varrho_0 c}{S_k}\dfrac{Z + i\dfrac{\varrho_0 c}{S_k}\operatorname{tg}(kL_1)}{\dfrac{\varrho_0 c}{S_k} + iZ\operatorname{tg}(kL_1)}}{}, \tag{35}$$

where: ϱ_0 – rest density of the medium, c – adiabatic propagation velocity of a sound wave, S_k – cross-sectional area of the stator channel, l_1 – length of stator channel, Z – impedance loading the outlet of stator channel.

In accordance with the theoretical generator model [9] we can note that

$$Z = nZ_0 \tag{36}$$

where n is the number of openings in the stator and Z_0 is the impedance of the horn inlet.

It was accepted in numeric calculations of the input impedance of the stator channel Z_2 that openings in the stator enter the catenoidal horn ($T = 0$) with dimensions as given in paragraph 2. Furthermore, the following parameters were accepted: $n = 50$, $l_1 = 10^{-2}$ m, and the diameter of the stator opening equal to $1.5 \cdot 10^{-3}$ m.

Calculation results of real and imaginary parts of the elementary relative impedance of the inlet of the stator channel and the horn are presented in Figs. 7 and 8. Both diagrams were drawn in the frequency range from zero to four kHz, what corresponds to the range of application of the assumption about the plane wave in the horn. A comparison between diagrams in Figs. 7 and 8 frequency characteristics of the inlet impedance of the horn itself in Figs. 5 and 6 shows that the introduction of a stator as a separate element in the acoustic system of an axial generator does not influence the shape of impedance frequency characteristics, but causes a considerable decrease of its average value. This occurs, because resonant and antiresonant frequencies, and proportions of individual maxima and minima are in both diagrams nearly identical. While, values of real parts of the impedance at a fixed frequency are at least four times smaller for the inlet of the stator-horn system than for the inlet of the horn itself. This is due to the reflection of a wave at the connection of the stator channel outlet with the horn inlet and has to cause a considerable decrease of the acoustic power emitted by the generator. A theoretical power frequency characteristic of a generator with given above dimensions of the

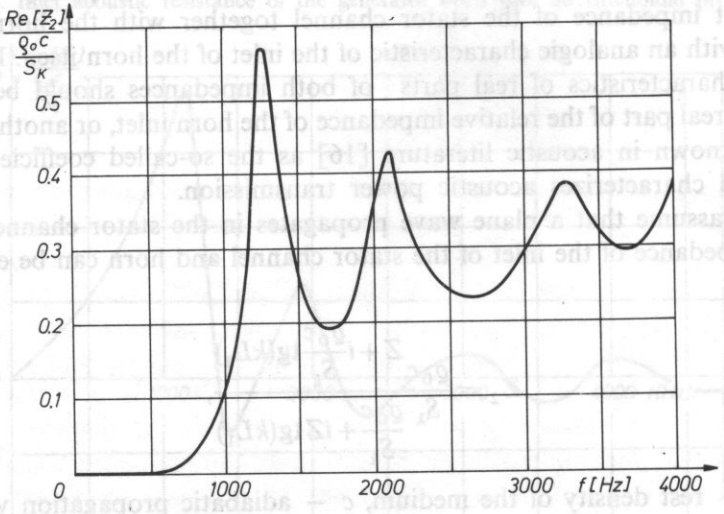

Fig. 7. Inlet acoustic resistance of the stator channel and horn

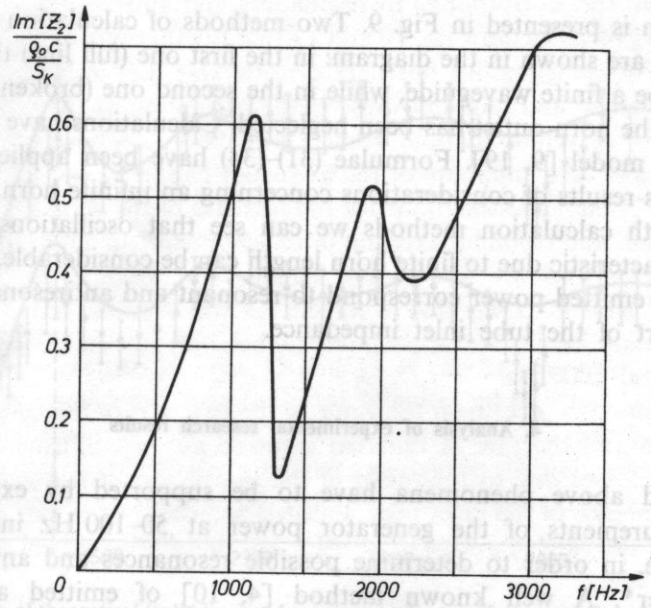

Fig. 8. Inlet acoustic reactance of the stator channel and horn

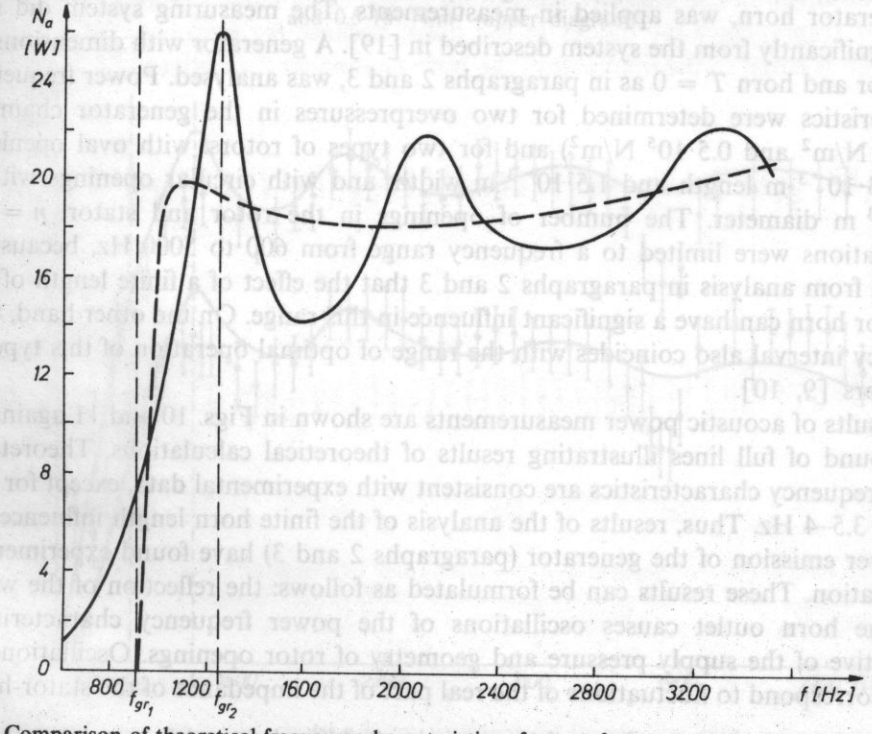

Fig. 9. Comparison of theoretical frequency characteristics of power for a generator collaborating with a catenoidal horn with finite length (solid line) and infinite length (dashed line). Openings in the rotor were taken to be circular and the overpressure in the generator chamber was taken to be equal to $0.5 \cdot 10^5$ N/m^2

stator and horn is presented in Fig. 9. Two methods of calculation of the emitted acoustic power are shown in the diagram: in the first one (full line) the generator is considered to be a finite waveguide, while in the second one (broken line) the wave reflected from the horn outlet has been neglected. Calculations have been based on the theoretical model [9, 19]. Formulae (31)–(34) have been applied to the finite horn, as well as results of considerations concerning an infinite horn, given in [18]. Comparing both calculation methods we can see that oscillations of the power frequency characteristic due to finite horn length can be considerable, while maxima and minima of emitted power correspond to resonant and antiresonant frequencies of the real part of the tube inlet impedance.

4. Analysis of experimental research results

Mentioned above phenomena have to be supported by experiment. This requires measurements of the generator power at 50–100 Hz intervals on the frequency scale, in order to determine possible resonances and antiresonances of radiated power*. A well known method [4, 10] of emitted acoustic power determination on the basis of directional characteristic measured in the far field of the generator horn, was applied in measurements. The measuring system did not differ significantly from the system described in [19]. A generator with dimensions of the stator and horn $T = 0$ as in paragraphs 2 and 3, was analysed. Power frequency characteristics were determined for two overpressures in the generator chamber ($0.2 \cdot 10^5$ N/m^2 and $0.5 \cdot 10^5$ N/m^2) and for two types of rotors: with oval openings with a $3 \cdot 10^{-3}$ m length and $1.5 \cdot 10^{-3}$ m width, and with circular openings with a $1.5 \cdot 10^{-3}$ m diameter. The number of openings in the rotor and stator: $n = 50$. Investigations were limited to a frequency range from 600 to 5000 Hz, because it resulted from analysis in paragraphs 2 and 3 that the effect of a finite length of the generator horn can have a significant influence in this range. On the other hand, this frequency interval also coincides with the range of optimal operation of this type of generators [9, 10].

Results of acoustic power measurements are shown in Figs. 10 and 11 against a background of full lines illustrating results of theoretical calculations. Theoretical power frequency characteristics are consistent with experimental data, except for the interval 3.5–4 Hz. Thus, results of the analysis of the finite horn length influence on the power emission of the generator (paragraphs 2 and 3) have found experimental confirmation. These results can be formulated as follows: the reflection of the wave from the horn outlet causes oscillations of the power frequency characteristic, irrespective of the supply pressure and geometry of rotor openings. Oscillations of power correspond to fluctuations of the real part of the impedance of the stator-horn

* Measuring points on power frequency characteristics have been given in previous papers [9, 10, 19] most frequently at 500–1000 Hz intervals.

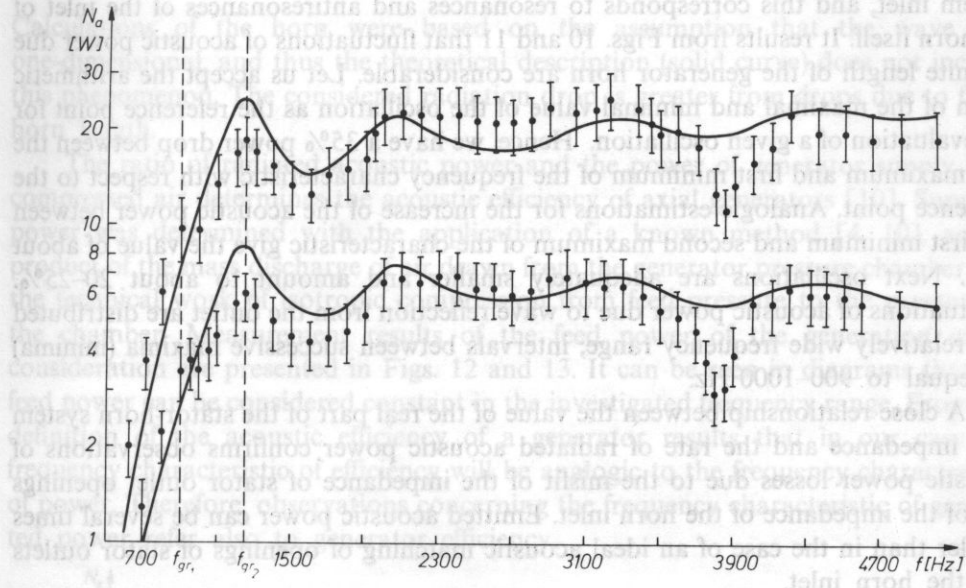

Fig. 10. Comparison of theoretical (solid line) and experimental power frequency characteristics of an axial generator collaborating with a rotor with circular openings at overpressure $0.2 \cdot 10^5$ N/m^2 (lower diagram) and $0.5 \cdot 10^5$ N/m^2 (upper diagram)

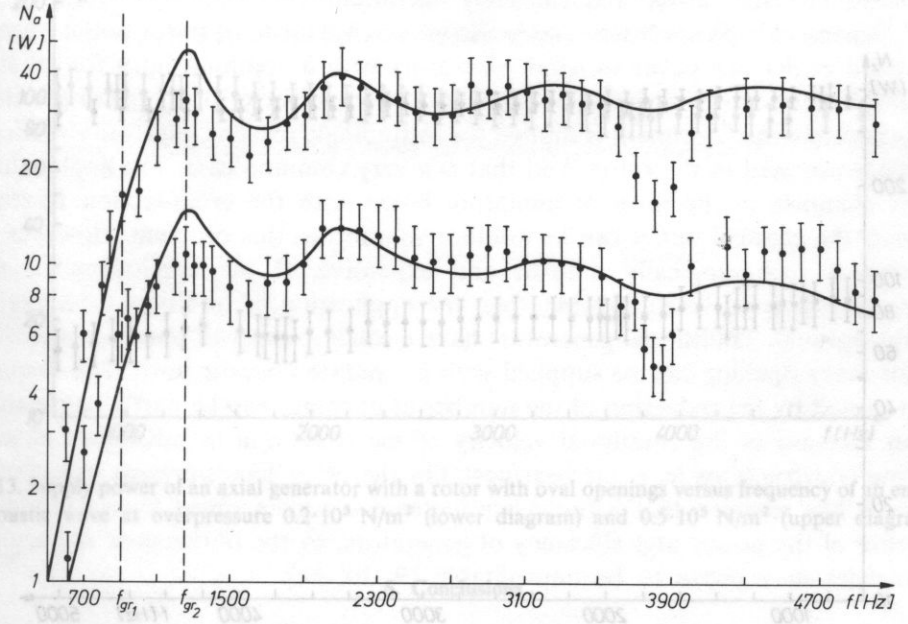

Fig. 11. Comparison of theoretical (solid line) and experimental power frequency characteristics of an axial generator collaborating with a rator with oval openings at overpressure $0.2 \cdot 10^5$ N/m^2 (lower diagram) and $0.5 \cdot 10^5$ N/m^2 (upper diagram)

system inlet, and this corresponds to resonances and antiresonances of the inlet of the horn itself. It results from Figs. 10 and 11 that fluctuations of acoustic power due to finite length of the generator horn are considerable. Let us accept the arithmetic mean of the maximal and minimal value of the oscillation as the reference point for the evaluation of a given oscillation. Hence, we have a 35% power drop between the first maximum and first minimum of the frequency characteristic with respect to the reference point. Analogic estimations for the increase of the acoustic power between the first minimum and second maximum of the characteristic give the value of about 60%. Next oscillations are adequately smaller and amount to about 20–25%. Fluctuations of acoustic power due to wave reflection from the outlet are distributed in a relatively wide frequency range; intervals between successive maxima (minima) are equal to 900–1000 Hz.

A close relationship between the value of the real part of the stator-horn system inlet impedance and the rate of radiated acoustic power confirms observations of acoustic power losses due to the misfit of the impedance of stator outlet openings and of the impedance of the horn inlet. Emitted acoustic power can be several times smaller than in the case of an ideal acoustic matching of openings of stator outlets and the horn inlet.

Measurements exhibit a minimum of radiation in the interval 3.5–4 kHz, which was not obtained in calculations. According to the author this radiation decrease is caused by transverse wave modes in the horn, because for frequency 3400 Hz the wavelength is equal to the diameter of the horn channel at the outlet ($0.5d_w = 0.1$ m).

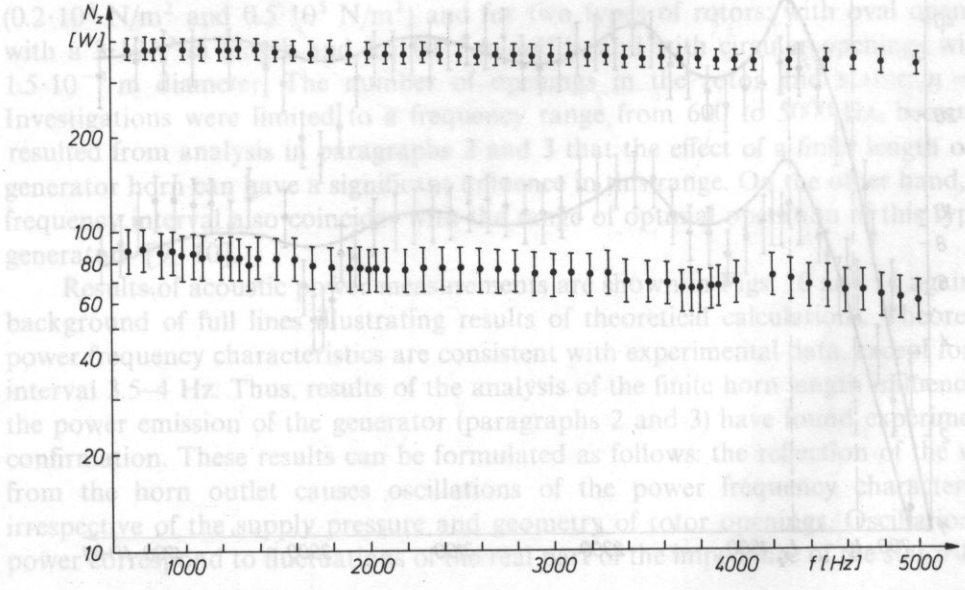

Fig. 12. Supply power of an axial generator with a rotor with circular openings versus frequency of an emitted acoustic wave at overpressure $0.2 \cdot 10^5$ N/m^2 (lower diagram) and $0.5 \cdot 10^5$ N/m^2 (upper diagram)

Calculations of the horn were based on the assumption that the wave was one-dimensional, and thus the theoretical description (solid curve) does not include this phenomenon. The considered radiation drop is greater from drops due to finite horn length.

The ratio of radiated acoustic power and the power of generator supply with compressed air determines the acoustic efficiency of axial generators [10]. Supplied power was determined with the application of a known method [4, 10], as the product of the mass discharge of air drawn from the generator pressure chamber and the technical work of isotropic compression from feed pressure to the pressure in the chamber. Measurement results of the feed power of the generation under consideration are presented in Figs. 12 and 13. It can be seen in diagrams that the feed power can be considered constant in the investigated frequency range. From the definition of the acoustic efficiency of a generator results that in our case the frequency characteristic of efficiency will be analogic to the frequency characteristic of power. Therefore, observations concerning the frequency characteristic of generated power refer also to generator efficiency.

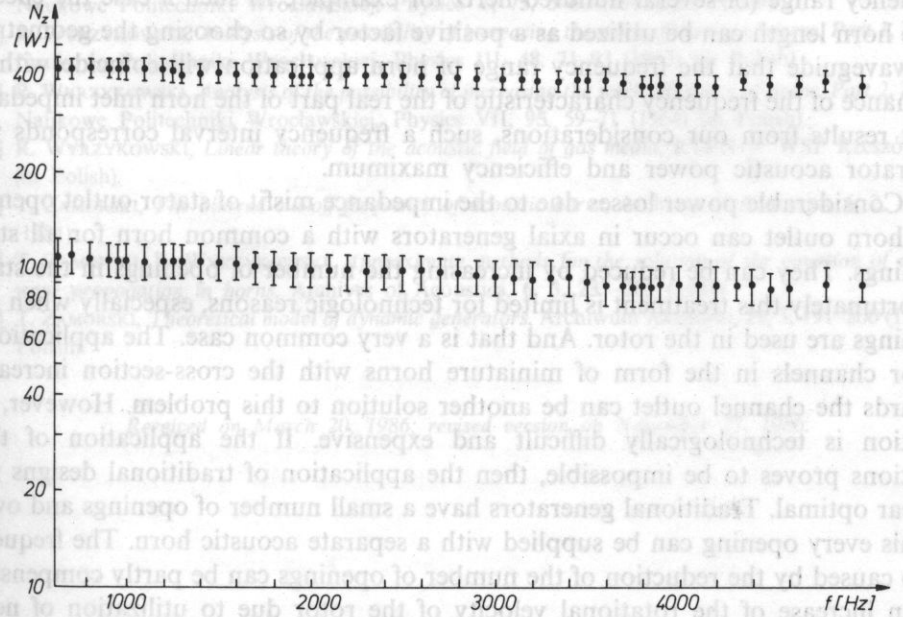

Fig. 13. Supply power of an axial generator with a rotor with oval openings versus frequency of an emitted acoustic wave at overpressure $0.2 \cdot 10^5$ N/m^2 (lower diagram) and $0.5 \cdot 10^5$ N/m^2 (upper diagram)

5. Conclusions

Dimensions of the generator horn outlet, and indirectly of its other parameters such as length or a constant determining the rate of flare, should be a result of a settlement between two opposed postulates. On one hand, the necessity of reduction

of wave reflections from the horn outlet requires the diameter of the horn outlet to be large with respect to wavelength, and on the other, the demand for reduction of energy loss due to transverse mode formation requires transverse dimensions of the horn to be small with respect to wavelength. Hence, the application of one horn in the generator can not ensure optimal radiation conditions in the whole frequency range of generator operation. This range can be divided into intervals – each of them requires the application of a different horn. This problem can be solved in practice in two different ways:

– by supplying the generator with a set of replaceable horns, which would be used in adequate intervals of generated frequencies,

– by designing a folding multi-element horn – its elements would be installed or taken off depending on the frequency interval.

If one horn would be used for the whole frequency range of generated waves, then the effect of a finite horn would have an adverse influence, because it would disturb the stability of frequency characteristics of generator power and efficiency. Solutions mentioned above will lead to the application of a given horn in a narrower frequency range (of several hundred hertz for example). In such a case the effect of finite horn length can be utilized as a positive factor by so choosing the geometry of the waveguide that the frequency range of horn application will coincide with the resonance of the frequency characteristic of the real part of the horn inlet impedance. As it results from our considerations, such a frequency interval corresponds with generator acoustic power and efficiency maximum.

Considerable power losses due to the impedance misfit of stator outlet openings and horn outlet can occur in axial generators with a common horn for all stator openings. They can be reduced by increasing the number of openings in the stator. Unfortunately this treatment is limited for technologic reasons, especially when oval openings are used in the rotor. And that is a very common case. The application of stator channels in the form of miniature horns with the cross-section increasing towards the channel outlet can be another solution to this problem. However, this solution is technologically difficult and expensive. If the application of these solutions proves to be impossible, then the application of traditional designs may appear optimal. Traditional generators have a small number of openings and owing to this every opening can be supplied with a separate acoustic horn. The frequency drop caused by the reduction of the number of openings can be partly compensated by an increase of the rotational velocity of the rotor due to utilization of newer bearing constructions (e. g. air bearings). On the other hand, present experimental research has revealed that a frequency increase is accompanied by a considerable decrease of the power and efficiency of generators, so the obtainment of very high frequencies may prove to be unprofitable [9, 10, 14].

References

[1] C. H. ALLEN, J. RUDNICK, *A powerful high frequency siren*, JASA, **19**, 5, 857–865 (1974).

[2] R. C. JONES, *A fifty horsepower siren*, JASA, **18**, 2, 371–387 (1946).

[3] E. KAMKE, *Sprawocznik po obyknowiennym dyfferencjalnym urawnieniam, pieriewod s niemisckowo pod riedakciej S. W. Fomina*, Izd. Innostrannoj Litieratury, Moscow 1951.

[4] B. LEŚNIAK, *Investigations of an audio-frequency jet generator*, IPPT PAN, Warsaw 1974 (doctors thesis) (in Polish).

[5] B. MATUŁA, W. KASPRZYK, *New static and dynamic sirens in processes of hydro- and aerosol coagulation processes*, Proc. XVIII Open Seminar on Acoustics, Jadwisin 1971 (in Polish).

[6] B. MATUŁA, W. KASPRZYK, R. HNATKÓW, M. ROCZNIAK, *A new high frequency dynamic siren*, Proc. XX Open Seminar on Acoustics, Mierzyn 1973 (in Polish).

[7] E. P. MIEDNIKOW, *Dwie konstrukcji ekspierimientalnych zwukowych sirien*, Akust. Ż., **4**, 1, 59–63 (1958).

[8] A. PUCH, J. TRZEŚNIOWSKI, T. ZAMORSKI, *Design and results of investigations of an axial dynamic siren*, Proc. XXI Seminar on Acoustics, Rzeszów 1974 (in Polish).

[9] A. PUCH, *Generalized model of an axial dynamic generator*, Archives of Acoustics, **13**, 1, 17–34 (1978).

[10] A. PUCH, *The effect of the shape of the holes of the rotor and stator on the acoustic parameters of a dynamic axial generator*, Archives of Acoustics, **5**, 4, 369–380 (1980).

[11] W. W. WIAŁCEW, W. G. CHORAGUANI, *Moszcznaja niskoczastotnaja zwukowaja siriena*, Akust. Ż., **7**, 3, 377–378 (1961).

[12] R. WYRZYKOWSKI, *Acoustic calculation of a siren*, Proc. I Conf. on Ultrasonic Technology, PAN, PWN, Warszawa 1955 (in Polish).

[13] R. WYRZYKOWSKI, *The influence of pulse shape on wave shape and work conditions of a siren*, Zeszyty Naukowe Politechniki Wrocławskiej, Physics V, **75**, 5–60 (1963) (in Polish).

[14] R. WYRZYKOWSKI, *Analysis of the possibility of increasing the work efficiency of sirens, Part 1*, Zeszyty Naukowe Politechniki Wrocławskiej, Physics III, **48**, 71–93 (1963) (in Polish).

[15] R. WYRZYKOWSKI, *Analysis of the possibility of increasing the work efficiency of sirens, Part 2*, Zeszyty Naukowe Politechniki Wrocławskiej, Physics VII, **95**, 59–71 (1964) (in Polish).

[16] R. WYRZYKOWSKI, *Linear theory of the acoustic field of gas media*, RTPN – WSP Rzeszów 1972 (in Polish).

[17] T. ZAMORSKI, *The blurred cut-off frequency of acoustic horns*, Archives of Acoustics, **6**, 2, 135–146 (1981).

[18] T. ZAMORSKI, R. WYRZYKOWSKI, *Approximate methods for the solution of the equation of acoustic wave propagation in horns*, Archives of Acoustics, **6**, 3, 237–285 (1981).

[19] T. ZAMORSKI, *Theoretical model of dynamic generators*, Archiwum Akustyki, **19**, 3, 191–200 (1984) (in Polish).

Received on March 20, 1986; revised version on November 27, 1986.

ARCHIVES OF ACOUSTICS
12, 2, 149–155 (1987)

INTERACTION OF A TWO-LAYERED HALF-CYLINDRICAL SHELL WITH ACOUSTIC MEDIUM

OĽGA ŠIMKOVÁ

Institute of Materials and Machine Mechanics, Slovak Academy of Sciences
(836-06 Bratislava, ul. Februárového vitazstva 75)

Some numerical results of investigations into the coupling between the acoustic field inside a two-layered half-cylindrical shell and the vibrations of the containing structure are presented in this paper. An analytical approach has been used to find resonant frequencies of the system as a whole.

1. Introduction

Interaction effects that exist between the structure and the enclosed acoustic medium have been receiving increasing attention during past years. Such effects can cause resonant frequencies of the whole structure to be considerably different from these in vacuum.

2. Equations of motion

The differential equations of motion of a double-layered cylindrical shell were derived by MARKUŠ [1]. With an internal fluid enclosed they can be written in the following form [2]

$$
\begin{aligned}
&RA_1(\partial^2 u/\partial x^2) - A_{1\nu}\partial w/\partial x + 1/2R(A_1 - A_{1\nu})\partial^2 u/\partial\varphi^2 + \\
&\quad + (1/2)(A_1 + A_{1\nu})\partial^2 v/\partial x\,\partial\varphi - Rm_0\partial^2 u/\partial t^2 = 0, \\
&[D_{1\nu}/4R + (1/2)(A_1 + A_{1\nu})]\partial^2 u/\partial x\,\partial\varphi + RP(\partial^2 v/\partial x^2) + \\
&\quad + (A_1/R + B_1/R^3)(\partial^2 v/\partial\varphi^2) - A_1/R(\partial w/\partial\varphi) - \\
&\quad - Rm_0(\partial^2 v/\partial t^2) = 0, \\
&A_{1\nu}\partial u/\partial x + (1/R)A_1(\partial v/\partial\varphi) - (1/R)A_1 w + D_{1\nu}(\partial^2 w/\partial x^2) - RB_1(\partial^4 w/\partial x^4) + \\
&\quad + (2/R^2)(\partial^4 w/\partial x^2\,\partial\varphi^2) + (1/R^4)(\partial^4 w/\partial\varphi^4) - Rm_0(\partial^2 w/\partial t^2) = -R\varrho(\partial\Phi/\partial t)\big|_{r=a},
\end{aligned}
\tag{1}
$$

where (u, v, w) are the components of displacement of the shell in the axial, circumferential and radial directions, respectively; r, φ and x are cylindrical coordinates as shown in Fig. 1; h_1, h_2 – thicknesses of separate layers; E_i, ν_i, $i = 1, 2$ – Young's moduli and Poisson's constants of the inner and outer layer, respectively.

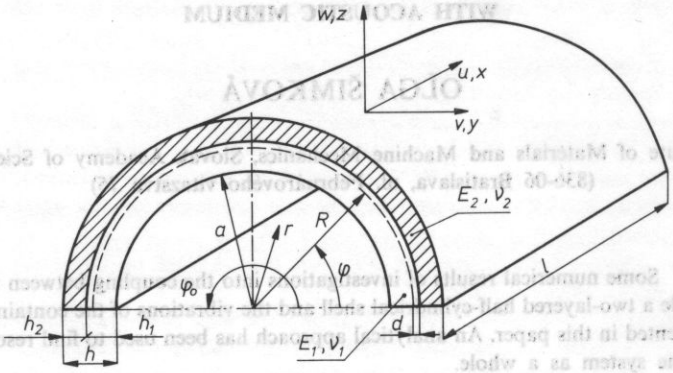

Fig. 1. Geometry and co-ordinate system of a two-layered shell

$$S_i = E_i(1-\nu_i^2),\ i = 1, 2; \quad A_1 = S_1 h_1 + S_2 h_2; \quad A_{1\nu} = S_1 h_1 \nu_1 + S_2 h_2 \nu_2;$$

$$B_1 = (1/3)(S_1 h_1^3 + S_2 h_2^3) - d(S_1 h_1^2 - S_2 h_2^2) + d^2(S_1 h_1 + S_2 h_2);$$

$$B_{1\nu} = (1/3)(S_1 h_1^3 \nu_1 + S_2 h_2^3 \nu_2) - d(S_1 h_1^2 \nu_1 - S_2 h_2^2 \nu_2) + d^2(S_1 h_1 \nu_1 + S_2 h_2 \nu_2);$$

$$D_{1\nu} = (S_1 h_1^2 \nu_1 - S_2 h_2^2 \nu_2) - 2d(S_1 h_1 \nu_1 + S_2 h_2 \nu_2);$$

$$d = (1/2)(S_1 h_1^2 - S_2 h_2^2)/(S_1 h_1 + S_2 h_2);$$

$$P = (1/2)(A_1 - A_{1\nu}) - 3D_{1\nu}/4R + 1/R^2(B_1 - B_{1\nu});$$

m_0 – mass per unit length of the shell; t – time; R – equivalent radius of the shell; $a = R - h_1 + d$; ϱ – density of the fluid; Φ – velocity potential of the fluid.

The velocity potential Φ satisfies the wave equation

$$\nabla^2 \Phi - (1/c_0^2)(\partial^2 \Phi / \partial t^2) = 0, \tag{2}$$

where ∇^2 is the Laplacian operator in the form

$$(1/r)(\partial/\partial r)\left[r(\partial/\partial r)\right] + (1/r^2)(\partial^2/\partial \varphi^2) + (\partial^2/\partial x^2)$$

and c_0 is the velocity of sound in the fluid. It is assumed that the shell and the fluid remain in contact and so

$$\partial w/\partial t = -\partial \Phi/\partial r|_{r=a}. \tag{3}$$

3. Solution of the problem

The task is to find resonant frequencies ω of the system described by equations (1)–(3). The normal modes are harmonic functions in the axial and circumferential directions, and Bessel functions in the radial direction.

Considering a simply-supported half cylindrical shell with the length l, solutions are taken to be in the form

$$\begin{aligned} u &= A\cos\lambda^* x \sin n\varphi e^{-i\omega t}, \\ v &= B\sin\lambda^* x \cos n\varphi e^{-i\omega t}, \\ w &= C\sin\lambda^* x \sin n\varphi e^{-i\omega t}, \\ \Phi &= DJ_n(\beta r)\sin\lambda^* x \sin n\varphi e^{-i\omega t}, \end{aligned} \tag{4}$$

where $J_n(\beta r)$ – Bessel function of the first kind and order n, $\lambda^* = m\pi/l$, $m = 1, 2, 3, \ldots$ bending mode number, $n = k\pi/\varphi_0$, $k = 1, 2, 3, \ldots$ circumferential mode number, ($\varphi_0 = \pi$ for a half-cylindrical shell).

Substituting solutions (4) in equations (2) and (3) we have

$$\beta^2 + \lambda^{*2} = \omega^2/c_0^2, \tag{5}$$

$$i\omega C = D\beta J_n'(\beta a). \tag{6}$$

The following relations between A, B and C can be obtained, from equations (1), using equation (6) to eliminate D:

$$\begin{aligned} A(H_1 - \Omega^2) + BH_2 + CH_3 &= 0, \\ AH_4 + B(H_5 - \Omega^2) + CH_6 &= 0, \\ AH_7 + BH_8 + C\{H_9 - \Omega^2[1 + K/F_n(\xi)]\} &= 0, \end{aligned} \tag{7}$$

where

$$H_1 = \lambda^2 + (1/2)[(A_1 - A_{1\nu})/A_1]n^2, \quad H_2 = (1/2)[(A_1 + A_{1\nu})/A_1]\lambda n,$$

$$H_3 = H_7 = (A_{1\nu}/A_1)\lambda, \quad H_4 = \lambda n[D_{1\nu}/4A_1R + (1/2)(A_1 + A_{1\nu})/A_1],$$

$$H_5 = (P/A_1)\lambda^2 + n^2[1 + B_1/(A_1R^2)], \quad H_6 = H_8 = n,$$

$$H_9 = 1 + (D_{1\nu}/A_1R)\lambda^2 + B_1/(A_1R^2)(\lambda^2 + n^2)^2, \quad \lambda = \lambda^* R, \quad \Omega = \omega^2 m_0 R^2 (1/A_1),$$

$$\beta = \sqrt{(1/R^2)(\Omega^2 A_1/(m_0 c_0^2) - \lambda^2)}, \quad K = \varrho a/m_0, \quad \xi = \beta a,$$

$$F_n(\xi) = [J_n'(\xi)/J_n(\xi)]\xi.$$

Equations (7) are valid simultaneously, when the determinant of coefficients vanishes. This condition can be written as

$$\Omega^6 - K_2(\Omega)\Omega^4 + K_1(\Omega)\Omega^2 - K_0(\Omega) = 0, \tag{8}$$

where

$$K_2(\Omega) = H_5 + H_1 + \mu H_9,$$

$$K_1(\Omega) = H_1 H_5 - H_2 H_4 + \mu(H_1 H_9 + H_5 H_9 - H_3 H_7 - H_6 H_8),$$

$$K_0(\Omega) = \mu(H_1 H_5 H_9 + H_3 H_4 H_8 + H_2 H_6 H_7 - H_3 H_5 H_7 - H_2 H_4 H_9 - H_1 H_6 H_8),$$

$$\mu = F_n(\xi)/(F_n(\xi) + K).$$

4. Numerical results

As an example, the transcendental equation (8) has been solved for the system with parameters as follows:

$$R = 0.5 \text{ m}, \quad E_1 = 2.1 \cdot 10^5 \text{ MPa}, \quad E_2 = 10^2 \text{ MPa}, \quad \nu_1 = 0.3, \quad \nu_2 = 0.4;$$

$$\gamma_1 = 7.8 \cdot 10^3 \text{ kgm}^{-3}, \quad \gamma_2 = 1.2 \cdot 10^3 \text{ kgm}^{-3}, \quad m_0 = \gamma_1 h_1 + \gamma_2 h_2, \quad h_1 = h_2.$$

Three positive real values of frequency parameter Ω were found for any acoustic medium enclosed, but only the lowest value Ω_1 (corresponding to the predominant shell bending mode) has been influenced by the interaction.

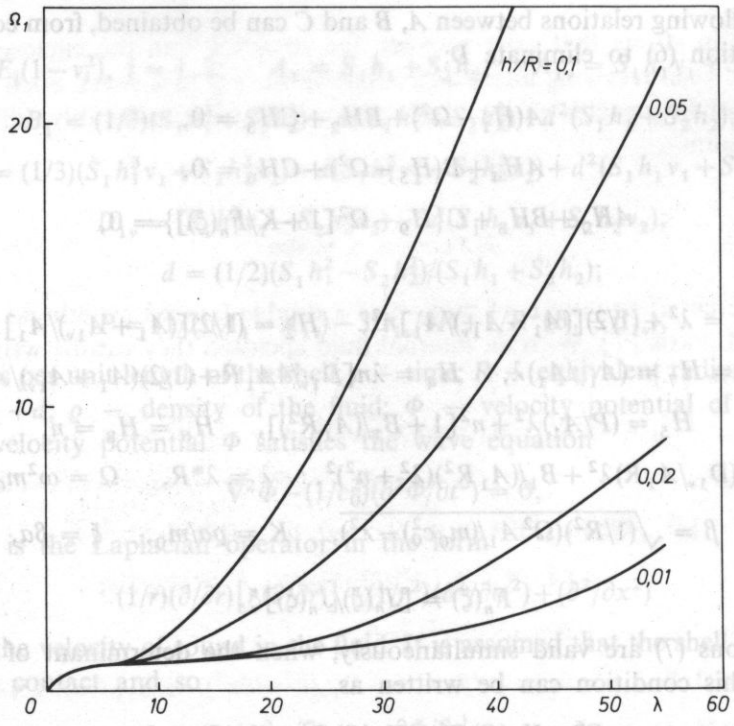

Fig. 2. Ω_1 versus λ for different ratios h/R, $n = 1$ (acoustic medium – air, $\varrho = 1.2 \text{ kgm}^{-3}$, $c_0 = 343 \text{ ms}^{-1}$)

Values of Ω_1 versus wave number λ for different ratios h/R and for circumferential mode number $n = 1$, with air as the acoustic medium ($\varrho = 1.2\ \mathrm{kgm^{-3}}$, $c_0 = 343\ \mathrm{ms^{-1}}$) are plotted in Fig. 2.

Resonant frequencies Ω_1 plotted in Fig. 2 are significantly influenced by the ratio h/R and they are higher for higher values of the wave number λ.

In the research carried out, the same shell as treated above has been analysed in interaction with different acoustic media. Results show only a slight difference between the values of frequency parameters for the coupled system with vacuum ($\varrho = 0$) and those with any gaseous acoustic medium under atmospheric pressure. However, the lowest values of frequency parameters are considerably reduced for any liquid medium. This is illustrated in Fig. 3 for a system with water as an acoustic medium ($\varrho = 1000\ \mathrm{kgm^{-3}}$, $c_0 = 1500\ \mathrm{ms^{-1}}$).

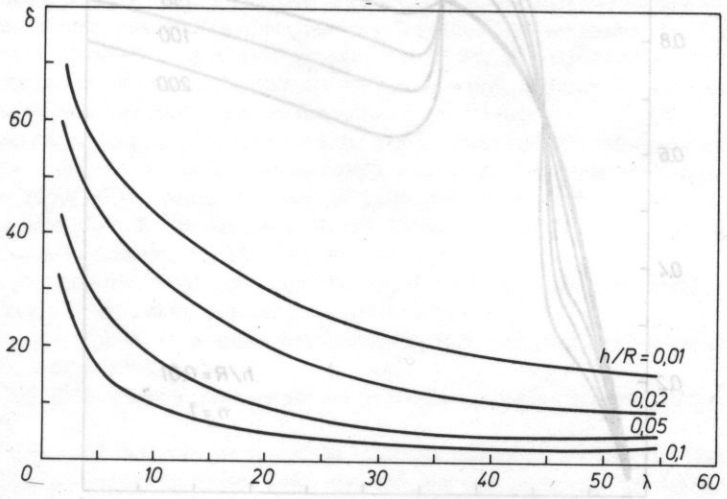

Fig. 3. Relative difference δ versus λ for different ratios h/R, $n = 1$ (acoustic medium – water, $\varrho = 1000\ \mathrm{kgm^{-3}}$, $c_0 = 1500\ \mathrm{ms^{-1}}$)

The relative difference

$$\delta = \frac{\Omega_{1(\mathrm{vacuum})} - \Omega_{1(\mathrm{water})}}{\Omega_{1(\mathrm{vacuum})}} \cdot 100 \quad [\%]$$

versus the wave number λ for different ratios h/R, $n = 1$ is plotted. The values of δ are lower for higher ratios h/R and they decrease with increasing wave number λ.

Let us pay our attention to air as the acoustic medium, again. A question arises, how the resonant frequency Ω_1 of the coupled system will be influenced by an increase of the wave impedance ϱc_0 of air.

It is well known, that the velocity of sound c_0 in any gaseous medium does not depend on its pressure. The wave impedance of air may thus be increased by pressurizing the structure (increasing the density of air ϱ).

The resonant frequency Ω_1 is presented in Fig. 4 in dependence on the wave number λ for different values of ϱ, for $h/R = 0.01$ and $n = 1$. The thick line stands for uncompressed air ($\varrho = 1.2\ \mathrm{kgm}^{-3}$). Compressed air tends to re-tune the enclosure in the following way: $\Omega_1' s$ increase for $\lambda < \pi$, then $\Omega_1' s$ decrease and for $\lambda > 4$ they increase again. There is a local maximum at $\lambda = \pi$, what means that an extreme of Ω_1 occurs when the length of the structure is set by an integer multiple of the relevant radius R of the shell. This conclusion holds, of course, for simply supported shells ($\lambda = m\pi R/l$) only.

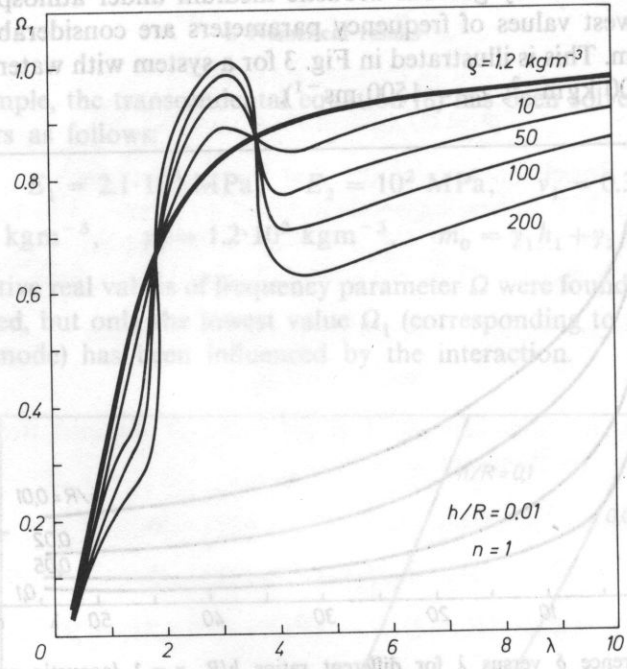

Fig. 4. Ω_1 versus λ for different values of ϱ, $h/R = 0.01$ and $n = 1$ (acoustic medium — compressed air)

5. Conclusion

The following concluding remarks can be yielded from the analysis carried out:

- eigenfrequencies of the system coupled with any gaseous medium under atmospheric pressure enclosed do not differ from those of the structure in vacuum;
- lowest values of the frequency parameter Ω_1 (corresponding to the predominant shell bending mode) are considerably reduced for any liquid medium;
- by pressurizing the enclosure with air inside, the structure may be "re-tuned" to higher, as well as to lower values of eigenfrequencies Ω_1 (depending on the wave number λ).

References

[1] Š. MARKUŠ, *Refined theory of damped axisymmetric vibrations of double-layered cylindrical shells*, J. Mech. Eng. Sci., **21**, 1 (1979).

[2] P. G. BENTLEY, D. FIRTH, *Acoustically excited vibrations in a liquid-filled cylindrical tank*, J. Sound Vib., **19**, 2 (1971).

Received on May 13, 1986; revised version on September 22, 1986.